BILINGUAL PUBLISHING GROUP

Journal of Environmental & Earth Sciences

Volume 6 • Issue 1 • April 2024 ISSN 2661-3190(Online)

Volume 6 Issue 1 • April 2024 • ISSN 2661-3190 (Online)

Journal of Environmental & Earth Sciences

BILINGUAL PUBLISHING GROUP

Volume 6 | Issue 1 | April 2024 | Page1-82
Journal of Environmental & Earth Sciences

Contents

Articles

Reviews

Case Report

BILINGUAL PUBLISHING GROUP

Journal of Environmental & Earth Sciences

https://journals.bilpubgroup.com/index.php/jees

ARTICLE

About Some Aspects of Use of Optical Sensors for Monitoring the Aquatic Environment

Ferdenant Mkrtchyan *, ***Vladimiir Soldatov, Maxim Mkrtchyan***

Kotelnikov Institute of Radioengineering & Electronics RAS, Fryazino Branch, Vvedensky Sq.1, Fryazino, Moscow, 141190, Russia

ABSTRACT

Multi-channel polarization optical technology is increasingly used for prompt monitoring of water systems. Optical devices during the assessment of water quality determine the intensity of light through the studied aquatic environment. Spectrophotometric devices measure the spectrum of weakening of light through the aquatic environment. Spectroellipsometric devices receive spectra in vertical and horizontal polarizations. The presented article develops an adaptive optical hardware and image system for monitoring water bodies. The system is combined. It consists of 2 parts: 1) automated spectrophotometer-refractometer, and 2) adaptive spectroellipsometer. The system is equipped with a corresponding algorithmic and software, including algorithms for identifying spectral curves, databases and knowledge of spectral curves algorithms for solving reverse problems. The presented system is original since it differs from modern foreign systems by a new method of spectrophotometric and spectroellipsometric measurements, an original elemental base of polarization optics and a comprehensive mathematical approach to assessing the quality of a water body. There are no rotating polarization elements in the system. Therefore, this makes it possible to increase the signal-to-noise ratio and, as a result, improve measurement stability and simplify multichannel spectrophotometers and spectroellipsometers. The proposed system can be used in various water systems where it is necessary to assess water quality or identify the presence of a certain set of chemical elements.

Keywords: Monitoring; Aquatic environment; Polarization optics; Water object; Pollutants; Spectral images; Classification; Identification

*CORRESPONDING AUTHOR:

Ferdenant Mkrtchyan, Kotelnikov Institute of Radioengineering & Electronics RAS, Fryazino Branch, Vvedensky Sq.1, Fryazino, Moscow, 141190, Russia; Email: ferd47@mail.ru

ARTICLE INFO

Received: 9 October 2023 | Revised: 7 November 2023 | Accepted: 13 November 2023 | Published Online: 28 November 2023

DOI: https://doi.org/10.30564/jees.v6i1.6006

CITATION

Mkrtchyan, F., Soldatov, V., Mkrtchyan, M., 2023. About Some Aspects on Use of Optical Sensors for Monitoring the Aquatic Environment. Journal of Environmental & Earth Sciences. 6(1): 1–10. DOI: https://doi.org/10.30564/jees.v6i1.6006

1. Introduction

The assessment of physicochemical parameters (PCP) of aquatic systems is the subject of many studies aimed at creating technical and algorithmic means for measuring and processing data on the state of the aquatic environment. Remote technologies have acquired particular relevance in recent years, allowing us to obtain operational information about water bodies and characterized by high productivity. The greatest effect is achieved when using multi-channel remote sensing systems, when, through the use of the necessary set of algorithmic tools, it is possible to significantly increase the reliability of the interpretation of observational data and successfully solve assessment problems of water quality. Work in this direction is being carried out at the Institute of Radio Engineering and Electronics named after. V.A. Kotelnikov RAS. The works formulate the basic principles of the integrated use of mathematical and technical means for solving problems of hydrophysical monitoring [1]. According to these principles, the procedure for synthesizing an automated data processing system for multichannel water quality measurements includes the creation of a set of hardware, algorithmic, model and software tools for collecting and analyzing information, taking into account the levels of its reliability and completeness [2,3].

The aquatic environment, as studies by many authors have shown, requires the collection of a large amount of data and, as a rule, laboratory analyzes for its assessment. The latter circumstance sharply worsens the functional characteristics of the monitoring system. The conducted studies excluded the stage of laboratory analysis from the procedure for assessing the quality of the aquatic environment, moving it to the beginning of the procedure for adopting the identification algorithm. This feature of the developed methodology is a fundamental difference between the proposed approach to assessing the physicochemical characteristics of water bodies from the developed approaches by other authors. In this case, the advantages of multichannel measurements in the optical and microwave regions of the spectrum are used, which, as shown by experimental measurements and theoretical models, creates the possibility of using highly efficient information technologies to solve problems of classification and identification of water bodies. The implementation of the methodology makes it possible to reduce the volume of observations and thereby increase the efficiency of the monitoring system.

The spectral composition of the radiation emerging from water carries information about the absorbing and scattering substances contained in the water. This is the physical basis of remote methods for analyzing the composition of natural waters. Knowledge of the spectral distribution of the brightness coefficient of waters with a known chemical composition makes it possible to determine some of the ingredients of the unknown composition of waters in the presence of characteristic features of the brightness of the water body under study.

Recently, spectral-polarization-optical methods and corresponding equipment for real-time research have been intensively developed: multichannel polarization spectrophotometers; spectropolarimeters; spectral ellipsometers and dichrometers; and refractometers. The use of effective polarization state modulators and multichannel analyzers in modern polarization-optical devices, as well as the development of programming methods, determine their high technical characteristics.

The joint use of technical and software tools for operational monitoring of the aquatic environment is poorly developed due to the complexity of synthesizing a comprehensive monitoring system. Particularly difficult are the tasks of combining algorithmic support with the level of information support of the monitoring system. The urgent task of environmental monitoring requires the development of compact precision polarization optical instruments for express analysis of liquid media. At the same time, the effectiveness of solving multiparameter problems is largely determined by the sensitivity and accuracy of devices, their versatility, and the ability to use a wide spectral range. Spectral measurements in the aquatic environment create an informative basis for the use of modern methods and algorithms for recognizing and identifying pollutants in this environment.

2. Materials and methods

2.1 Spectrophotometry and spectroellipsometry methods

Spectrophotometry and spectroellipsometry are optical techniques that use changes in the polarization state of light through reflection and refraction to characterize surfaces, interfaces, thin films in physics, and liquid solutions in hydrochemical studies in situ and in real time. Spectrophotometry and spectroellipsometry methods are used for non-destructive testing of the chemical and physical characteristics of solid materials and liquid solutions. These methods are based on recording the effects of optical polarization that occur when a light wave is reflected or deformed as a result of its interaction with the object under study. Diagnostics of liquids allows you to assess the concentration of chemical substances dissolved and suspended in the liquid, as well as identify stains of contaminants on the surface of the water.

Spectrophotometry is a method of research and analysis of substances based on measuring absorption spectra in the optical electromagnetic region. radiation. The basis of spectrophotometry is a physicochemical method for studying solutions and solids, based on the study of absorption spectra in the ultraviolet (200–400 nm), visible (400–760 nm) and infrared (> 760 nm) regions of the spectrum. The main dependence studied in spectrophotometry is the dependence of the absorption intensity of incident light on the wavelength. The result is a discrete spectrum, which, using traditional techniques, is converted into a continuous spectrum, which is visualized and analyzed. Optical spectral analysis is characterized by the relative ease of implementation, the absence of complex sample preparation for analysis, and the small amount of substance (10–30 mg) required for the analysis of a large number of elements.

The traditional approach to analyzing spectral images of solutions is based on cluster analysis. First, pattern recognition is trained by forming a cluster space. Then, based on the fact that the spectral image enters a given cluster, a decision is made on the composition of this solution. This fairly simple method works well for one-component solutions. In more complex cases, interpolation methods and more complex procedures are used. One of these procedures will consist of the following.

To solve the problem of recognizing the structure and content of chemical elements in an aqueous solution using a spectrophotometer, at the initial stage a database of standard samples is created. To create it, measurements were taken of samples of one-component and two-component solutions of various chemical elements.

Forming a database of standards for samples of aqueous solutions requires the creation of a formalized indicator for each sample. For this purpose, the Department of Computer Science of the Institute of Radio Engineering and Electronics of the Russian Academy of Sciences carried out measurements of one-component and two-component solutions with a resolution of 5% of the maximum possible concentration of a chemical element. This concentration was determined at the expert level. To develop an informative indicator of each spectrum, the encoding method adopted for signal recognition in radio engineering was used. For each spectrum, a vector indicator-image was created and clusters were formed.

Multichannel spectroellipsometry methods are among the most informative and sensitive methods for studying solid, liquid and gaseous objects. For example, the thickness and optical constants of monolayer coatings on the surface of liquids or the presence and structure of molecules of optically active substances in solutions are reliably measured.

Spectroellipsometers are designed for real-time measurements of the spectra of ellipsometric parameters Ψ and Δ (TanΨ, CosΔ) with subsequent transition, within the framework of a specific physical model of the structure under study, to the spectra of optical constants and geometric parameters (thicknesses of films and transition layers, degree of surface roughness, etc.).

The ability to accurately and quickly determine the spectra of optical constants of various materials and film thicknesses in the range from 1 nm to several microns has determined the widespread use of spectral ellipsometry in electronics, chemistry and electrochemistry, physics, biology, and medicine. Recently, spectroellipsometers have found interesting applications in the non-destructive determination of the critical dimensions of nanoelectronic structures. Laser ellipsometers with lateral resolution better than 0.1 µm are appearing. The use of spectral and laser ellipsometers as sensitive sensors is also of interest. The spectroellipsometer described below does not contain moving polarization elements, unlike widely used multichannel spectroellipsometers with rotating polarizers, analyzers and compensators, which allows for increasing the sensitivity of the spectroellipsometer in the absence of vibration noise.

The inverted geometry of the spectroellipsometer makes it possible to reduce the influence of background illumination during measurements with weak signals.

It should be noted that increasing the sensitivity and long-term stability of polarization-optical devices is achieved by using various modulators of the polarization state (photoelastic, Faraday, acousto-optical, etc.). In multichannel spectroellipsometers with rulers and photodetector arrays, the optimal use of rotating polarization elements (polarizer, compensator or analyzer). At the Institute of Radio Engineering and Electronics named after V.A. Kotelnikov RAS is developing a new approach to spectroellipsometry—spectroellipsometry with binary modulation of the polarization state, using an original binary polarization modulator, effectively replacing known expensive polarization elements [3–8].

In the spectroellipsometer with binary modulation (SEBM), radiation with two orthogonal polarization states is applied sequentially in time to the sample under study. The radiation beam reflected from the sample is either divided by a Wollaston [3-5] prism into two orthogonally polarized beams with azimuths A and A + 90º, which are simultaneously directed to two photodetectors, or passes through a polarization device that selects polarization sequentially in time with azimuths A and A + 90º, and arrives to a photodetector (linear or matrix of photodetectors).

The absence of moving polarization elements and the compactness of a SEBM of the polarization state provide a high signal-to-noise value and allow it to be used for measurements in field conditions. Currently, SEBM has a wide spectral range, high sensitivity and operational reliability. The use of these spectroellipsometers for diagnosing various water bodies has shown high efficiency.

2.2 Spectrophotometric and spectroellipsometric tools

Figure 1 shows the one developed at the Kotelnikov IRE RAS combined spectrophotometer and spectroellipsometer. The LED spectrophotometer (LSP) and LED spectroellipsometer (LSE) consist of two parts. The top part contains a spectrophotometer, and the lower part is a spectroellipsometer.

LSP is designed for training, which is a procedure for measuring the spectral characteristics and simultaneous independent measurement of the content of chemical elements in the aquatic environment. As a result, a database of standards is formed in the knowledge base, a comparison which provides a solution to the problem of identification. In particular, such a comparison can be realized within the framework of the calculation of the average square deviation of the measured spectral image of an object from the standards held in computer memory. The LSP software provides various algorithms for solving this problem, among which there is discriminant and cluster analysis.

Figure 1. A combined Led spectrophotometer and spectroellipsometer.

LSP can be used in various areas where it is required to assess the quality of an aqueous solution or to detect the presence of a specific set of chemical elements in an aqueous medium. LSP solves these tasks in the continuous monitoring of the aquatic environment. Installed for stationary measurement, it allows monitoring the dynamics of water quality in a stream, and when placed on board a vessel, measures the characteristics of a water body along the route.

The functionality of LSP can be expanded by increasing the volume of standards in the knowledge base. Switching to the natural light source allows solving the problems of detecting films of petroleum products and other substances in the aquatic environment, determining the degree of air pollution and assessing the state of other environmental objects whose spectral images in the visible range can vary.

As noted above, spectroellipsometry refers to optical technologies that use changes in the polarization of a light flux when it is reflected from a surface or refracted while passing through a liquid. Spectroellipsometry methods are used in the non-destructive study of the chemical and physical properties of solid and liquid substances [4-6,15]. These methods are based on recording optical polarization effects that occur when a light wave is reflected or distorted when interacting with the substance under study. In solid state physics, spectroellipsometry provides the ability to simultaneously measure the amplitude and phase characteristics of the sample under study and allows one to accurately determine simultaneously the thickness of films and the optical constants of the film material. When diagnosing liquids, it is possible to assess the concentrations of dissolved and suspended chemicals, as well as identify stains of pollutants on the water surface.

The characteristics of LSP and LES are shown in **Table 1**.

Table 1. Technical parameters of LSP and LSE.

Parameter	Value	
	LSP	LSE
Spectral range, nm	360–800	450–930
Spectral resolution,	10	10
Light flux registration time, sec	0.15	0.15
Long term stability, %	0.1–0.5	0.1–0.5
Sizes of measuring device, mm		
height	200	300
length	300	600
Measuring precision, degree		
Δ	-	0.01
Ψ	-	0.003
Weight of measuring device, kg	3	5
Power consumption, W	10	30
Sources of radiation: a complex of LEDs		
UVLED365-SMD	365	365
VL380-3528	380	380
VL400-3228	400	400
RLCU-415	415	415
SMC470	470	470
SMC525	525	525
SMC660	660	660
SMC780	780	780
Terms of use:		
operating temperature	15°–35 °C	15°–35 °C
relative humidity	95% at a temp. 20 °C.	95% at a temp. 20 °C.

LED Spectroellipsometer includes:

• a polarizer that converts a linearly polarized light flux into elliptical polarization;

• an analyzer that evaluates the parameters of the ellipse;

• power supply that supplies voltage according to the selected operating mode of the spectroellipsometer;

• light source with known spectral characteristics;

• fiberglass cable;

• broadband filters.

LES measures in real time the spectra of two ellipsometric angles Ψ and Δ ($0 \leq \Psi \leq 90°$, $0 \leq \Delta < 360°$; TanΨ, CosΔ) [3–8]. Based on these parameters, by solving the inverse problem of spectroellipsometry within the framework of a specific physical and mathematical model of the object (structure) under study, a transition to geophysical and geochemical parameters is realized (content of a chemical element, types of spots on the water surface, temperature, salinity, transparency, etc.).

Three measurement modes are possible:

1) In the first case, the measurement procedure is limited to taking a sample of the solution and placing it in a special cuvette with known optical characteristics. This limitation is leveled by the fact that here at the output we obtain two spectra reflecting the ellipsometric angles that determine the ratio of the complex amplitude refractive indices of light for two polarizations. Possible distortions of the spectra may occur in the case of uncontrolled changes in the characteristics of the cuvette.

2) Direct measurements of the integral flux of scattered and refracted light by lowering the light guide and receiver into a liquid medium. In this case, external interference is excluded.

3) Use of sunlight reflected from the water surface. In this case, the level of illumination of the surrounding space is simultaneously recorded to calibrate the obtained spectra. The level of instability of the recorded spectra is determined by the instability of the illumination of the surrounding space during the signal registration time (fractions of a second).

In any mode of measuring the optical characteristics of the test object η at the output of the spectroellipsometric system according to the basic equation $\rho = r_p/r_s = \mathrm{Tan}\Psi\exp(i\Delta)$, where Ψ and Δ are the ellipsometric angles that determine the ratio of the complex amplitude reflection coefficients r_p and r_s for p and s polarizations, two spectra are obtained [3–6]:

1) $S_\Psi(\lambda,\eta)$—spectral distribution of the tangent of the spectroellipsometric angle Ψ.

2) $S_\Delta(\lambda,\eta)$—spectral distribution of the cosine of the spectroellipsometric angle Δ.

Spectral curves $S_\Psi(\lambda,\eta)$ and $S_\Delta(\lambda,\eta)$ are functions of the optical characteristics of the diagnosed object η. Based on these spectra, one can estimate the physical or chemical parameters of an object by solving the inverse problem of spectroellipsometry.

The algorithmic and functional capabilities of LES make it possible to implement a training procedure for spectral pattern recognition. In this case, a database of spectral standards is formed in LES, and the inverse problem of spectroellipsometry is solved by searching this database for spectra close to the new spectrum obtained. The accuracy of solving the problem depends on the method of assessing this proximity.

2.3 One method for solving the inverse problem

For the experiment, 6 solutions of copper sulfate ($CuSO_4$) of various concentrations were prepared, namely 5%, 10%, 15%, 20%, 25%, 30%. By mixing two solutions in certain proportions, you can get a third solution of intermediate concentration from the list above. To obtain the proportions of two solutions, it is necessary to solve the inverse problem by comparing the readings of the spectrophotometer of the linear combination of two solutions with the readings of the instrument of the third solution. The problem is described by a system of linear equations:

$$A\overline{x} = \overline{B} \tag{1}$$

where the vector corresponds to the spectrum of the third solution. We will solve (1) by the Cramer method. Consider a combination of 3 solutions: 5-20-10, i.e. we need to mix two solutions with a concentration of 5% and 20% in order to obtain a concentration of 10%. We will choose two reference channels: $\lambda_1 = 380$ *nm and* $\lambda_2 = 525$ *nm*.

Channel selection can be optimized according to various criteria. The simplest is the choice of the maximum channel separation. But since the channels $\lambda = 660$ *nm and* $\lambda = 780$ *nm* with are extremely noisy, we will exclude them from consideration and stop at the $\lambda = 525$ nm channel. The 365 nm channel, being the leftmost channel, was omitted to align the pair of channels to the center of the frequency range.

$$A = \begin{vmatrix} \cdot 76683 & \cdot 21598 \\ \cdot 77462 & \cdot 39918 \end{vmatrix} \quad \bar{b} = \begin{vmatrix} \cdot 59794 \\ \cdot 75117 \end{vmatrix}$$

det $A = 0.13881$, det $A_x = 0.076448$, then $x = \det A_x / \det A = 0.55077$

det $A_y = 0.11284$ $y = \det A_y / \det A = 0.81299$

Here the designation is accepted: $x_1 = x$, $x_2 = y$. How to evaluate the quality of a popular result? Here, too, different optimality criteria are possible, for example, the normalization error. In our case, it is 0.36376. The second criterion is to minimize the deviation of the obtained proportion of the first solution with a concentration of 5% from the theoretical estimate. In our case, this deviation is 0.11589. In this method, we did not take into account the normalization condition.

Let us now consider how the normalization condition affects the quality of the solution. Under these conditions, solving the second equation for, corresponding to the channel $x = 525$ nm, we obtain $x = 0.93753$, which, according to the second criterion, gives an error equal to 0.27087, which is more than 3 times greater than the corresponding error. But by sorting through all the channels, we can easily find the optimal one, in this case it is a channel with a wavelength $\lambda = 380$ nm, and the corresponding error is 0.02674, which is an order of magnitude less than the error obtained with the first method according to the second criterion. Even the worst 470 nm channel has an error comparable to the error of the first method, namely 0.38460. Solving the problem for the 380 nm and 365 nm channels using the 1st method, we get an error for both criteria even greater than for the previous pair of channels. Thus, it is obvious that the optimization of the decision procedure should still be carried out taking into account the normalization condition, especially since the enumeration of options in this case is much smaller. Another thing is when the answer to the problem is unknown, i.e. the third solution has an unknown intermediate concentration. In this case, it is necessary to sort through all possible pairs of spectral channels and perform optimization according to the first criterion.

We have studied all 20 combinations of three solutions and obtained optimal error estimates for the second criterion. The worst channels and their corresponding error estimates were also found.

We will distinguish between combinations of two types: general (**Table 2**) and symmetrical (**Table 3**) combination. We call a combination of 3 solutions symmetrical if the proportions of two of them in the third solution are equal.

These combinations in our experiment are:

1. 5-15-10; **2.** 5-25-15; **3.** 10-20-15; **4.** 10-30-20; **5.** 20-30-25; **6.** 15-25-20

The remaining combinations of solutions will be called combinations of the general. Let us now present the final optimization results with the indication of the minimum and maximum errors and the corresponding channel.

Table 2. General combinations.

View	Channel	Minimum	Channel	Maximum
5-25-10	365	0.01204	470	0.29281
5-20-10	380	0.02674	470	0.38460
5-20-15	380	0.01976	470	0.45743
5-25-20	525	0.07403	400	0.17518
5-30-10	365	0.00899	470	0.23067
5-30-15	400	0.01896	470	0.27361
5-30-20	470	0.00402	365	0.19830
5-30-25	525	0.00824	470	0.08216
10-25-15	525	0.00869	400	0.20545
10-25-20	525	0.15824	400	0.23776
10-30-15	415	0.00831	525	0.11976
10-30-25	470	0.02498	365	0.09608
5-30-20	525	0.19170	365	0.28458
15-30-25	525	0.04214	365	0.10876

Table 3. Symmetrical combinations.

View	Channel	Minimum	Channel	Maximum
5-15-10	470	0.00000	365	0.16476
5-25-15	365, 380, 470	0.00000	415, 525	0.00001
10-20-15	380	0.00000	365	0.00043
10-30-20	365	0.00000	400	0.00020
20-30-25	365	0.00000	380	0.00004
15-25-20	470	0.11649	400	0.34918

It can be seen from the tables that symmetrical combinations of solutions are the most stable when solving inverse problems. This is apparently due to the fact that the errors of symmetrical solutions have different signs and the same weights, which leads to their mutual cancellation when summed up to the 5th decimal place.

As for the accuracy of optical instruments, it is determined directly by the accuracy of the spectral values, as well as the reliability of the final results of diagnostics of aquatic environments. The spectrophotometer measures the spectral curve $S(\lambda)$, and the spectroellipsometer measures the spectral curves $S_\Psi(\lambda)$ and $S_\Delta(\lambda)$, respectively. Optical diagnostics of water systems is carried out directly by analyzing spectral curves using specific algorithms and models [8,9,11,14–17].

3. Results and discussion

3.1 Application of LSP

LSP was used to determine the hardness of water.

Water hardness is a combination of chemical and physical properties of water associated with the content of dissolved salts of alkaline earth metals, mainly calcium and magnesium. Natural waters contain calcium and magnesium sulphates and bicarbonates, i.e. Ca^{2+} and Mg^{2+} cations, SO_4^{2-} and HCO_3^- anions.

LSP was tested when determining the concentration of different solutions of $CaCl_2$ and $MgSO_4$ for different concentrations. The results are shown in **Table 4**.

For LSP, a Pascal program was developed that implements solution identification algorithms based on the standard deviation and discriminant analysis procedures.

LSP was also used to determine the content of Ca++ and Mg++ ions in drinking water. When comparing the results of analyses of drinking water with SES data, the discrepancy was 2–3%.

Table 4. Concentrations of different solutions of $CaCl_2$ and $MgSO_4$.

Solution $CaCl_2$			**Solution $MgSO_4$**
Conc. %	λ	Indication. LSP	
0.25	365	–0.000013833	0.000013665
	380	–0.000016537	0.000000078589
	400	–0.000015107	–0.0000088009
	415	–0.000033185	–0.000017852
	470	–0.000015903	0.00000034272
	525	–0.000041114	–0.000019528
	660	–0.000044677	–0.000022124
	780	–0.000062126	–0.000038044
0.5	365	0.000054099	0.00011439
	380	0.000040307	0.00010519
	400	0.000058027	0.00013196
	415	0.000057663	0.00016455
	470	0.000063689	0.00014422
	525	0.000069659	0.00019617
	660	0.000059451	0.00017979
	780	0.000048948	0.00019018
1	365	0.00016419	0.00015503
	380	0.00017495	0.00024768
	400	0.00022308	0.00025534
	415	0.00025486	0.00031383
	470	0.00023397	0.0002794
	525	0.0003413	0.00043667
	660	0.0003493	0.00043667
	780	0.00037174	0.00047805

3.2 Application of LSE

LSE was used to assess water quality in Lake Baikal and the Siberian rivers Angara and Yenisei. Heavy metals and oil spills were discovered both in Lake Baikal and in the Angara and Yenisei rivers along the course.

In many countries, there is an increase in the concentration of heavy metals and petroleum products along the Arctic coast [13,14]. The main reason for the increase in this pollution is mainly the Siberian rivers, including the Angara and Yenisei. These rivers contain large industrial cities such as Angarsk, Irkutsk, and Krosnoyarsk. LSEs have been used to estimate concentrations of heavy metals and oil spills in waters above and below these cities. The results of these measurements are shown in **Table 5**.

Table 5. Heavy metal concentration (ppb) in the river water samples was assessed using the LSE.

Measurement location	As	Cd	Cr	Cu	Ni	Pb	Zn
Lake Baikal	4.18	0.33	6.7	13.6	14.8	1.36	24.3
r. Angara to the dam	6.59	0.47	8.7	15.3	16.5	2.13	21.8
r.Angara after the dam	12.8	1.15	9.8	16.1	20.2	4.07	59.3
r.Yenisei to the confluence of the r.Angara	11.4	0.87	10.4	19.4	21.4	5.72	41.9
r.Yenisei after the confluence of the r.Angara	9.23	0.68	13.8	15.6	19.8	6.87	18.6

Based on the measurement results, the following conclusions can be drawn. In the Angara River and in the Yenisei River, all heavy metals are unevenly distributed. This is the result of a fast current and the turbulence of these rivers, as well as due to the rocky bottom of these rivers. It can be noted, in particular, that at the bottom of the Angara there are low areas where heavy metals accumulate and are periodically washed out. To obtain a real picture of the water quality of the Angara and Yenisei, it is necessary to develop a regional model of the water balance of the system of these rivers. This model should take into account the sources of pollution entering this system with inflows and wastewater [10–14].

4. Conclusions

The technology discussed in this paper for the combined use of spectrophotometry, spectroellipsometry and detection and classification algorithms can be used in determining the concentration of aqueous solutions (including medical solutions), as well as diagnosing the quality of wastewater from industrial enterprises in real time.

Also, LSP and LSE can be made in the form of a portable device, with the help of which the operator can monitor the quality of water resources in real time without taking samples and conducting chemical analyses in the laboratory. In a stationary version, they allow monitoring of the dynamics of water quality in a stream, and when placed on a ship—measure water parameters throughout the entire route. The functions of LSP and LSE can be achieved by increasing the volume of standards in the knowledge base.

Author Contributions

Ferdenant Mkrtchyan conceived the study design, developed the models, and drafted the manuscript; Vladimir Soldatov and Maxim Mkrtchyan were involved in data acquisition and analysis and worked on aspects of the experiment. All authors have read and agreed to the published version of the manuscript.

Conflict of Interest

The authors declare no conflict of interest.

Acknowledgement

"The Study Was Supported By The Russian Science Foundation Grant No. 23-21-00115, https://rscf.ru/en/project/23-21-00115/".

References

[1] Mkrtchyan, F.A., Varotsos, C.A., 2018. A new monitoring system for the surface marine anomalies. Water, Air, & Soil Pollution. 229, 1–10.
DOI: https://doi.org/10.1007/s11270-018-3938-3

[2] Mkrtchyan, F.A. (editor), 2018. On the effectiveness of remote monitoring systems. Earth Observing Systems XXIII; 2018 Sep 7; San Diego, California, United States. 10764, 361–367.
DOI: https://doi.org/10.1117/12.2322522

[3] Kovalev, V.I., Rukovishnikov, A.I., Kovalev, S.V., et al., 2016. LED broadband spectral ellipsometer with switching of orthogonal polarization states. Journal of Optical Technology. 83(3), 181–184.

DOI: https://doi.org/10.1364/JOT.83.000181

[4] Kovalev, V.I., Rukovishnikov, A.I., Kovalev, S.V., et al., 2014. An LED multichannel spectral ellipsometer with binary modulation of the polarization state. Instruments and Experimental Techniques. 57, 607–610.
DOI: https://doi.org/10.1134/S002044121405008X

[5] Kovalev, V.I., Ali, M., Kovalev, S.V., et al., 2014. Possibilities of achromatization of coaxial asymmetric phase shifters with an even number of reflections. Optics and Spectroscopy. 117, 118–120.
DOI: https://doi.org/10.1134/S0030400X1407011X

[6] Krapivin, V.F., Nitu, C., Mkrtchyan, F.A., et al., 2018. Information-instrumental tools of microwave and optical environmental monitoring. The Scientific Bulletin of Electrical Engineering Faculty. 18(1), 11–18.
DOI: https://doi.org/10.1515/sbeef-2017-0016

[7] Mkrtchyan, F.A., Krapivin, V.F., Kovalev, V.I., et al., 2009. An adaptive spectroellipsometric technology for ecological monitoring of sea water. PICES Scientific Report. 36, 215–218.

[8] Mkrtchyan, F.A., Krapivin, V.F., Kovalev, V.I., et al., 2009. An adaptive spectroellipsometer for ecological monitoring. Microwave and Optical Technology Letters. 51(11), 2792–2795.
DOI: https://doi.org/10.1002/mop.24730

[9] Lazareva, O., Kan, J., Chen, C., et al., 2022. Coupled dynamics of aqueous biogeochemistry in contrasting floodplain environments: Implications for Critical Zone carbon sequestration along redox gradients. Applied Geochemistry. 145, 105413.
DOI: https://doi.org/10.1016/j.apgeochem.2022.105413

[10] Liao, F., Wang, G., Shi, Z., et al., 2018. Distributions, sources, and species of heavy metals/trace elements in shallow groundwater around the Poyang Lake, East China. Exposure and Health. 10, 211–227.
DOI: https://doi.org/10.1007/s12403-017-0256-8

[11] Mkrtchyan, F.A., Krapivin, V.F., Kovalev, V.I., et al. (editors), 2010. An adaptive spectroellipsometric identifier for ecological monitoring of the aquatic environment. PIERS 2010 Cambridge-Progress in Electromagnetics Research Symposium; 2010 Jul 5-8; Cambridge, USA. p. 365–368. (in Russian).

[12] Plana, Q., Alferes, J., Fuks, K., et al., 2019. Towards a water quality database for raw and validated data with emphasis on structured metadata. Water Quality Research Journal. 54(1), 1–9.
DOI: https://doi.org/10.2166/wqrj.2018.013

[13] Prasad, A.N., Mamun, K.A., Islam, F.R., et al. (editors), 2015. Smart water quality monitoring system. 2015 2nd Asia-Pacific World Congress on Computer Science and Engineering (APWC on CSE); 2015 Dec 2–4; Nadi, Fiji. New York: IEEE. p. 1–6.
DOI: https://doi.org/10.1109/APWCCSE.2015.7476234

[14] Varotsos, C.A., Krapivin, V.F., Mkrtchyan, F.A., 2019. New optical tools for water quality diagnostics. Water, Air, & Soil Pollution. 230, 1–12.
DOI: https://doi.org/10.1007/s11270-019-4228-4

[15] Mkrtchyan, F.A., Krapivin, V.F., Klimov, V.V. (editors), 2019. The possibilities of using LED photometry and ellipsometry technology for monitoring the aquatic anvironment. 2019 Photonics & Electromagnetics Research Symposium-Spring (PIERS-Spring); 2019 Jun 17–20; Rome, Italy. New York: IEEE. p. 908–914.
DOI: https://doi.org/10.1109/PIERS-Spring46901.2019.9017591

[16] Nitu, C., Krapivin, V.F., Mkrtchyan, F.A., 2020. Advanced ecology. Monitoring, diagnostics, prognosis. Vol. 1. Matrix Rom: Bucharesti. pp. 1–396.

[17] Nitu, C., Krapivin, V.F., Mkrtchyan, F.A., 2021. Advanced ecology. Monitoring, diagnostics, prognosis. Vol. 2. Matrix Rom: Bucharesti. pp. 1–374.

BILINGUAL PUBLISHING GROUP

Journal of Environmental & Earth Sciences

https://journals.bilpubgroup.com/index.php/jees

ARTICLE

Exploring Variability in Sea Level at a Tide Gauge Station through Control Charts

H. Bâki İz

Independent Scholar, Boca Raton Florida, 33496, USA

ABSTRACT

Monitoring temporal changes in sea level is important in assessing coastal risk. Sea level anomalies at a tide gauge station, if kinematically conceived, include systematic variations such as trend, acceleration, periodic oscillations, and random disturbances. Among them, the non-stationary nature of the random sea level variations of known or unknown origin at coastal regions has been long recognized by the sea level community. This study proposes the analyses of subgroups of random residual statistics of a rigorously formulated kinematic model solution of tide gauge variations using X-bar and S control charts. The approach is demonstrated using Key West, Florida tide gauge records. The mean and standard errors of 5-year-long subgroups of the residuals revealed that sea level changes at this location have been progressively intensifying from 1913 to the present. Increasing oscillations in sea level at this locality may be attributed partly to the thermal expansion of seawater with increasing temperatures causing larger buoyancy-related sea level fluctuations as well as the intensification of atmospheric events including wind patterns and the impact of changes in inverted barometer effects that will alter coastal risk assessments for the future.

Keywords: Climate change; Sea level variance; X-bar; S control charts

1. Introduction

Monitoring sea level changes during the 20th and 21st centuries is important in assessing anthropogenic contributions to climate change mechanisms [1]. Recent sea level rise studies emphasize observing systematic changes, such as trends, accelerations, periodic oscillations, and unexplained random contributors to sea level changes of known or unknown origin.

*CORRESPONDING AUTHOR:
H. Bâki İz, Independent Scholar, Boca Raton Florida, 33496, USA; Email: h.baki.iz@gmail.com

ARTICLE INFO
Received: 23 September 2023 | Revised: 9 December 2023 | Accepted: 19 December 2023 | Published Online: 27 December 2023
DOI: https://doi.org/10.30564/jees.v6i1.5983

CITATION
İz, H.B., 2023. Exploring Variability in Sea Level at a Tide Gauge Station through Control Charts. Journal of Environmental & Earth Sciences. 6(1): 11–18. DOI: https://doi.org/10.30564/jees.v6i1.5983

Among them, systematic sea level changes are induced by wind stress, atmospheric pressure, precipitation, river discharge, currents, temperature and salinity of the water long periodic solar radiation variations and lunar tidal activities [2]. Sub-seasonal to decadal periodic movements of sea level, locally and regionally, are also induced by atmospheric pressure variations, sea surface winds, and ocean circulation patterns [3]. Linear and nonlinear systematic changes in sea level are represented by trend and acceleration/deceleration respectively using kinematic models.

Random sea level anomalies are due to the instrumental errors and transient roughness of the sea level over short or long timescales because of climatic changes. Irregular and episodic discharges from a nearby river, or seasonal variations due to the components of atmospheric pressure or temperature variations may have random components. Some of the sea level variability is attributed to the thermal expansion of seawater, which accelerates with increasing temperature and larger buoyancy-related sea level fluctuations [4]. Climate model simulations with increasing greenhouse gas emissions suggest that future sea level variability, such as the annual and interannual oscillations that alter local astronomical tidal cycles and contribute to coastal impacts, are expected to increase in many regions [4].

Recently, Woodworth et al. [5] stated that coastal sea level variability can be better understood than those in the deep ocean. Their study discussed the underlying forcing factors exhaustively. The systematic components of resulting coastal sea level variability can be modeled kinematically, which will be demonstrated as a byproduct of this study, such that the remaining unknown or unmodeled random variability in sea level can be scrutinized at tide gauge (TG) stations. Increasing oscillations in sea level are expected due to the thermal expansion of seawater with increasing temperatures causing larger buoyancy-related sea level fluctuations as well as the observed intensification of atmospheric events because of climate change [6] that will alter coastal risk assessments for the future.

The random appearance of the sea level changes has long been identified as having non-stationary properties [3]. The stationarity of random sea level variations can be understood formally as the statistical properties of a physical system that remain unchanged over time [7]. Two types of stationary series are identified: One having a *constant mean* and another, fluctuating about that mean with a *constant variance* [8]. A study by Iz and Ng [9], already demonstrated by examining globally distributed 1862 stations' tide gauge data from the Permanent Service for Mean Sea Level (PSMSL) that random excursions in sea levels are preponderantly *non-stationary in variance*. This study conjures further and demonstrates that there is more to be learned from the time progression of *non-stationary variances* in sea level anomalies for climate change related risk assessments at coastal regions.

In the following sections, the Key West TG station record is used to examine the random properties of the sea level fluctuations at this locality as an example. Systematic and random sea level variations observed at this station are represented by a rigorous kinematic model. An Ordinary Least Squares (OLS) solution to the kinematic model is then carried out and the solution residuals are analyzed using their subgroups' statistics inspired by X-bar and S control charts. The reliability of the finding, an increase in the variance of the random changes in sea level at this TG station from 1913 to the present, is quantified by bootstrapping the residuals and analyzing alternative random realization of residual subgroups' stationary/non-stationary properties.

2. An extended kinematic model of sea level variations

The following extended kinematic model represents observed sea level height anomalies at a TG station. It consists of a trend, a uniform acceleration, and periodic sea level variations to represent observed sea level anomalies h_t^{obs} at an epoch t with random disturbances ε_t,

$$h_t^{obs} = h_0 + v_0(t - t_0) + \frac{a}{2}(t - t_0)^2 + \\ + \sum_{h=1}^{17} \left\{ \alpha_h \sin\left[\frac{2\pi}{P_h}(t - t_0)\right] + \gamma_h \cos\left[\frac{2\pi}{P_h}(t - t_0)\right] \right\} + \varepsilon_t \tag{1}$$

where, the reference datum h_0 is defined in the middle of the record at an epoch t_0. The trend is the initial velocity v_0 at t_0 when $a \neq 0$, and a is the constant rate of change in the sea level velocity (i.e., the uniform acceleration). P_h are the periods of systematic sea level oscillations. Their amplitudes can be constructed using α_h *and* γ_h sin and cosine components respectively.

What is markedly different in this model as compared to the previous studies of a similar nature① is the inclusion of various prospective low frequency sea level variations at a TG station explicitly in a top-down approach. The origins of these oscillations in sea level were conjured by Munk et al. [10] and Keeling and Whorf [11]. Under their scenarios, interactions of the ocean, meteorological forcing, and sea surface temperature materialize as natural broad band sea level variations. They modulate astronomical forcings, such as lunar node tide systematically or as random beatings resulting in sub and super harmonics of known periods (**Table 1**). Similarly, the variations in total solar radiation with a period of P = 11.1 years, yield subharmonics with periods: 2 × P = 22.2 years and longer. An earlier wavelet analysis by Yndestad [12] also identified several lunar node subs and super harmonics in Arctic Sea level, temperature, ice extent and winter index time series data, including the signature of nodal harmonics in pole position time series (**Table 1** in Yndestad [13]), and a strong cross correlation with Chandler wobble.

Although the observed amplitudes of such oscillation are small, they can bias sea level trends and acceleration estimates. Their unmodeled effects confound short TG and Satellite Altimetry, SA, time series thereby hindering the search for a global GMSL acceleration caused by anthropogenic global warming. İz [14] demonstrated that once these effects are modeled and the corresponding model parameters are estimated, spectral analyses of the TG residuals reveal additional statistically significant sea level variations at the decadal scale due to the ocean surface wind forcings and periodic changes in atmospheric pressure along the coastal lines of some of the TG stations [15].

All the above-mentioned effects are therefore incorporated into the kinematic model. The periodicities consist of a mix of seventeen sub and super harmonics attributed to the compounding of the nodal tides, solar radiation, and annual and sub annual variations with natural sea level variations (**Table 1**). In total, the extended kinematic model includes 37 unknown parameters.

As far as the statistical properties of the model are concerned, the disturbances denoted by ε_t may be autocorrelated of first order, AR(1). First order autocorrelations AR(1) exist with varying magnitudes in globally distributed tide gauge stations once the low frequency sea level variations are modeled. The autocorrelations are always positive and can be as large as ρ = 0.4 or more. Such AR(1) disturbances can be represented as follows,

Table 1. Compounded Luni-Solar and other periodicities all in years.

Nodal subharmonics	Nodal superharmonics	Nodal superharmonics	Solar	Chandler	Annual subannuals
74.5	18.6	3.7	11.1	429.5/365.4 = 1.2	1.00
55.8	9.3	3.1	22.2		0.50
37.2	6.2	2.6	0.25		
	4.7	2.3			

① With the exception of the earlier studies by this investigator.

$$\varepsilon_t = \rho\varepsilon_{t-1} + u_t \tag{2}$$

In this expression, $-1 \leq \rho \leq 1$ is the unknown autocorrelation coefficient of the AR(1) process. Furthermore, the stochastic processes for the random noise u_t and ε_t, have the following assumed distributional properties,

$$E(u_t) = 0,\ E(u_t^2) = \sigma_u^2,\ E(u_t u_{t-1}) = 0 \tag{3}$$

where σ_u^2 is the variance of u_t. The square root of its estimate is denoted by, $\hat{\sigma}_u$ or stated simply as the standard error, SE. The error of omission of a positive AR(1) correlation reduces the effective length of the total series statistically in proportion to the magnitude of ρ, and leads to a Type I error in testing null-hypotheses when assessing the solution parameters. The above expression together with Equation (2) gives,

$$E(\varepsilon_t) = 0, E(\varepsilon_t^2) = \sigma_\varepsilon^2 = \frac{\sigma_u^2}{1-\rho^2} \tag{4}$$

If the observation equation represented by Equation (1) at an epoch t-1 is multiplied by ρ and subtracted from the following observation equation at t, the effect of AR(1) is removed,

$$\begin{aligned} h_t - \rho h_{t-1} = {} & [h_{t_0} - \rho h_{t_0-1}] + v_0[(t-t_0) + \rho(t_{t-1}-t_0)] \\ & + \frac{a}{2}[(t-t_0)^2 + \rho(t_{t-1}-t_0)^2] \\ & + \sum_{k=1}^{n}\left(\alpha_h \sin\left[\frac{2\pi}{P_k}(t-t_0)\right]\right. \\ & \left. - \rho\alpha_k \sin\left[\frac{2\pi}{P_k}(t_{t-1}-t_0)\right]\right) \\ & + \sum_{k=1}^{n}\left(\gamma_k \cos\left[\frac{2\pi}{P_k}(t-t_0)\right]\right. \\ & \left. - \rho\gamma_k \cos\left[\frac{2\pi}{P_k}(t_{t-1}-t_0)\right]\right) + u_t \end{aligned} \tag{5}$$

Because the random errors in this representation are identically and independently distributed, *i.i.d*., with zero expected value, i.e., $u_t \sim (0, \sigma_u^2)$,the observation equations based on Equation (5) can be solved using the OLS method. In the following section, OLS is used to generate the residuals needed for the graphical analyses of random excursions in sea level at Key West, Florida TG station.

3. Tide gauge records

Key West, Florida, monthly TG time series data displayed in **Figure 1** are used for the OLS solution and the graphical analyses of the residuals. The record is referenced to the Revised Local Reference, RLR, defined by the Permanent Mean Sea Level, PSMSL. No corrections including post glacial rebound, nor inverted barometric effects were applied to the data. The records were downloaded from the PSMSL repository in November 2020 [16].

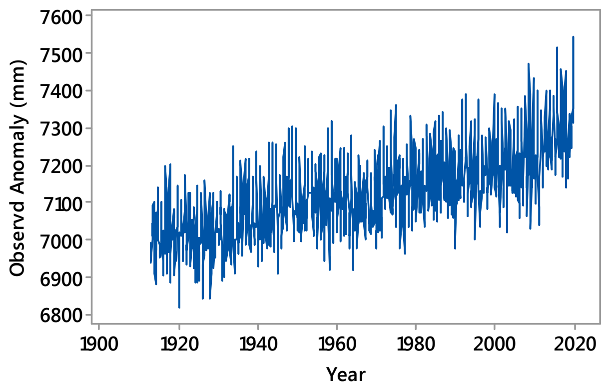

Figure 1. Monthly averaged sea level height anomalies at Key West, Florida, TG station.

4. Ordinary least squares solution

The observation equation given by Equation (5) is a function of the unknown AR(1) correlation coefficient ρ on the left-hand side. If several OLS solutions are carried out for the values within the interval [$-1 \leq \rho \leq 1$], the solution with the smallest SE is adopted as the optimal value for the model based on Equation (5). This process is known as the Hildreth-Lu procedure [17]. All the statistically significant parameters for the Key West Florida TG station, i.e., those with p-values②, $p < 0.05$, were estimated using this approach.

The solution statistics tabulated in **Tables 2 and 3** indicate that the model explains more than 72% of the sea level variations together with well-defined

② *p-value* is the probability of obtaining a test statistic result at least as extreme or as close to the one that was observed, if the null hypothesis is true (Goodman, 1999). Smaller *p-values* for the model parameters in this study provide statistical evidence (*independent of the significance level*) that the magnitudes of estimates cannot be attributed to chance alone.

Table 2. OLS solution statistics. Trend and uniform acceleration estimates are statistically significant at α = 0.05.

Time span year	Initial velocity mm/year	Uniform acceleration mm/year^2	SE mm.	Adj. R^2 %	DW	ρ
1913–2020	2.45 ± 0.06	0.018 ± 0.005	41.2	71.8	1.9	0.4

Table 3. Statistically significant amplitudes of periodicities and their SEs. Units are in mm.

Period (year)	75	37	37	12.4	11	6	Annual	Semi-annual
Amplitude	11.78	18.05	18.05	6.77	6.49	6.95	81.28	39.23
SE	±2.87	±2.89	±2.79	±2.76	±2.75	±2.70	±2.38	±1.87

sea level trends and uniform acceleration estimates. The Durbin-Watson statistic, DW = 1.9, is close to its expected value of 2, which indicates the solution residuals are free from unmodeled systematic effects.

The statistically significant low frequency sea level variations experienced at the TG station shown in **Table 3** have amplitudes large enough to bias the trend and acceleration estimates and their statistics. More importantly, they confound the randomness of the residuals if they are not incorporated into the model.

Figures 2 and 3 reveal that the residuals are unambiguously free from any unmodeled systematic sea level variations. This outcome is also a testament to the effectiveness of the top-down modeled low frequency sea level changes. Because the model removes all the systematic variations from the sea level anomalies, the remaining unexplained sea level variations at this TG station are the random effects whose statistical properties will be studied in the following section.

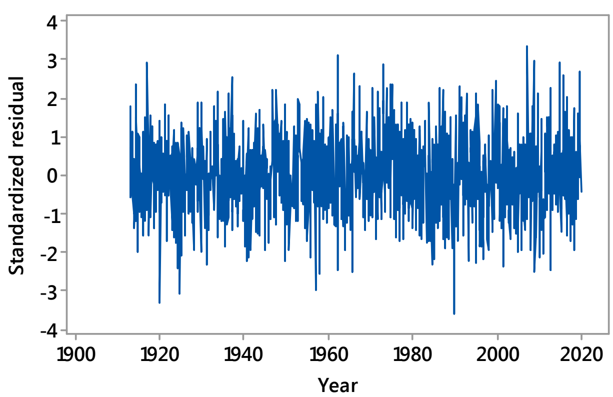

Figure 2. Standardized residuals (residuals divided by their standard errors).

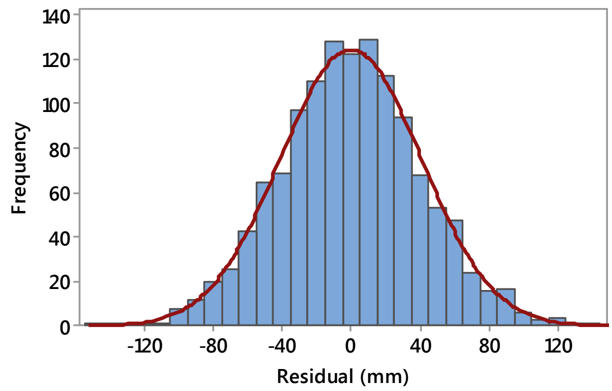

Figure 3. The histogram of the standardized residuals exhibits a normal-like distribution.

5. The analyses of the residuals using $\bar{x}$ and s control charts

In statistical quality control, X-bar and S control charts (also known as Shewhart charts [18]) are used to monitor variation in a business or industrial process during which samples are collected at regular intervals and analyzed [18]. In this study, inspired by these charts, subgroups of residuals will be created and the time evolution of their means and standard errors will be investigated using what is labelled in this study as X-bar and S control charts. As previously stated, part of the displayed sea level variability by these charts' statistics can be attributed to the thermal expansion of seawater, which is expected to increase with rising sea surface temperature in many regions as demonstrated by simulation studies [18].

A prerequisite for the analyses of the residual charts would be their randomness, i.e., Normal-like distribution of the standardized residuals shown in

Figure 2, and their statistical independence. The histogram with a Normal distribution fitting is shown in **Figure 3** and the DW test result confirms that the conditions for randomness are effectively fulfilled. The correlogram generated with 5-year lags reveals that there are no statistically significant leftover autocorrelations in the residual series (**Figure 4**).

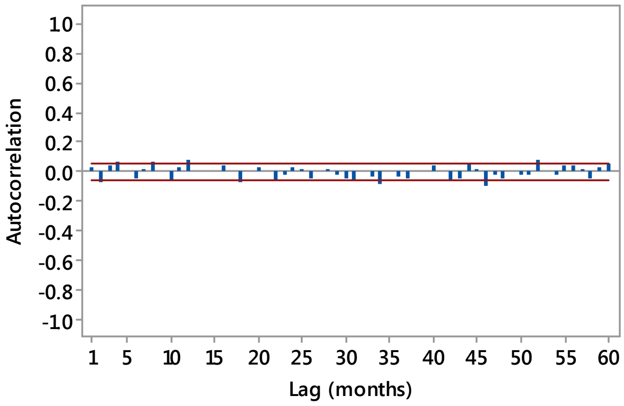

Figure 4. Correlogram of the residuals with 5% significance intervals based on 5-year lags.

At this point, X-bar and S residual charts can be constructed. **Figure 5** is the X-bar residual chart generated by the averages of 5-year subgroups standardized residuals. The time progression of the 5-year subgroup residual averages varies randomly about the zero mean of the entire standardized residuals series and reveals that the residuals are stationary in mean. But S residual chart exhibits a contiguously increasing variance in the sea level, i.e., residuals are non-stationary in variance (**Figure 6**). A simple linear regression, using the standard errors of the subgroup means as dependent variables, shows that there is a statistically significant ($\alpha = 0.05$) rate of increase of 0.009 ± 0.003 rad/year in sea level variance since 1913. For the moment, assessing the physical significance of the estimated rate increase would be challenging since this is an underresearched topic in sea level studies, which requires similar assessments at other globally distributed TG stations for clarity.

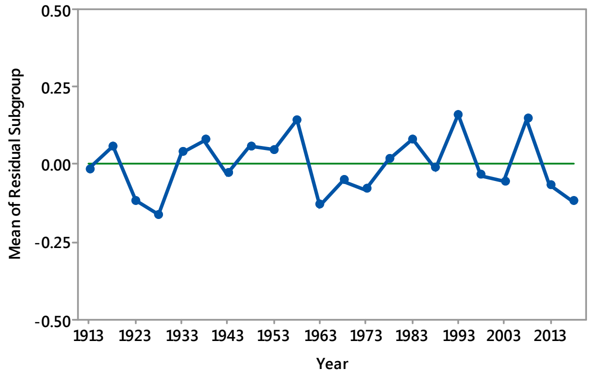

Figure 5. X-bar residual chart constructed using means of 5-year long subgroup residuals.

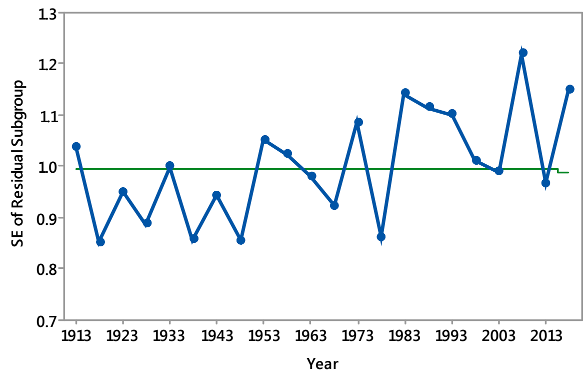

Figure 6. The S residual chart was constructed using the standard errors of 5-year long subgroups of residuals.

Meanwhile, although the trend of the S residual chart is statistically significant and visually noticeable on the graph, it is still questionable if the intensification is due to chance only, because the regression explains only Adj $R^2 = 28\%$ of the variation. To verify, one hundred monthly residual series were generated by randomly shuffling the original standardized residuals. The s residual charts were then created for each shuffled residual series and the trends of the s residual charts were estimated (**Figure 7**). Out of one hundred bootstrapped subgrouped S residual charts, only the trend of one series' S residual chart (shown in **Figure 7** with a red diamond shape) exceeded the trend of the original (shown as a red circular dot) indicating that the odds for getting the intensification of the residuals' variances of this magnitude by chance alone is about 1 out of 100.

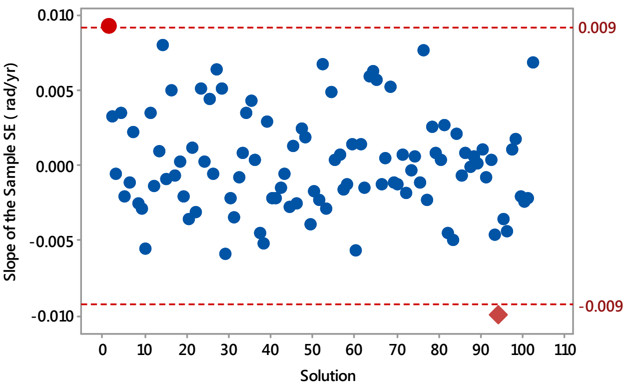

Figure 7. The S residual chart trends (rad/year) are estimated from the S residual charts of 100 randomly shuffled standardized monthly residual series. Red dot is the trend of the original series' residuals' S chart. Only one trend out of 100 bootstrapped series trends (shown with a red diamond shape) has a magnitude larger than the original trend of the *s* residual chart.

6. Conclusions

This study demonstrated the use of S residual charts to investigate random properties of sea level variations at Key West TG station. The residuals of an OLS solution to a rigorous kinematic model representing sea level anomalies revealed that random sea level fluctuations at this station are stationary, however, the variances of the random sea level changes have been steadily increasing since 1913 up to the present. Evidently, there is more to be learned about the nature of random sea level variations at globally distributed TG stations using graphical analyses of their stationary/non-stationary properties. The origin and potential ramifications of the increasing variance in sea level rise for coastal risk assessments will require further investigations.

Conflict of Interest

I declare no conflict of interest.

Funding

This research received no external funding.

Acknowledgement

I express my gratitude to the anonymous referees for dedicating their time and providing valuable comments.

References

[1] Climate Change 2001: The Scientific Basis [Internet]. IPCC [cited 2002 Sep 24]. Available from: https://www.ipcc.ch/report/ar3/wg1/

[2] Lambeck, K., 1980. Earth's variable rotation: Geophysical causes and consequences. Cambridge University Press: Cambridge. pp. 449.

[3] Pugh, D.T., 1987. Tides, surges and mean sea level. John Wiley & Sons Ltd.: Hoboken. pp. 300–330.

[4] Widlansky, M.J., Long, X., Schloesser, F., 2020. Increase in sea level variability with ocean warming associated with the nonlinear thermal expansion of seawater. Communications Earth & Environment. 1(1), 9. DOI: https://doi.org/10.1038/s43247-020-0008-8

[5] Woodworth, P.L., Melet, A., Marcos, M., et al., 2019. Forcing factors affecting sea level changes at the coast. Surveys in Geophysics. 40(6), 1351–1397. DOI: https://doi.org/10.1007/s10712-019-09531-1

[6] Bhatia, K.T., Vecchi, G.A., Knutson, T.R., et al., 2019. Recent increases in tropical cyclone intensification rates. Nature Communications. 10(1), 635. DOI: https://doi.org/10.1038/s41467-019-08471-z

[7] Emery, W.J., Emery, W.J., 2001. Data analysis methods in physical oceanography, second and revised edition. Elsevier: Amsterdam. pp. 373–374.

[8] Kendall, M., 1973. Time-series, second edition. Charles Griffin and Company Ltd.: London. pp. 70–85.

[9] İz, H.B., Ng, H.M., 2005. Are global tide gauge data stationary in variance? Marine Geodesy. 28(3), 209–217. DOI: https://doi.org/10.1080/01490410500204546

[10] Munk, W., Dzieciuch, M., Jayne, S., 2002. Millennial climate variability: Is there a tidal connection? Journal of Climate. 15(4), 370–385. DOI: https://doi.org/10.1175/1520-0442(2002)

015<0370:MCVITA>2.0.CO;2

[11] Keeling, C.D., Whorf, T.P., 1997. Possible forcing of global temperature by the oceanic tides. Proceedings of the National Academy of Sciences. 94(16), 8321–8328.
DOI: https://doi.org/10.1073/pnas.94.16.8321

[12] Yndestad, H., 2006. The influence of the lunar nodal cycle on Arctic climate. ICES Journal of Marine Science. 63(3), 401–420.
DOI: https://doi.org/10.1016/j.icesjms.2005.07.015

[13] Yndestad, H., Turrell, W.R., Ozhigin, V., 2008. Lunar nodal tide effects on variability of sea level, temperature, and salinity in the Faroe-Shetland Channel and the Barents Sea. Deep Sea Research Part I: Oceanographic Research Papers. 55(10), 1201–1217.
DOI: https://doi.org/10.1016/j.dsr.2008.06.003

[14] Iz, H.B., 2006. How do unmodeled systematic mean sea level variations affect long-term sea level trend estimates from tide gauge data? Journal of Geodesy. 80, 40–46.
DOI: https://doi.org/10.1007/s00190-006-0028-x

[15] Iz, H.B., 2018. The effect of regional sea level atmospheric pressure on sea level variations at globally distributed tide gauge stations with long records. Journal of Geodetic Science. 8(1), 55–71.
DOI: https://doi.org/10.1515/jogs-2018-0007

[16] Tide Gauge Data [Internet]. Permanent Service for Mean Sea Level (PSMSL). Available from: http://www.psmsl.org/data/obtaining/

[17] Hildreth, G., Lu, T., 1960. Demand relations with autocorrelated disturbances. Michigan State University Agricultural Experiment Station: East Lansing.

[18] Shewhart X-bar and S Control Charts [Internet]. National Institute of Standards and Technology. Available from: https://www.itl.nist.gov/div898/handbook/pmc/section3/pmc321.htm

Journal of Environmental & Earth Sciences
https://journals.bilpubgroup.com/index.php/jees

ARTICLE

Irrigation and Thermal Buffering Using Mathematical Modeling

Yara Yasser Elborolosy[*], *Harsho Sanyal, Joseph Cataldo*

The Albert Nerken School of Engineering at the Cooper Union, New York, NY 10003, US

ABSTRACT

Two methods of irrigation, drip, and sprinkler were studied to determine the response of the Javits green roof to irrigation. The control study was dry unirrigated plots. Drip irrigation consisted of irrigation tubes running through the green roof that would water the soil throughout and sprinkler irrigation used a sprinkler system to irrigate the green roof from above. In all cases, the irrigated roofs had increased the soil moisture, reduced temperatures of both the upper and lower surfaces, reduced growing medium temperatures and reduced air temperatures above the green roof relative to the unirrigated roof. The buffered temperature fluctuations were also studied via air conditioner energy consumption. There was a 28% reduction in air conditioner energy consumption and a 33% reduction in overall energy consumption between dry and irrigated plots. Values of thermal resistance or S were determined for accuracy and for this study, there was little change which is ideal. A series of infra-red and thermal probe measurements were used to determine temperatures in the air and sedum. It was determined that the sprinkler irrigation did a better job than the drip irrigation in keeping cooler temperatures within the green roof. A Mann-Whitney U test was performed to verify the variation in moisture temperatures buffering energy consumption. By getting a p-value < 0.05, it indicates that the model is accurate for prediction and medium temperatures were statistically different.

Keywords: Green roofs; Irrigation; Drip; Sprinkler; Thermal buffering

1. Introduction

Green roofs have emerged as a promising solution to address a myriad of urban environmental challenges, offering a multifaceted approach that combines sustainability and innovation [1]. Recent research has delved into novel methods and strate-

*CORRESPONDING AUTHOR:
Yara Yasser Elborolosy, The Albert Nerken School of Engineering at the Cooper Union, New York, NY 10003, US; Email: yaraelborolosy7392@gmail.com

ARTICLE INFO
Received: 13 September 2023 | Revised: 22 December 2023 | Accepted: 25 December 2023 | Published Online: 27 January 2024
DOI: https://doi.org/10.30564/jees.v6i1.5959

CITATION
Elborolosy, Y.Y., Sanyal, H., Cataldo, J., 2024. Irrigation and Thermal Buffering Using Mathematical Modeling. Journal of Environmental & Earth Sciences. 6(1): 19–32. DOI: https://doi.org/10.30564/jees.v6i1.5959

gies to enhance the performance and sustainability of green roofs, shedding light on their potential to transform urban landscapes into more eco-friendly and resilient environments. The materials and hydrological performance of green roofs have become focal points of investigation. Zhang and Chen [2] conducted a comprehensive review, emphasizing the significance of the materials used and their hydrological attributes. Such insights are essential for understanding the environmental benefits associated with green roofs. Furthermore, Wang, Guo, and Cao [3] provided an expansive review that underscores the role of green roofs in improving the urban environment. Their research encompasses various environmental aspects, making it highly pertinent to discussions on the potential advantages and drawbacks of this technology. These insights are essential for understanding the benefits of having green roofs. It was determined that green roofs significantly reduce indoor temperatures during hot summer months [4]. They act as an insulating layer, reducing the transfer of heat from the external environment to the interior of the building. This effect contributes to a more comfortable living environment and can result in decreased energy consumption for air conditioning [3,5].

Sustainable development is a key consideration, and Liu, Liu, and Cao [6] delve into the long-term viability of green roofs. Their research outlines the crucial factors contributing to the sustainable growth of this technology, elucidating its prospects for the future. Urban stormwater management is another pressing concern that green roofs can address. Bass and Lee [7] offer valuable insights into their potential in this context, highlighting the role of green roofs in managing and mitigating urban stormwater runoff. The thermal performance of green roofs is also a subject of interest, particularly in diverse climatic conditions. Wu, Huang, and Zhang [8] have explored how green roofs influence heat transfer and thermal comfort in varying climates. Their findings offer practical data that can guide the effective implementation of green roofs in different environmental contexts.

The use of green roofs has the disadvantage of constant irrigation. In contrast, this technology contributes to the cleaning of rainwater, reducing pollution, lowering carbon emissions, improving the thermal and acoustic comfort, and lowering the temperature of external environment [9]. A field size of about 0.25 m, with robust balances, a sensitivity of about 1–2 g, and a maximum weight load of 60 kg was measured by lysimeters [10]. These lysimeters were suitable for measuring various types of green roofs and could be used to measure light rain events as well as the dew on the vegetation in the morning hours. It was found that the irrigation system should be stopped 3 days before a rain event so the potential water capacity in the soil GR is high. Dry summer irrigation reduces temperature by up to 5 °C and on the vegetation layer by up to 10 °C [10].

Thermal regulation GR affects vegetation and irrigation by less than 25% of the potential ET is applied as limited irrigation lowers heat flux [11]. Plant diffusion increased the thermal insulation capacity. Water limited irrigation treatment was shown to increase thermal insulation capacity when compared to complete well-watered irrigation, suggesting that the air/water substrate has a greater effect on insulation than ET. Height, LAT and transpiration notes should be considered [12]. GR thermal insulation modeling (experiment) selection of plant species may be important. Heat reduction by evaporative cooling from GR (extensive) was explored by J. Heusinger et al. [13] by applying irrigation in different climate zones. There were three irrigation models: 1) no irrigation, 2) sustainable irrigation by harvested runoff, and 3) unrestricted irrigation. These models were used to study heat reduction potential in terms of surface energy partitioning and sensible heat flux and compare white roofs. Green roofs compared to black roofs reduced excess heat by 15–51% with sustainable irrigation by 48–75% unrestricted irrigation but dropped 3% unirrigated [13]. T. Sun et al. [14] confirm that the medium layer depth affects heat and moisture transport significantly. They found a deeper layer to redistribute more water into the bottom section, thus limiting surface evaporation, while a thin layer does not store enough water, dries up fast, and decreases performance. Therefore, an optimal layer thickness exists somewhere in the middle. The different irrigation scenarios are then investigated, given a fixed medium layer depth. Higher irrigation control limits (i.e., soil moisture at which irrigation is initiated) enhance the thermal performance of green roofs, but this enhancement plateaus at high limits [14,15]. Using a low-speed wind tunnel and the plant's transpiration, the thermal performance of the green roof was evaluated in the controlled weather conditions [16]. Green roof samples with two types of plants were tested. The results showed that plants' evapotranspiration represents about 13% of the thermal resistance for ryegrass and about 27.7% of the thermal resistance for periwinkle. Greywater was about 30% lower in temperature than those irrigated with clean water shown by their thermal performance for green roof irrigation [16]. From the top surface of the soil to the ceiling inside the chamber, temperature profiles were measured across the section of each roof. A comparison of the two shading strategies demonstrated that while the mesh provided more cooling over a daily cycle, the daytime cooling potential, which is crucial in a desert climate, was higher with lightweight gravel [16].

In a study in a green roof module [17] five commercial substrate types or systems were subjected to three irrigation methods (overhead, drip, and sub-irrigation) to determine substrate water distribution and retention. Substrates subjected to overhead irrigation or those with a moisture retention fabric (MRF) retained the greatest amount of water. Sub-irrigation resulted in the least amount of water retention and the most wastewater, except when an MRF was present. Substrate volumetric moisture content exhibited similar results. The MRF was effective in retaining water, but for sub-irrigation a visible waterfront was not visible as water did not reach the surface via capillary action [17]. Differences can be attributed to the fact that overhead irrigation distributed water over 100% of the area, whereas in many cases the waterfront radiating from the drip or sub emitters never merged leaving dry areas In between emitters [18]. Results show that overhead was the most favorable for plant growth and health [19]. Since green roof substrates tend to be coarse to allow adequate drainage, water does not move laterally to a great extent as it would in finer substrates. For this reason, drip and sub-irrigation may not be the most efficient irrigation methods [17].

C. Van Mechelen et al. [20] concluded overhead irrigation may be a better choice, as it distributes water more uniformly and leads to higher substrate water holding capacity (WHC), less runoff, and better plant growth and health compared to drip irrigation. Another strategy to adapt to the irrigation requirement is by optimal design of green roof materials, such as developing green roof substrates with higher WHC [21]. The addition of sandy loam soil and the use of amended soils (i.e., a mix of red gravel, vermiculite and bark compost), perlite-based substrates, foam sheets and fiberglass can all improve the WHC of the green roof system. Some water-holding additives, like hydrophilic gels, are also currently being explored [21]. A second way to conserve water is by finding alternative irrigation sources. For example, gray water, which is the wastewater from in and around the house (including bathroom sinks, showers and washing machines, but excluding water originating from toilet flushing, dishwashers, and kitchen sinks), could be reused for irrigation purposes [20]. Another possibility is rainwater harvesting in which runoff is collected and stored. Runoff harvested from green roofs themselves has been shown to be sufficiently clean enough to be reused for urban irrigation. In the third category, irrigation quantity can be minimized through monitoring and control of irrigation regimes [22]. Meteorological factors, mainly relative humidity and number of sunshine hours as they affect water consumption the most, are important to consider for green roof irrigation systems. Otherwise, irrigation should be turned on when the substrate moisture drops below a specified level, such as the stress point, which is the point when the transition between readily available water in the substrates larger pores and less available water in the small pores occurs). Irrigation can be controlled using a smart controller, which turns on when necessary (at night or when soil moisture drops below the stress point) but deactivated when rainfall is registered [23].

During the establishment phase and the first growing season throughout summer, it is advised to use irrigation on all green roof types and climates. Afterwards, irrigation is only necessary on extensive green roofs in arid climates and temperate climates with dry periods [24]. In this study on Javits Convention green roof, two methods of irrigation were studied: overhead sprinklers, and dry irrigation (half inch tubes with small holes every 18 inches). There were two sets of roof plots, one being wet irrigation and the second with no irrigation. Both plots were monitored with temperature and humidity probes. The intake air temperatures on four RTUs were also determined. The ceiling temperatures were also measured under the dry and wet plots. The energy consumed by the conference center was determined for the irrigation activities and the savings in cost.

A mathematical model is presented to compare the results of thermal buffering to a 2018 model using the error function [25]. There was a good correlation found between these two models. Eumorfopoulou and Aravanteuos [26] calculation has been completed, using the stationary method to determine the thermal behavior of the planted roof and the way it influences the thermal protection of buildings in accordance with Greek climate conditions. They reduce solar radiation, daily thermal variations, and annual thermal fluctuations. This was also more recently verified by Wei and Jim [9].

This paper aims to contribute to the ongoing discourse on green roofs by exploring the impacts of different irrigation methods, with a specific focus on overhead sprinklers and dry irrigation, on the Javits Convention green roof. The study will assess the resulting effects on temperature, humidity, and energy consumption within the conference center, providing valuable insights into the benefits and challenges of these irrigation methods. As we advance our understanding of green roofs through recent research, we can harness their potential to create more sustainable and environmentally resilient urban landscapes. By integrating the latest findings into our study, we can make informed decisions that contribute to a greener, more sustainable future.

2. Methods

The JGR is an extensive green roof, and the key components are provided in Alvizuri [27]. A portable infrared camera was used to image the interior and exterior of the roof. The Javits Center green roof layer consists of several layers: the top vegetation layer, vegetation mat, growing medium, water retention mat, and drainage layer. Below the green roof, the structure segment of the roof is positioned, such as bitumen, concrete, thermal insulation, and steel beam. The soil probes were calibrated in the same soil as the Javits roof under the sedum. The moisture was determined to have increased from 0.1 to 0.85 content by mass using a gravimetric water content test. The thermal resistance for the green roof was determined using published values. The thermal resistance R equals 0.017 m^2k/w and the thermal transmissivity U equals 9.837 w/m^2k. The value of R and U for the Javits roof from the sedum mat the metal deck was 2.65 m^2k/w and 0.377 w/m^2k [27]. Although typical volumetric moisture content found in green roofs can vary for the range of R found on the Javits roof, the volumetric moisture content on the Javits roof has little change [28]. See Alvizuri [27] for the relationship between the diffusivity and U. Variation of temperature distribution through the green and structural Javits roof with a temperature of 29 °C was determined from the mathematical model [9].

The air temperatures were reported at six locations on a four-foot-high rectangular rack. See the experimental section for descriptions of the measuring equipment [29]. There was no temperature gradient difference observed between the two irrigation plots. The drip and sprinkler irrigation schedule is shown in **Figure 1** [29]. The dry temperatures were over 20 degrees higher than the wet plots. **Figure 1** [29] shows the location of the dry and wet plots and equipment locations used to measure moisture, humidity, air and soil temperatures, and AMPS in the RTU intake.

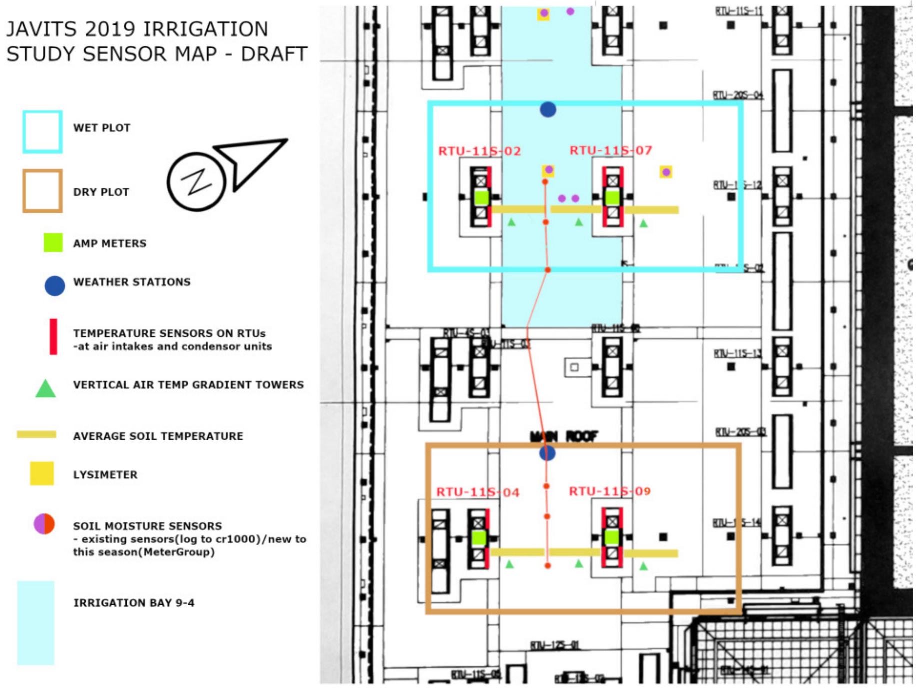

Figure 1. Layout of monitoring plan.

3. Results

A graph of the error function mathematical model is shown in Alvizuri [27] for three different roof temperatures. The moisture content of the irrigated plots was always higher than the dry plots (S4, S2). There was little change in the moisture for the air temperature during the survey. The values of the air temperature and relative humidity measured on the weather station are given in the experimental section.

From **Figure 2** it can be determined that there are higher values of the available kW per unit for 8/14 through 8/16. The occupancy status of S2 and S4 differed significantly over the study period. S4 also shows some operational challenges during the monitoring period. Operation of S7 and S9 were comparable during the monitoring with the occupancy differing only on one day during the study period.

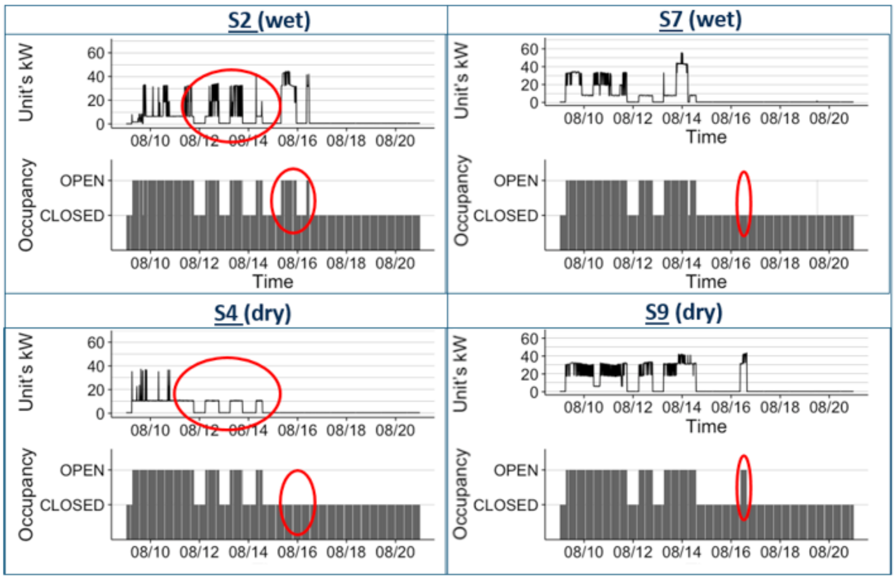

Figure 2. kW consumed and occupancy status.

There is also a 33% reduction in energy consumed between the two units (but the same irrigation activity benefits multiple units) shown in **Figure 3** (S7 is wet, S9 is dry).

There was no gradient observed between two different unirrigated plots. The thermal resistance R in $\frac{m^2k}{w}$ and thermal transmittance U in $\frac{w}{m^2k}$ was calculated for the five layers of green and six layers of structural roof for the JGR. The table of values for R is given in **Table 1**.

For the five layers of the green roof system, R is 0.108 and U is 9.837. These values were used to determine the value of the thermal conductivity α in Equation (1) [27].

$$\alpha = \frac{k}{\rho C_p} \tag{1}$$

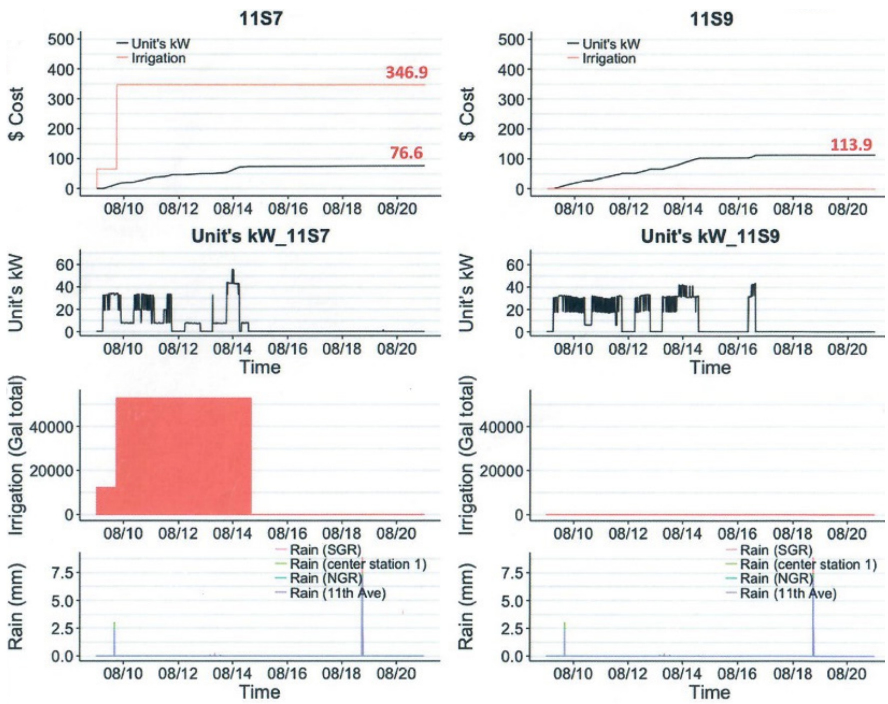

Figure 3. Comparison between S7 and S9.

Table 1. R values for Javits roof.

Item	d (m)	K (w/mk)	R
Sedum mat	0.019	0.5	0.0038
Soil	0.0119	1.16	0.01026
Fleece	0.014	0.5	0.028
Drain mat	0.0127	0.5	0.0254
Base felt	0.0093	0.07	0.133
Vermiculite aggregate	0.036	0.094	0.383
Polystyrene foam	0.0762	0.045	1.693
Insulated concrete	0.0085	0.2	0.0425
Asphalt membrane	0.0127	0.75	0.0169
Recovery board	0.0127	0.045	0.282
Metal deck	0.0068	54	0.000126
		Sum R	2.653
		U	0.377

where:

k = thermal conductivity

ρ = density

C_p = specific heat capacity

The α values were used to determine the temperature variation in the green roof for each layer in the error function equation and are given in **Figure 4** with the upper layer of the green roof showing a sharp drop in temperature from the surface of the roof to the ceiling of the convention center.

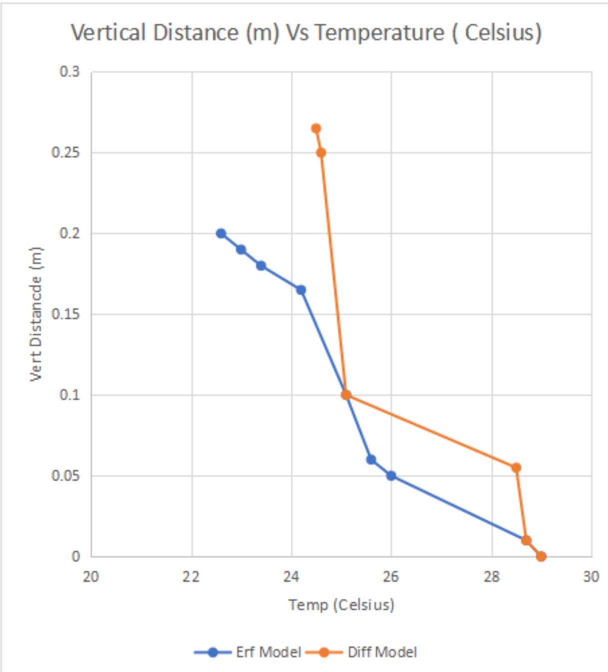

Figure 4. Vertical distance vs temperature.

Variation of temperature distribution through the green and structural Javits roof with the roof temperature of 29 °C was determined from the mathematical model [9]. There are only a few computer simulations in the literature to which the results of a simulation given in J. Alvizuri et al. [27,29] to determine values of the temperature variation through a green roof and calculations of R and α as shown in **Table 1**. These values have been used in the determination of ET for the roof and the calculation of the Penman-Monteith equation for the water balance. The ET for the water balance is less than three percent of the storage and precipitation.

Infrared photos of the north and south roofs and ceilings are shown in J. Alvizuri et al. [27] before the sedum was installed on the south roof. The average temperature of the south roof was 16.5 °C higher with the ceiling temperature 12.1 °C higher than the North roof. When the sedum was installed on the south roof, the difference in the roof and ceiling temperature was within experimental error. The temperature of the ceiling under wet plots is consistently lower than under dry plots.

One experimental study took place at the Cooper Union and involved the construction of a two-part model roof: half of this area was a non-vegetated control section, and the other half was coated with geomembrane, soil, and sod, to simulate a green roof. To act as a source of simulated rainfall, a 4' × 4' grid of PVC pipes was built and placed above the roof model. The roof model is on a 2% slope, with holes at the bottom for runoff collection. A uniform level of precipitation was applied to both roofs over five trials. Reference John Alvizuri et al. [27] has a view of the lab model, showing the overhead rain maker.

5. Discussion

The error function mathematical model [9] was used to simulate 53 pairs of internal surface temperatures. On average, the model predictions were within 3% of the measured values. This validation indicates that the error function mathematical model is very accurate at predicting the ceiling temperatures of this green roof and the temperature heat diffusion profile through the layers of the structure. From the results from Alvizuri [27], the differential model can be used with similar results of accuracy.

Equation (2) was used to compare the results to the results [29]:

$$\frac{d^2T}{dx^2} = 0 \tag{2}$$

where T is temperature and x is vertical distance (Holman, 1981). Solving the differential equation gives the relationship between temperature and distance is linear as following Equation (3):

$$T = Cx + vw\ D \tag{3}$$

where C and D are both constants. Since only how much temperature is changed by each layer is of interest, only the constant C will be discussed further.

Among several data sets, one of the planted roofs with medium-high vegetation with thermal insulation is selected, because its setting is similar to the Javits Center. The thermal behaviors of green roofs of many buildings in Greece [26] are analyzed by measuring temperatures at different layers throughout the green roof. It gives data on how temperature gets affected by each layer. Also, only summer data is selected, because the project is concentrated on the green roof's cooling impact on the building. From the data given, the slope of temperature through each layer is calculated, with the unit of °C/m. All the slopes come out to be negative, meaning the temperature cools throughout the depth of the green roof. **Table 2** summarizes the results.

Table 2. Temperature gradient slopes through each layer of the Greek building.

Layer	Temperature Slope (°C/m)
Soil	–1.67
Drainage	–4
Membrane protection against the roots	0
Bitumen membrane	–33.3
Perlite-concrete	–10
Foam expanded polystyrene	–75
Reinforced concrete slab	–0.67
Roof plaster	–6.67

The two mathematical models are shown in a graph (**Figure 4**). There is a close comparison between these models. Van Woert et al. [19] ran tests on three roof models at a slope of 2% and found that vegetative roofs retained 66.6% rainfall; media roofs retained 50% rainfall and the gravel ballast roof retained 27.2% rainfall.

Figure 5 shows plots taken with the air temperature ranging from 26 °C to 48 °C on August 19 by the IR camera.

The sedum data indicates that on this day, the S7 plot is over 14 °C higher than the wet plots at 13:00 and between 15:00 and 16:00 hours. This leads to an indoor ceiling difference of about 4 °C at 13:00. The wet sedum plots consistently have roof sedum temperature with higher dry readings greater than 10–15 °C and indoor ceiling temperature of 3–4 °C compared to the dry plots. Similar variations were determined for S6 and S9 plots. These temperature reductions were recorded using the sprinkler irrigation. There was a similar temperature reduction using drip irrigation with sedum roof having a temperature on the dry sedum of 5–10 °C higher than the wet and 2–3 °C plots higher on the dry ceiling temperature. These values were repeated for different days (August 9 and 12) showing similar temperature reductions due to irrigation. The sprinkler always reduces the temperature more than the drip irrigation (**Figure 6**).

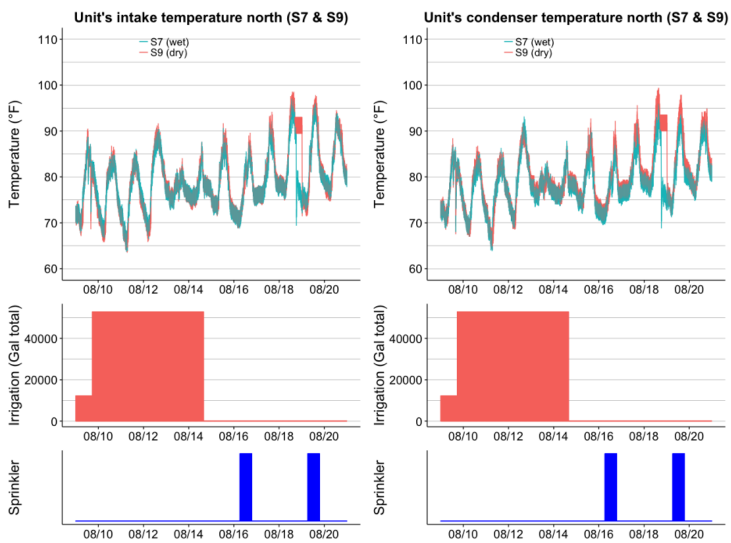

Figure 5. Air temperature above the green roof.

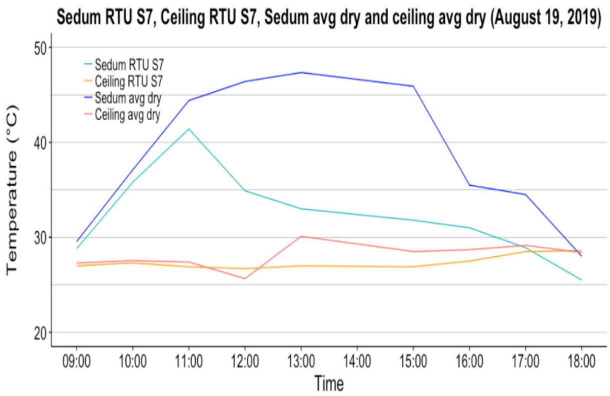

Figure 6. Comparison of drip to sprinkler irrigation.

In **Figure 7**, the temperature variation over a ten-day period (August 10 to 20) on the top and bottom of the sedum is shown for plots S2 (irrigated) and S4 (unirrigated). From August 10 to August 14, drip irrigation on 8/16 and 8/20 sprinkler irrigation was conducted. The difference in the wet versus dry for drip irrigation for the top sedum was less than 6 °C and for the sprinkler was over 17 °C. The bottom of the sedum in **Figure 7** had values for a drip irrigation 3 °F lower and a maximum 7 °F lower for sprinkler irrigation. The max temperature variation for the bottom of the sedum for both drip and sprinkler irrigation varied from 5 to 17 °C lower than the top of the sedum.

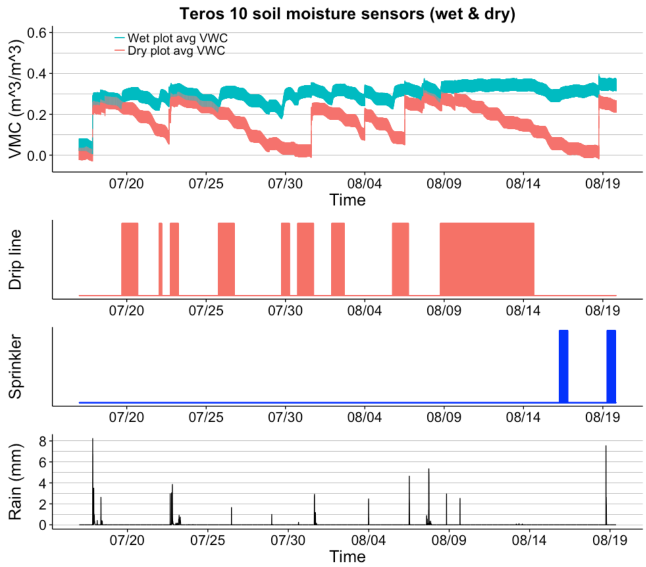

Figure 7. Comparison of the ceiling temperatures.

Table 3 summarizes the Mann-Whitney U tests' results to determine if there were statistically significant differences in the median of the sedum temperatures at the top and bottom in each region and between irrigated and non-irrigated regions. Instances, where the p-value is less than 0.05, indicate that median temperatures were statistically different [30]. The U test proves that p-values less than 0.05 indicate that the model is accurate in its predictions. In each region, the median temperatures at the top

Table 3. Results of Whitney Mann U test at top and bottom of sedum.

Hypothesis	Drip Line Period (Daytime)	Drip Line Period (Nighttime)	Sprinkler Period (Daytime)	Sprinkler Period (Nighttime)
Temperature at the top and bottom of sedum in	P-value			
Irrigated	Not similar (< 0.001)	Not similar (< 0.001)	Similar (0.087)	Not similar (< 0.001)
Non-irrigated	Not similar (< 0.001)	Not similar (< 0.001)	Not similar (< 0.001)	Not similar (< 0.001)
Non-irrigated	-	-	Not similar (< 0.001)	Not similar (< 0.001)
Temperature at the top of sedum between	P-value			
Irrigated and non-irrigated	Not similar (0.001)	Similar (0.756)	Not similar (< 0.001)	Not similar (< 0.001)
Irrigated and non-irrigated	-	-	Not similar (< 0.033)	Not similar (0.015)
Temperature at the bottom of sedum between	P-value			
Irrigated and non-irrigated	Not similar (< 0.001)	Not similar (< 0.001)	Not similar (< 0.001)	Not similar (< 0.001)
Irrigated and non-irrigated	-	-	Not similar (0.007)	Similar (0.173)

and bottom of the sedum were significantly different (**Table 3**) except for S1 during the sprinkler daytime period. A greater degree of variability was also observed at the top (**Figure 7**) and could be attributable that sedum itself effectively buffers temperature fluctuations.

The comparison of irrigated and non-irrigated plots suggested median temperatures were statistically significantly different, with only two exceptions: the comparisons of temperatures at the top of sedum between drip line nighttime, and at the bottom of sedum between sprinkler nighttime. This indicates that the sedum buffers temperature fluctuations.

Table 4 summarizes the results of Mann-Whitney U tests which determine the significance of the differences in the median of the ambient air temperatures between irrigated and non-irrigated regions. Instances where median temperatures were statistically different were drip line daytime for the entire tower (top, middle, and bottom) during sprinkler daytime for the entire tower and during sprinkler nighttime at the top and bottom of the tower.

The difference in maximum condenser temperature for irrigated and non-irrigated during drip line daytime ranged from –1.2 to 21 °C whereas the sprinkler period daytime ranged from 2.3 to 5.2 °C. The Mann-Whitney U test suggested condenser temperatures were statistically significant during the sprinkler daytime and sprinkler nighttime [30,31]. The U test results for intake and condenser temperatures between irrigated and non-irrigated plots are given in **Table 3**.

A comparison of the ceiling temperature under irrigated and non-irrigated was completed. The fluctuation in the ceiling temperatures under both irrigated and non-irrigated plots displays similar patterns. The temperature of the ceiling was significantly different and consistently lower. The maximum temperature during the drip line daytime was 29 °C and 30 °C for the irrigated and non-irrigated plots, respectively. The difference in maximum ceiling temperature during drip line daytime ranged from 0.6 to 1 °C and for the sprinkler period daytime ranged from 1 to 1.7 °C.

6. Conclusions

The differential function equation is compared to the error function curve showing a close correlation to the two different methods. Since water can either travel through some layers without any hindrance, such as the drainage layer, or cannot penetrate at all into a layer, such as the structure portion of roof, hy-

Table 4. Results of Whitney Mann U test at the top of the tower.

Hypothesis	Drip Line (Daytime)	Drip Line (Nighttime)	Sprinkler (Daytime)	Sprinkler (Nighttime)
Temperature at the top of tower in	P-value			
Irrigated S1 and non-irrigated S4 are	Similar (0.147)	Similar (0.270)	Not similar (< 0.001)	Not similar (< 0.003)
Irrigated S2 and non-irrigated S5 are	Not similar (0.003)	Similar (0.123)	Not similar (< 0.001)	Not similar (< 0.001)
Irrigated S3 and non-irrigated S6 are	-	-	Similar (0.958)	Similar (< 0.059)
Temperature at the middle of tower in	P-value			
Irrigated S1 and non-irrigated S4 are	Similar (0.712)	Similar (0.234)	Not similar (< 0.001)	Similar (0.860)
Irrigated S2 and non-irrigated S5 are	Not similar (0.024)	Similar (0.140)	-	-
Irrigated S3 and non-irrigated S6 are	-	-	-	-
Temperature at the bottom of tower in	P-value			
Irrigated S1 and non-irrigated S4 are	Similar (0.103)	Similar (0.234)	Not similar (< 0.001)	Similar (0.860)
Irrigated S2 and non-irrigated S5 are	Not similar (0.025)	Similar (0.898)	-	-
Irrigated S3 and non-irrigated S6 are	-	-	Similar (0.658)	Similar (0.463)

draulic parameters of such layers are not acquirable. In this case, heat transfer theory has been used to predict the temperature gradient [32]. There is no heat generation source within each layer, the temperature gradient in only one direction, vertical direction, is of interest, and steady state is chosen to be analyzed; therefore, the heat transfer equation of steady-state one-dimensional heat flow with no heat generation is used.

Figure 1 shows the layout of the drop and sprinkler irrigation and the layout of the Javits 2019 roof. **Figure 2** shows that there are higher values of the available kW per unit for 8/14 through 8/16. There is also a 33% reduction in energy consumed between the two units (but the same irrigation activity benefits multiple units) shown in **Figure 3** (S7 is wet, S9 is dry). The α values were used to determine the temperature variation in the green roof for each layer in the error function equation and are given in **Figure 4** with the upper layer of the green roof showing a sharp drop in temperature from the surface of the roof to the ceiling of the convention center. **Figure 5** shows plots taken with the air temperature ranging from 26 °C to 48 °C on August 19 by the IR camera. **Figure 6** shows the sprinkler always reduces the temperature more than the drop irrigation. A comparison of the ceiling temperature is shown in **Figure 7** for plots S2 and S4 from August 10 to August 20, 2019. The maximum temperature for the dry plot was 86°F and the wet plot was 84°F. The fluctuations in the ceiling temperatures under both plots display the same patterns. The wet plots' ceiling temperature is consistently lower than under the dry plots. Sedum effectively buffers temperature fluctuations. These temperatures were measured with the probes.

The results in **Table 2** compare favorably with Abualfaraj [29]. A different mathematical model was used to compare the results to the error function model in Abualfaraj [29] with interesting results. By using a different temperature model approach compared to Abualfaraj [29] and the effects of irrigation the following benefits of a green roof were determined:

- Increased the moisture content.
- Reduced the growing media temperature.
- Reduced the temperature of its upper and lower surfaces.
- Reduce the air temperature just above it.
- Reduce the ceiling temperature under the irrigated roof plots.

Over a 10-day test, these differences amounted to a 28% reduction in air conditioner energy consumption and there was a 33% reduction in energy consumption between dry and wet plot intakes. The Mann-Whitney U test was used to verify the conclusions of the variation in moisture, temperature buffering and energy consumption with values of $p < 0.05$. An error function mathematical model was used to determine the behavior of the thermal buffering of the JGR. This model was used to predict 53 pairs of internal temperatures [27]. This model has a close comparison to the differential equation model. The differential function is compared to the error function curve showing a close correlation to the two different methods. By using irrigated green roofs, the effects of climate change can be adapted to and even mitigated. Irrigation activities were effective at keeping the growing medium moist during the dry periods with a better than 3% accuracy. The soil moisture increasing in response to precipitation was elevated in the green roof due to irrigation and increased the roof's ability to become a thermal buffer. In addition, green roofs help mitigate storms, reduce energy use by buildings, mitigate the heat island effect, establish habitats for birds and bees, and increase water and air quality. By continuing to implement green roofs with sprinkler irrigation, we will be able to reap the full benefits of green roofs as we continue to adapt to the changing climate.

7. Limitations

The use of green roofs has the disadvantage of constant irrigation. The lysimeters were only suitable for measuring various types of green roofs and were used to measure light rain events as well as the dew on the vegetation in the morning hours. The irrigation system should be stopped 3 days before a rain event so the potential water capacity in the soil green roof is high. The limited irrigation to lower heat flux is less than 25% of the potential ET. Height, LAT and transpiration should be considered. Plant species are important to the irrigation of green roofs. The climate should also be considered in the design of green roofs. Limiting surface evaporation does store enough water, dries fast, and decreases performance. The enhancement is high to limit irrigation. Daytime cooling was high and provided more cooling during the day with light-weight gravel.

Author Contributions

In this study, the author contributions were as follows:

Harsho Sanyal: Conceived and designed the research, collected, and organized research data, conducted data analysis, and wrote the manuscript.

Yara Elborolosy: Contributed to data analysis, contributed to manuscript writing, and reviewed the manuscript.

Joseph Cataldo: Contributed to the study design, data analysis, and provided critical revisions to the manuscript.

All authors reviewed and approved the final version of the manuscript.

Conflict of Interest

The authors declare that they have no conflicts of interest related to this research. This research received no specific grant from any funding agency in the public, commercial, or nonprofit sectors. The authors have no financial interests or relationships that could be perceived as influencing the research presented in this paper.

References

[1] Jamei, E., Chau, H.W., Seyedmahmoudian, M., et al., 2023. Green roof and energy—role of climate and design elements in hot and temperate climates. Heliyon. 9, e15917.
DOI: https://doi.org/10.1016/j.heliyon.2023.e15917

[2] Wani, S., Selvaraj, T., Faria, P., et al., 2023. Study on ancient green materials and technology used in Udaipur palace, India: An input to abate climate changes in modern construction. Environmental Science and Pollution Research. 30, 93952–93969.
DOI: https://doi.org/10.1007/s11356-023-28785-2

[3] Wang, J., Garg, A., Huang, S., et al., 2022. An experimental and numerical investigation of the mechanism of improving the rainwater retention of green roofs with layered soil. Environmental Science and Pollution Research. 29, 10482–10494.
DOI: https://doi.org/10.1007/s11356-021-16369-x

[4] Richter, M., Dickhaut, W., 2023. Long-term performance of blue-green roof systems—Results of a building-scale monitoring study in Hamburg, Germany. Water. 15(15), 2806.
DOI: https://doi.org/10.3390/w15152806

[5] Bollman, M.A., DeSantis, G.E., Waschmann, R.S., et al., 2021. Effects of shading and composition on green roof media temperature and moisture. Journal of Environmental Management. 281, 111882.
DOI: https://doi.org/10.1016/j.jenvman.2020.111882

[6] Mihalakakou, G., Souliotis, M., Papadaki, M., et al., 2023. Green roofs as a nature-based solution for improving urban sustainability: Progress and perspectives. Renewable and Sustainable Energy Reviews. 180, 113306.
DOI: https://doi.org/10.1016/j.rser.2023.113306

[7] Raimondi, A., Becciu, G., 2021. Performance of green roofs for rainwater control. Water Resources Management. 35, 99–111.
DOI: https://doi.org/10.1007/s11269-020-02712-3

[8] Lokesh, S., Kadiwal, N., Chandrashekar, R., et

al., 2023. Heat transfer study of green roof in warm and humid climatic conditions. Materials Today: Proceedings. 92, 327–337.
DOI: https://doi.org/10.1016/j.matpr.2023.05.010

[9] Wei, T., Jim, C.Y., Chen, Y., et al., 2022. Complementary influence of green-roof and roof-slab thermal conductivity on winter indoor warming assessed by finite element analysis. Energy Reports. 8, 14852–14864.
DOI: https://doi.org/10.1016/j.egyr.2022.11.019

[10] Kaiser, D., Köhler, M., Schmidt, M., et al., 2019. Increasing evapotranspiration on extensive green roofs by changing substrate depths, construction, and additional irrigation. Buildings. 9(7), 173.
DOI: https://doi.org/10.3390/buildings9070173

[11] Azeñas, V., Cuxart, J., Picos, R., et al., 2018. Thermal regulation capacity of a green roof system in the mediterranean region: The effects of vegetation and irrigation level. Energy and Buildings. 164, 226–238.
DOI: https://doi.org/10.1016/j.enbuild.2018.01.010

[12] Shahmohammad, M., Hosseinzadeh, M., Dvorak, B., et al., 2022. Sustainable green roofs: A comprehensive review of influential factors. Environmental Science and Pollution Research. 29, 78228–78254.
DOI: https://doi.org/10.1007/s11356-022-23405-x

[13] Heusinger, J., Sailor, D.J., Weber, S., 2018. Modeling the reduction of urban excess heat by green roofs with respect to different irrigation scenarios. Building and Environment. 131, 174–183.
DOI: https://doi.org/10.1016/j.buildenv.2018.01.003

[14] Sun, T., Bou-Zeid, E., Ni, G.H., 2014. To irrigate or not to irrigate: Analysis of green roof performance via a vertically-resolved hygrothermal model. Building and Environment. 73, 127–137.
DOI: https://doi.org/10.1016/j.buildenv.2013.12.004

[15] Xiong, S., 2020. Study on the reverse heat conduction behavior of steel. Open Journal of Safety Science and Technology. 10(1), 24–31.
DOI: https://doi.org/10.4236/ojsst.2020.101002

[16] Jaffal, I., Ouldboukhitine, S.E., Belarbi, R., 2012. A comprehensive study of the impact of green roofs on building energy performance. Renewable Energy. 43, 157–164.
DOI: https://doi.org/10.1016/j.renene.2011.12.004

[17] Rowe, D.B., Kolp, M.R., Greer, S.E., et al., 2014. Comparison of irrigation efficiency and plant health of overhead, drip, and sub-irrigation for extensive green roofs. Ecological Engineering. 64, 306–313.
DOI: https://doi.org/10.1016/j.ecoleng.2013.12.052

[18] Vandegrift, D.A., Rowe, D.B., Cregg, B.M., et al., 2019. Effect of substrate depth on plant community development on a Michigan green roof. Ecological Engineering. 138, 264–273.
DOI: https://doi.org/10.1016/j.ecoleng.2019.07.032

[19] VanWoert, N.D., Rowe, D.B., Andresen, J.A., et al., 2005. Green roof stormwater retention: Effects of roof surface, slope, and media depth. Journal of Environmental Quality. 34(3), 1036–1044.
DOI: https://doi.org/10.2134/jeq2004.0364

[20] Vanuytrecht, E., Van Mechelen, C., Van Meerbeek, K., et al., 2014. Runoff and vegetation stress of green roofs under different climate change scenarios. Landscape and Urban Planning. 122, 68–77.
DOI: https://doi.org/10.1016/j.landurbplan.2013.11.001

[21] Shetty, N.H., Elliott, R.M., Wang, M., et al., 2022. Comparing the hydrological performance of an irrigated native vegetation green roof with a conventional Sedum spp. green roof in New York City. PLoS One. 17(4), e0266593.

DOI: https://doi.org/10.1371/journal.pone.0266593

[22] Zheng, X., Sarwar, A., Islam, F., et al., 2023. Rainwater harvesting for agriculture development using multi-influence factor and fuzzy overlay techniques. Environmental Research. 238, 117189.
DOI: https://doi.org/10.1016/j.envres.2023.117189

[23] Jain, R.K., 2023. Experimental performance of smart IoT-enabled drip irrigation system using and controlled through web-based applications. Smart Agricultural Technology. 4, 100215.
DOI: https://doi.org/10.1016/j.atech.2023.100215

[24] Zhang, H., Lu, S., Fan, X., et al., 2021. Is sustainable extensive green roof realizable without irrigation in a temperate monsoonal climate? A case study in Beijing. Science of the Total Environment. 753, 142067.
DOI: https://doi.org/10.1016/j.scitotenv.2020.142067

[25] Xie, P., Barbarossa, V., Erisman, J.W., et al., 2024. A modeling framework to assess the crop production potential of green roofs. Science of the Total Environment. 907, 168051.
DOI: https://doi.org/10.1016/j.scitotenv.2023.168051

[26] Eumorfopoulou, E., Aravantinos, D., 1998. The contribution of a planted roof to the thermal protection of buildings in Greece. Energy and Buildings. 27(1), 29–36.
DOI: https://doi.org/10.1016/S0378-7788(97)00023-6

[27] Alvizuri, J., Cataldo, J., Smalls-Mantey, L.A., et al., 2017. Green roof thermal buffering: Insights derived from fixed and portable monitoring equipment. Energy and Buildings. 151, 455–468.
DOI: https://doi.org/10.1016/j.enbuild.2017.06.020

[28] Sailor, D.J., Hagos, M., 2011. An updated and expanded set of thermal property data for green roof growing media. Energy and Buildings. 43(9), 2298–2303.
DOI: https://doi.org/10.1016/j.enbuild.2011.05.014

[29] Abualfaraj, N., Cataldo, J., Elborolosy, Y., et al., 2018. Monitoring and modeling the long-term rainfall-runoff response of the Jacob K. Javits center green roof. Water. 10(11), 1494.
DOI: https://doi.org/10.3390/w10111494

[30] Dehaene, H., De Neve, J., Rosseel, Y., 2021. A Wilcoxon-Mann-Whitney test for latent variables. Frontiers in Psychology. 12, 754898.
DOI: https://doi.org/10.3389/fpsyg.2021.754898

[31] Hart, A., 2001. Mann-Whitney test is not just a test of medians: Differences in spread can be important. BMJ. 323(7309), 391–393.
DOI: https://doi.org/10.1136/bmj.323.7309.391

[32] Inyang, U.E., Uwa, I.J., 2022. Heat transfer in helical coil heat exchanger. Advances in Chemical Engineering and Science. 12, 26–39.
DOI: https://doi.org/10.4236/aces.2022.121003

Journal of Environmental & Earth Sciences
https://journals.bilpubgroup.com/index.php/jees

REVIEW

Nature-based Natural-hazard Preparedness: A Cross Section of Categorized Examples

Kyoo-Man Ha

Faculty of Resilience, Rabdan Academy, Abu Dhabi, 114646, UAE

ABSTRACT

Despite prevailing interests, no rigorous research has been conducted to examine the role of nature in natural-hazard preparedness. This systematic review aimed to describe how nature can reduce the impacts of natural hazards during the preparedness stage. The study focuses on the land, water, and air systems and on three types of stakeholders: international organizations, developed countries, and developing countries. Further, it provides supplementary strategies, such as immediate actions, local engagement, and research and development, that the stakeholders should apply to enhance their nature-based natural-hazard preparedness. We suggest integrating costs and benefits analysis, local culture, societal challenges, and environmental justice into the implementation of nature-based solutions. Finally, this review outlines the framework of nature-based natural-hazard preparedness by discussing the relationship between nature and society.

Keywords: Nature-based solutions; Costs and benefits; Land; Integration; Society

1. Introduction

Human beings have continuously deteriorated the quality of land, water, and air resources. Over 75% of the world's lands have been considerably altered by human activities. Consequently, more than two-thirds of all wildlife have been dramatically affected by environmental crises since the beginning of the 1970s. Approximately two-thirds of salt waters and over 85% of wetlands have also been polluted. Additionally, air pollution has contributed to approximately 11.65% of human deaths as well as the extinction of many biotic vectors [1].

Regardless of national boundaries, human-in-

*CORRESPONDING AUTHOR:
Kyoo-Man Ha, Faculty of Resilience, Rabdan Academy, Abu Dhabi, 114646, UAE; Email: ha1999@hotmail.com; kmanha@ra.ac.ae

ARTICLE INFO
Received: 3 October 2023 | Revised: 17 December 2023 | Accepted: 19 December 2023 | Published Online: 1 March 2024
DOI: https://doi.org/10.30564/jees.v6i1.5995

CITATION
Ha, K.M., 2024. Nature-based Natural-hazard Preparedness: A Cross Section of Categorized Examples. Journal of Environmental & Earth Sciences. 6(1): 33–44. DOI: https://doi.org/10.30564/jees.v6i1.5995

duced activities have aggravated the impacts of natural hazards [2]. Recent examples include the building collapse during the Türkiye and Syria earthquakes in 2023, long-lasting droughts in California, flooding in Afghanistan and Pakistan in 2022, and outbreaks of infectious diseases. The occurrence of natural hazards has resulted in several visible and invisible impacts, including ecological disturbances, human deaths, risks to basic human needs, and social inequalities.

Nonetheless, understanding the costs and benefits of nature or the application of nature-based solutions may allow multiple nations to prepare for the occurrence of dire natural hazards [3]. Nature-based solutions, such as the use of natural-hazard-resistant species like the Ghaf trees, seagrasses, and steppe-land birds against drought, storm surges, and air pollution, respectively, can help in taking measures against natural-hazard impacts in advance, leading to the restoration of nature and resolution of societal challenges. In addition, various species can be utilized as natural-hazard indicators (e.g., using tree nuts and medicinal herbs; leaf loss in plants; rats, snakes, and weasels; and birds and fish as indicators of droughts, food insecurity, earthquakes, and tsunamis, respectively).

As nature-based solutions enhance natural conditions and contribute to natural-hazard preparedness in each nation, they benefit both the natural environment and human beings [4]. In this context, we should ask ourselves "How have major stakeholders in different regions addressed the role of nature (i.e., land, water, and air) in natural-hazard preparedness?" The goal of this review was to study this role of nature, considering natural-hazard preparedness as the final goal. The findings of this review are expected to help reduce the human loss, economic damages, and social inequalities resulting from natural disasters.

To frame supplementary strategies, this study initially examined nature-based solutions for natural-hazard preparedness based on three factors: land, water, and air. These three factors were further analyzed through the lens of three types of stakeholders: international organizations, developed nations, and developing nations. Since the stakeholders try to improve the current status of their nature-based natural-hazard preparedness with supplementary strategies, they have to address factors such as the local culture, participation, integration, societal challenges, emergency training, and environmental justice.

2. Literature review

Nature-based solutions (also known as nature-based approaches or ecological engineering) use nature as a tool to productively transform unsustainable human activities [5]. "Nature-based solutions" is an umbrella term referring to aspects such as biodiversity, ecosystem services, lessons learned from nature, and nature-focused interventions. However, the main focus of the present study is the application of nature-based solutions for natural-hazard management.

Natural hazards are naturally occurring phenomena such as hurricanes accompanied by floods, earthquakes and tsunamis, snowstorms, sandstorms, droughts, sinkholes, and landslides. They also include quasi-natural hazards such as climate change, desertification, and the spread of coronavirus disease 2019 (COVID-19). The disaster-management cycle includes the phases of natural-hazard prevention/mitigation, preparedness, response, and recovery. The preparedness phase involves preparing for emergencies before, during, and after the occurrence of natural hazards [6]; it lasts for the entirety of the disaster-management cycle.

There are approximately 18 kinds of natural hazards, which are characterized by the scale of their occurrence [7]. Irrespective of an individual's place of residence, natural hazards may impact their lives, regardless of regional boundaries and personal desires. The occurrence of natural hazards is beyond human control on countless occasions, necessitating the adoption of preventive measures.

Despite its progressive approach, nature-based solutions have remained a divisive and contentious strategy [8]. While being used for climate change mitigation, the term "nature-based solutions" has contributed to a lack of informed consent, an inability to access natural resources, privatization of an intrinsic nature, and the violation of human rights. Further, due to the ambiguous scope of nature-based solutions, the term has been frequently interpreted for various individual and institutional interests, thereby leading to its inconsistent application.

Involvement of a high extent of risks has been reported for certain applications of nature-based solutions [9]. Some politicians and businessmen have maintained that nature-based solutions would help regional economies to move away from a fossil-fuel economy. However, activities such as tree planting in large areas for carbon sequestration could have serious consequences if the stakeholders entirely supplanted the native trees with non-native species. Similarly, the production of bioethanol from corn grains could dramatically increase the use of pesticides.

Thus, nature-based solutions have both benefits and associated costs [10]. However, nature-based solutions have proved to be a more sustainable approach against natural hazards than the establishment of built infrastructure (or hard-engineering approach), since they promote preparedness capacity and emergency resilience. As an added investment for nature, restored natural habitats may boost biodiversity, green job creation, and economic performance, and offer other benefits under appropriate cultural contexts. Thus, nature-based solutions promote well-being and regeneration in human society.

A universal formula cannot be applied to nature-based solutions since related contexts, including the changing intensity of natural hazards, politics, and social inequalities, also need to be considered in the approach. However, this has not been the case in most of its applications [11]. Moreover, the successful implementation of nature-based solutions for natural-hazard preparedness is not possible without the investment of an appropriate amount of funds.

Since the first introduction of the term "nature-based solutions" by the international community (through its inclusion in the title of the annual report of the World Bank in 2008), researchers have focused increasingly on related topics such as climate change [12,13]. These studies have directly or indirectly involved several disciplines, including climatology, ecology, economics, agriculture, pisciculture, ornithology, medical sciences, natural resource management, legislation, and public policy.

However, not many have studies focused on nature-based solutions for disaster management [14]. Although some researchers and policymakers have mentioned nature-based solutions in their domains, no rigorous study has been attempted in relation to natural-hazard preparedness. Moreover, the relationships between nature and society and the collaboration among stakeholders have not been thoroughly examined in the field of natural-hazard preparedness.

Despite the lack of sufficient research, Keesstra et al. (2018) highlighted the importance of the concept of connectivity in nature-based solutions [15]. Although natural hazards were not discussed in detail, they strongly indicated that systems thinking would be useful to visualize how nature-based solutions will improve the environment. Connectivity includes multiple lives, processes, and feedback to outline the mainstream of ecology under a complicated environment.

In 2020, the International Union for Conservation of Nature (IUCN) proposed an international standard for nature-based solutions [16]. The IUCN highlighted the necessity of a global standard to solve the challenges of nature-based solutions, including those of biodiversity, ecosystem, and economic aspects. Without a global standard, the outcome of nature-based solutions would be unreliable. However, though the IUCN proposed a global standard as a framework for nature-based solutions, it only briefly discussed the issue of natural hazards in its theoretical process.

When the Federal Emergency Management Agency (FEMA) published a book on guidelines for nature-based solutions in 2021, it entirely focused on the impacts of climate change in local regions [17]. FEMA assumed that climate change was a big barrier in local communities, which would build their resilience and adaptation to climate change by weaving characteristics of nature into their built environment. The FEMA further maintained that corresponding implementation strategies would differ among individual communities.

Reflecting the East Asian saying "Humans shall play nature (i.e., land, water, and air) off against nature (the occurrence of natural hazards)", this study directly examines natural-hazard preparedness employing nature-based solutions. In doing so, this research aims to provide a holistic framework for natural-hazard preparedness by comprehensively addressing all natural hazards, the inconsistent application of nature-based solutions, related risks, and benefits and costs of nature-based solutions, among others. Based on multidisciplinary studies, this review focuses on the relationship between nature and society and includes stakeholders.

3. Methods

The systematic literature review in this paper focused on a holistic framework for natural-hazard preparedness and consisted of four steps: (1) formulating a research question, (2) identifying relevant texts, (3) analyzing the texts, and (4) summarizing the obtained evidence [18]. Namely, the PRISMA checklist, which includes numerous items such as the justification for the literature review, the selection procedure, text extraction, and text synthesis among many, was specifically the primary source of information used in this section [19].

After proposing a single research question regarding the role of nature in natural-hazard preparedness (following the analytical framework in **Figure 1**), the appropriate text data was identified. The criterion of inclusion was that the texts had to be related to nature-based solutions, the occurrence of natural hazards, and the phase of natural-hazard preparedness. To this end, several keywords were inputted into the search engines, including "nature-based solutions", "natural hazards and risks", and "natural disaster management".

This review created its own units of analysis. As the Earth is the geographical scope of this research, all stakeholders were comprehensively categorized into analytical units such as international organizations, developed nations, and developing nations [20]. While the international organizations (e.g., the United Nations and international non-governmental organizations) were considered to deal with international affairs, all countries, both developed and developing nations, were considered to manage their own regional affairs.

The four spheres of the Earth are defined as the geosphere, hydrosphere, atmosphere, and biosphere. Thus, there are three space systems (i.e., geosphere,

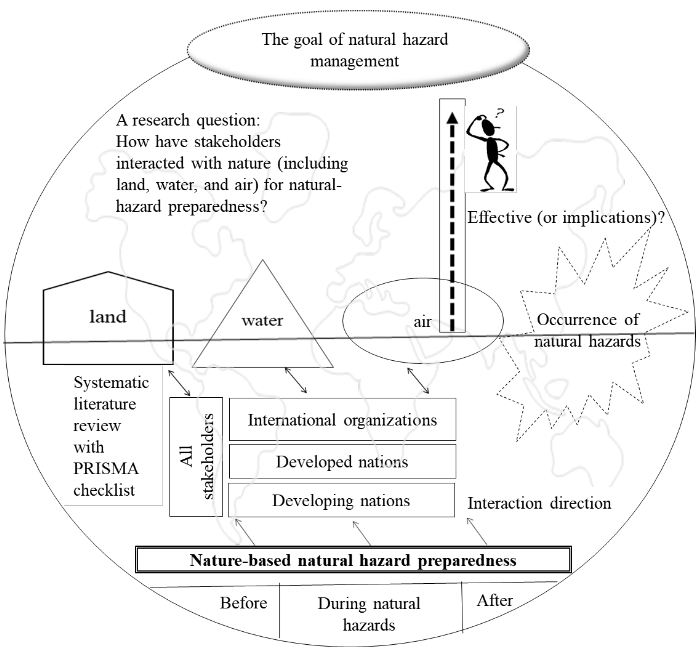

Figure 1. Analytical framework.

hydrosphere, and atmosphere) where life (i.e., biosphere) can exist [21]. They are generally termed as land, water, and air. In the present review, three analytical categories were used: land (forests, peat bogs, swamps, etc.), water (whales, salt marshes, seagrass beds, various fish, etc.), and air (various birds, insects, biotic vectors, etc.).

To summarize the evidence, appropriate texts were coded by interpreting and recording them [22]. Three units of analysis were repeatedly and flexibly classified into three analytical categories to monitor the effectiveness of the current application of nature-based solutions. In addition, supplementary strategies for nature-based solutions and their meaningful implications were provided, when applicable. This step was implemented to answer the research question.

4. Current state of nature-based natural-hazard preparedness

4.1 Land

The United Nations Environment Programme (UNEP) considers climate change to be an emergency and maintains the significance of implementing both tree planting and climate-smart agriculture. It has been difficult for the UNEP to achieve a full mitigation of climate change because of the slow pace of efforts of multiple nations [23]. The World Bank has attempted to mitigate the impacts of certain natural hazards, such as mudslides and floods, by promoting cost-effective strategies. Despite their economic efficiency, planting non-native trees in a region could pose serious threats (or be toxic) to local species.

Even though many European countries have supported nature-based solutions, European soil has become impermeable (also known as soil sealing) owing to urbanization, leading to an increase in heat and floods [24]. The United Arab Emirates (UAE) has planted Ghaf trees as a national initiative because they are drought-resistant and help prevent desertification. However, an increase in land pollution and the immigrant population has decreased the number of Ghaf trees.

Harbin City in China has implemented a Sponge City program to promote biodiversity and urban wells; they absorb rainwater from the ground to mitigate floods. However, the associated cost of building the urban infrastructure is not sustainable. Many nations in Africa have planned to establish forests and wetlands to decrease droughts and water shortages in their region. However, context-specific traditional knowledge has not been well integrated into these endeavors.

4.2 Water

Considering the role of whales in carbon dioxide (CO_2) sequestration (via their faeces, phytoplankton, carbon sinks, and the carbon cycle), the International Monetary Fund estimated the value of the financial benefits of whales at about 2 million US dollars per individual, in 2019 [25]. Therefore, whales are much more efficient in absorbing CO_2 than small fish and other marine organisms. Nonetheless, the number of whales in the ocean is decreasing, and policymakers are not sufficiently aware of the value of whales in terms of natural-hazard preparedness.

Australia has attempted to protect its seagrasses, mangroves, tidal marshes, commercial fish, and other species to prepare for the impacts of storm surges through international partnerships with neighboring countries. However, the involved parties have shown a lack of appropriate theoretical backgrounds. Similarly, Canada has implemented plans to protect approximately 30% of its seas until 2030, for natural-hazard preparedness [26]. Moreover, storing huge amounts of CO_2 in the ocean successfully will require further involvement of the local communities.

Even though Bangladesh has continuously implemented nature-based solutions, such as various-term actions and instruments, the country has faced considerable challenges related to coastal afforestation. Moreover, their efforts have been mostly managed in a scattered way [27]. While the Pacific islands such as Samoa, Kiribati, and Vanuatu have actively utilized their indigenous ecological knowledge, such as the reliance on bio-indicators as early warning systems, these countries have not fully implemented coastal planning against natural hazards.

4.3 Air

After officially adopting nature-based solutions in the 21st century, the IUCN has made partial efforts to stabilize the concentrations of greenhouse gases in the atmosphere. Further, it has continued to reduce the impacts of natural hazards via the Global Standard and other guidelines. Nonetheless, its policies related to the air systems still lack information on targeted customers. The Red Cross has prioritized making partnerships with environmental organizations for natural-hazard preparedness [28], but it has mainly focused on land and water, without equally supporting the air systems.

Authorities of Andalusia in Spain have tried to protect the steppe-land birds in their region by improving the air quality and replacing traditional fence marks with plastic ones. Despite an increase in the number of birds, Andalusia still requires both interoperability among communication channels and relevant training programs. In addition, the number of bees, butterflies, and moths has greatly decreased in many developed nations because of their poor air quality. An insufficient number of pollinators will lead to disruptions in the ecosystems, food security, and natural-hazard preparedness.

Even though the African nations have tried to improve their air quality, key sources of air pollution have not been well managed. The lenient regulations for vehicle air filters, use of solid fuels during cooking, and burning of private waste are some examples of this mismanagement [29]. These issues are complicated owing to their interconnections with regional conflicts. Additionally, many birds in South America have been killed by lead contamination. However, negligible information is available on the relationship between lead contamination and the bird population.

5. Implications

Nature-based solutions will expedite the decrease of the Earth's temperature if all stakeholders (i.e., international organizations, developed nations, and developing nations) systematically take appropriate actions [30]. For example, forests in the United States have absorbed about 10% of the country's gas emissions; however, nature-based solutions would compensate for approximately 30% of the climate change impacts in the future [31]. In essence, nature-based solutions derived from nature will contribute to lessening the impacts of natural hazards, while maintaining protection against them when they arise.

Comparatively speaking, hard solutions, also known as engineered solutions, are effective at handling high-frequency events, while nature-based solutions will be better at handling low-frequency ones [32,33]. As a result, nature-based solutions—like conversation projects—are self-sustaining, but hard solutions still need significant financial outlays for associated costs. If attempts are made to substantially work on the major aspects of nature, climate change, biodiversity loss, and natural-hazard preparedness will be widely improved in multiple regions. Therefore, nature-based solutions should be planned and implemented on a long-term basis.

Nature-based solutions may help prepare against various dire risks, arising as consequences of the natural-hazard occurrence [34]. The solutions involve preparing for events such as high temperatures, rising sea levels, melting glaciers, extreme weather events, disruptions to human livelihoods, and the spread of infectious diseases. Tree planting, coastal ecosystem improvement, the recovery of biotic vectors, and other actions are essential to mitigate the intensity of frequent natural hazards. By applying these measures, the consequent human loss, financial instability, infrastructure failure, and psychological impact on individuals will be reduced.

At the national level, major stakeholders should integrate nature-based solutions with the phase of natural-hazard preparedness [35]. Nature-based solutions are a long-standing alternative for the whole field of emergency preparedness. From a strategic viewpoint, nature-based solutions should be adapted for each nation during policy design and implemented based on the information given in **Table 1**. Even though natural hazards can occur anywhere, the national organizations and their policies are more

Table 1. Supplementary strategies for nature-based natural-hazard preparedness.

Units	Alternatives
5.1 Land	The UNEP must provide practical goals for climate change by further encouraging various nations' quick actions. The World Bank should consider not only financial benefits but also evidence-based science. European countries must improve stakeholder engagement against low soil permeability. In addition, the UAE needs to strongly prohibit the illegal uprooting of Ghaf trees or other species. Chinese local governments should solve the economic challenge of building Sponge Cities with potential changes in financial regulation. The African nations need to systematically document local knowledge.
5.2 Water	Policymakers need to study the role of whales in decreasing the amount of greenhouse gas emissions and consider policies to increase their numbers. Australia should develop and provide appropriate theoretical education for those who are working on coastal ecosystems. Similarly, Canada needs to involve local communities to achieve CO_2 storage in the ocean. Bangladesh requires high-level organized efforts for its nature-based solution, and the Pacific islands need to embrace coastal planning.
5.3 Air	The IUCN should include birds, insects, and other endangered species as well as air pollution sources for targeted customers, and the Red Cross should expand its partnerships with organizations working on air systems. After facilitating technological improvement and policy change for interoperability, Spain should provide appropriate training to stakeholders. All developed nations should increase the number of pollinators by avoiding the use of chemicals, attracting biotic vectors, decreasing outdoor lighting during the night, and applying other environmental strategies. While dealing with regional conflicts, the African nations need to discuss air-related issues in their formal agenda. Researchers in South America need to study the exact impacts of lead poisoning on bird species and other wildlife.

proficient at coordinating various efforts than the stakeholders at other levels.

Nature-based solutions have been regarded as a powerful tool for natural-hazard preparedness but the corresponding supplementary strategies must be implemented to ensure effectiveness [36]. Implementation should not be based on a lesson observed but on a lesson learned. The stakeholders need to adopt further actions such as identifying, analyzing, evaluating, and prioritizing human and material resources, while equally considering the positive factors and vulnerabilities in the region. In doing so, the practical implementation of each supplementary strategy will be established.

The implications of the supplementary strategies are firmly based on the local culture [37]. Nature is interconnected with the local culture via human interaction and the local environment. The phase of natural-hazard preparedness is also influenced by local culture. Indigenous people have accumulated traditional knowledge from their ancestors, which is based on their perception of land, water, and air as a part of the local culture. Similarly, their methods of emergency preparedness depend on their local culture; in a sense, natural-hazard preparedness has always been an important part of the local culture.

Participation must be fully acknowledged while implementing supplementary strategies [38]. The three stakeholders mentioned in this study must willingly participate in the management of all aspects of their nature-based solutions. Otherwise, the desired effects cannot be achieved in the expected time, particularly considering that the land, water, and air systems are interconnected with each other. Professionals from various fields, including decision-makers, technical specialists, emergency responders, and residents, should also be allowed to work for natural-hazard preparedness.

An integrated emergency management system must be further expanded in multiple regions. The three stakeholders must initiate extensive international networks among themselves, with a global goal in mind. The national integration of governments, industries, voluntary organizations, mass media, academic researchers, and other local communities should be attempted. Integration based on consensus building should be embodied at various levels, such as internal, external, horizontal, vertical, and diagonal levels [39].

Assuming that all three stakeholders are involved in delivering the supplementary strategies, they will accordingly act on the societal challenges surrounding the land, water, and air systems [40]. Subsequently, natural-hazard preparedness will consider the major societal barriers such as politics, governance issues, economic costs and benefits, social inequalities, and multiple environmental factors. Since these societal challenges are differently situated in many local communities, strategic interests and accumulated capacities will continue to be required.

Key stakeholders will need to enhance their implementation of the supplementary strategies [41]. While the potential of including benefits and costs in nature-based solutions has not been substantially recognized in some regions yet, major stakeholders will integrate nature and natural hazards with political alliances, multilateral funding, research and development, and other factors. Further measures should be adopted to fully embody the extent of supplementary strategies around natural-hazard preparedness. For example, stakeholders need to include nature-based solutions in emergency training and exercises related to natural hazards. Even though nature-based solutions have begun to be included in the academic curricula, emergency training and exercises have been rarely mentioned. While raising the extent of public awareness regarding supplementary strategies, detailed concepts, related benefits and costs, and other techniques should be provided for the diverse trainees.

Supplementary strategies will achieve a certain level of environmental justice in relation to natural hazards [42]. Environmental justice involves equally distributing environmental benefits and costs to various regions, while ensuring that all the stakeholders are involved in decision making. In further preparations for natural hazards, all stakeholders should enhance their disaster-response capabilities. Further, disadvantaged populations should be ensured social justice through policies such as non-discrimination and inclusion [43].

Nature-based solutions with supplementary strategies will eventually keep pace with the concept of systems thinking in the field [44]. Recalling that supplementary strategies involve numerous components and their interactions (e.g., interactions among land, water, and air, dynamic relationships among international organizations, developed nations, and developing nations, and so forth), systems thinking may apply to hierarchical structure, feedback loops, and other synergies in addition to those variables and interconnectedness. It will be easier to get ready for the occurrence of different natural hazards if the system is observed and then improved overall.

6. Conclusions

The main goal of this research was to investigate the role of nature in natural-hazard preparedness. This review has discussed previous studies, barriers, and other implications. The goal of this study was achieved by elucidating that the subject has been rigorously studied, in terms of land, water, and air systems, by international organizations, developed countries, and developing countries.

A major theme of this review has been that the three stakeholders will advance the current status of nature-based natural-hazard preparedness by referring to supplementary strategies. In doing so, each stakeholder implements assigned roles at the national level such as further studies on whales' contribution to carbon sequestration, actions for the increase in the number of pollinators, and other organized efforts. Simultaneously, the stakeholders also need to address the effects of nature-based solutions, the local culture, active participation, complete integration, societal barriers, emergency training, and environmental justice.

This review has provided a comprehensive framework of the relationships between nature and society via nature-based natural-hazard preparedness. This framework may be utilized as a theoretical reference by various stakeholders during the preparations for natural hazards, while including all players, all risks, and the costs and benefits of nature-based solutions. On the other hand, limitations in the timely future implementation of nature-based natural-hazard preparedness by the international community are only partially discussed in this paper. This limitation arises because of the existence of many disagreements and challenges around the land, water, and air systems. Without taking necessary action, the effects of nature-based natural-hazard preparedness will not be rapidly established.

Researchers should study nature-based solutions in other phases of the natural-hazard management cycle such as natural-hazard prevention/mitigation, response, and recovery in the future. They may refer to the framework of the nature-based natural-hazard preparedness provided in this paper. To address the limitations of this research, the ways to efficiently implement the suggested nature-based natural-hazard preparedness in affected nations or local communities should be further studied. Such efforts may help reduce not only the physical impacts but also the social impacts of natural hazards in multiple regions.

Acknowledgments

Not applicable.

Conflict of Interest

The author declares that he has no financial or non-financial conflicts of interest with this manuscript.

Availability of Data and Materials

The author confirms that the data supporting the findings of this study are available within the article.

Financial Support

Not applicable.

References

[1] A Market Review of Nature-based Solutions: An Emerging Institutional Asset Class [Internet]. Green Purposes Company. Available from: https://finance.earth/wp-content/uploads/2021/05/Finance-Earth-GPC-Market-Review-of-NbS-Report-May-2021.pdf

[2] Leake, I., 2023. Climate extremes drive negative vegetation growth. Nature Reviews Earth & Environment. 4, 68. DOI: https://doi.org/10.1038/s43017-023-00392-2

[3] Sowinska-Swierkosz, B., Garcia, J., 2022. What are Nature-based solutions (NBS)? Setting core ideas for concept clarification. Nature-Based Solutions. 2, 100009. DOI: https://doi.org/10.1016/j.nbsj.2022.100009

[4] Guerrin, J., Serra-Llobet, A., Bonnefond, M., et al., 2023. What are Nature-based Solutions for flood-risk management? Appropriations of a global concept in France and in the US. Techniques Sciences Methodes. 10(10), 97–119. (in French). DOI: https://doi.org/10.36904/tsm/202310097

[5] Antolin-Lopez, R., Garcia-de-Frutos, N., 2021. Nature-based solutions. Encyclopedia of the UN sustainable development goals: Partnerships for the goals. Springer: Switzerland. pp. 804–814. DOI: https://doi.org/10.1007/978-3-319-95963-4_12

[6] Are You Ready? An In-depth Guide to Citizen Preparedness [Internet]. Federal Emergency Management Agency. Available from: https://www.ready.gov/sites/default/files/2021-11/are-you-ready-guide.pdf

[7] Wickenberg, B., 2024. Collaborating for nature-based solutions: Bringing research and practice together. Local Environment. 29(1), 118–134. DOI: https://doi.org/10.1080/13549839.2023.2254797

[8] Seeking Clarity on Nature-based Climate Solutions for Adaptation [Internet]. International Institute for Sustainable Development. Available from: https://www.iisd.org/system/files/2022-06/seeking-clarity-nature-based-climate-solutions-adaptation-en.pdf

[9] Nature-based Solutions to Climate Change: A Rocha Worldwide Family Position [Internet]. A Rocha International. Available from: https://www.

arocha.org/wp-content/uploads/2021/10/Nature-based-Solutions-to-climate-change-A-Rocha-worldwide-family-position-October-2021.pdf

[10] Nelson, D.R., Bledsoe, B.P., Ferreira, S., et al., 2020. Challenges to realizing the potential of nature-based solutions. Current Opinion in Environmental Sustainability. 45, 49–55. DOI: https://doi.org/10.1016/j.cosust.2020.09.001

[11] Economic Costs and Benefits of Nature-based Solutions to Mitigate Climate Change [Internet]. Cambridge Econometrics. Available from: https://www.camecon.com/wp-content/uploads/2021/03/The-economic-costs-benefits-of-nature-based-solutions_final-report_FINAL_V3.pdf

[12] Bianciardi, A., Cascini, G., 2023. How would nature design and implement nature-based solutions?. Nature-Based Solutions. 3, 100047. DOI: https://doi.org/10.1016/j.nbsj.2022.100047

[13] Mercado, G., Wild, T., Hernandez-Garcia, J., et al., 2024. Supporting nature-based solutions via nature-based thinking across European and Latin American cities. Ambio: A Journal of Environment and Society. 53(1), 799–4. DOI: https://doi.org/10.1007/s13280-023-01920-6

[14] Alves, P.B.R., Djordjević, S., Javadi, A.A., 2022. Understanding the NEEDS for ACTING: An integrated framework for applying nature-based solutions in Brazil. Water Science and Technology. 85(4), 987–1010. DOI: https://doi.org/10.2166/wst.2021.513

[15] Keesstra, S., Nunes, J., Novara, A., et al., 2018. The superior effect of nature based solutions in land management for enhancing ecosystem services. Science of the Total Environment. 610–611, 997–1009. DOI: http://dx.doi.org/10.1016/j.scitotenv.2017.08.077

[16] International Union for Conservation of Nature (IUCN), 2020. Global standard for nature-based solutions. IUCN: Gland, Switzerland. pp. 1–22. DOI: https://portals.iucn.org/library/node/49070

[17] Building Community Resilience with Nature-based Solutions [Internet]. FEMA. Available from: https://www.fema.gov/sites/default/files/documents/fema_riskmap-nature-based-solutions-guide_2021.pdf

[18] Leveraging Evidence for Access and Development (LEAD), 2021. Conducting a systematic review: Methodology and steps. LEAD at KREA University: Chennai, India. pp. 1–29.

[19] Dawson, J.K., Twum, F., Acquah, J.B.H., et al., 2023. PRISMA archetype-based systematic literature review of security algorithms in the cloud. Security & Communication Networks. 9210803. DOI: https://doi.org/10.1155/2023/9210803

[20] Rizvi, S.A.F., 2020. Cost effectiveness of health expenditures: A macro level study for developing and developed countries. International Journal of Humanities and Applied Social Science. 26–42. DOI: https://doi.org/10.33642/ijhass.v5n9p3

[21] Bjelic, S.N., Markovic, N.A., 2023. A more advanced theoretical model of the sphere earth's EM in a foreign homogeneous EM field. Military Technical Courier. 71(2), 362–391. DOI: https://doi.org/10.5937/vojtehg71-42923

[22] Pollak, I., Stiehl, K.A.M., Scrank, B., 2023. Engaging children in intervention development—A comparison of four qualitative methods and their suitability to elicit information relevant for early intervention development. International Journal of Qualitative Methods. 22, 1–15. DOI: https://doi.org/10.1177/16094069231204775

[23] Nature-based Solutions for Climate Change Mitigation [Internet]. United Nations Environment Programme (UNEP) & IUCN. Available from: https://wedocs.unep.org/xmlui/bitstream/handle/20.500.11822/37318/NBSCCM.pdf

[24] Demaziere, C., 2021. Exploring the creation of the metropolitan city-region government: The cases of England, France and Italy. European Planning Studies. 29(11), 2038–2055. DOI: https://doi.org/10.1080/09654313.2021.1923666

[25] Theochari, A.P., Baltas, E., 2024. The nature-based solutions and climate change scenarios toward flood risk management in the greater Athens area—Greece. Natural Hazards. DOI: https://doi.org/10.1007/s11069-024-06409-3

[26] Roadmap 2030: Delivering on Canada's Land and Ocean Protection Targets [Internet]. Canadian Parks and Wilderness Society (CPAWS). Available from: https://cpaws.org/wp-content/uploads/2022/06/cpaws_roadmapto2030_digital_v2.pdf

[27] Mahood, R., Zhang, L., Li, G., 2023. Assessing effectiveness of nature-based solution with big earth data: 60 years mangrove plantation program in Bangladesh coast. Ecological Processes. 12, 11. DOI: https://doi.org/10.1186/s13717-023-00419-y

[28] Capgras, J., Mushamuka, F.B., Feuilleaubois, L., 2023. Optimisation of selection and placement of nature-based solutions for climate adaptation: a literature review on the modelling and resolution approaches. Environment Systems & Decisions. 43, 577–598. DOI: https://doi.org/10.1007/s10669-023-09933-y

[29] Abera, A., Friberg, J., Isaxon, C., et al., 2021. Air quality in Africa: Public health implications. Annual Review of Public Health. 42, 193–210. DOI: https://doi.org/10.1146/annurev-publhealth-100119-113802

[30] Girardin, C.A., Jenkins, S., Seddon, N., et al., 2021. Nature-based solutions can help cool the planet—if we act now. Nature. 593, 191–194. DOI: https://doi.org/10.1038/d41586-021-01241-2

[31] Opportunities to Accelerate Nature-based Solutions: A Roadmap for Climate Progress, Thriving Nature, Equity, & Prosperity [Internet]. White House. Available from: https://www.whitehouse.gov/wp-content/uploads/2022/11/Nature-Based-Solutions-Roadmap.pdf

[32] Lehner, F.V., Tiffer-Sotomayor, R., Díaz, A., et al., 2021. Biodiversity-friendly agricultural practices in the Indigenous Agricultural Systems in the Biodiversity Corridor of the Alto Paraná Atlantic Forest (Paraguay). Research in Ecology. 3(3), 1–7. DOI: https://doi.org/10.30564/re.v3i3.3358

[33] Miralles-Wilhelm, F., 2023. Nature-based solutions in agricultural landscapes for reducing tradeoffs between food production, climate change, and conservation objectives. Frontiers in Water. 5, 1247322. DOI: https://doi.org/10.3389/frwa.2023.1247322

[34] Badura, T., Lorencova, E.K., Ferrini, S., et al., 20 21. Public support for urban climate adaptation policy through nature-based solutions in Prague. Landscape and Urban Planning. 215, 104215. DOI: https://doi.org/10.1016/j.landurbplan.2021.104215

[35] Matthews, J., Cruz, E.O.D., 2022. Integrating nature-based solutions for climate change adaptation and disaster risk management: A practitioner's guide. Asian Development: Metro Manila, Philippines. pp. 1–66. DOI: http://dx.doi.org/10.22617/TIM220215-2

[36] Nature-based Solutions for Climate Change [Internet]. Forests Ontario. Available from: https://downloads.ctfassets.net/e09p19lzfrfe/3rqYvnSgdICpJG2x50HXkX/29094ac1f9cd442aac12c08a2593d5a1/FO_OE21_STUDY-GUIDE_FA.pdf

[37] Sarkki, S., Haanpaa, O., Heikkinen, H.I., et al., 2024. Mainstreaming nature-based solutions through five forms of scaling: Case of the Kiiminkijoki River basin, Finland. Ambio: A Journal of Environment and Society. 53(2), 212–226. DOI: https://doi.org/10.1007/s13280-023-01942-0

[38] Integrated Emergency Management Plan [Internet]. Purdue University. Available from: https://www.purdue.edu/ehps/emergency-

preparedness/emergency-plans/iemp-docs/iemp-final.pdf

[39] Eyankware, M.O., Igwe, E.O., Ogwah, C., et al., 2020. Achieving sustainable use and management of water resources for irrigation in Nigeria. Journal of Environmental & Earth Sciences. 2(2), 47–55.
DOI: https://doi.org/10.30564/jees.v2i2.2505

[40] Dick, J., Carruthers-Jones, J., Carver, S., et al., 2020. How are nature-based solutions contributing to priority societal challenges surrounding human well-being in the United Kingdom: a systematic map. Environmental Evidence. 9, 25.
DOI: https://doi.org/10.1186/s13750-020-00208-6

[41] Seddon, N., Chausson, A., Berry, P., et al., 2020. Understanding the value and limits of nature-based solutions to climate change and other global challenges. Philosophical Transactions of the Royal Society B. 375(1794).
DOI: http://dx.doi.org/10.1098/rstb.2019.0120

[42] Kato-Huerta, J., Geneletti, D., 2022. Environmental justice implications of nature-based solutions in urban areas: A systematic review of approaches, indicators, and outcomes. Environmental Science & Policy. 138, 122–133.
DOI: https://doi.org/10.1016/j.envsci.2022.07.034

[43] Inclusion, Diversity, and Equity [Internet]. KPMG. Available from: https://assets.kpmg.com/content/dam/kpmg/ie/pdf/2022/04/ie-inclusion-diveristy-equity-YM.pdf

[44] Martín, E.G., Giordano, R., Pagano, A., et al., 2020. Using a system thinking approach to assess the contribution of nature based solutions to sustainable development goals. Science of the Total Environment. 738, 139693.
DOI: https://doi.org/10.1016/j.scitotenv.2020.139693

BILINGUAL PUBLISHING GROUP

Journal of Environmental & Earth Sciences

https://journals.bilpubgroup.com/index.php/jees

ARTICLE

Stochastic Analysis and Modeling of Velocity Observations in Turbulent Flows

***Evangelos Rozos**[1*]**, Jorge Leandro**[2]**, Demetris Koutsoyiannis**[3]*

[1] *Institute for Environmental Research & Sustainable Development, National Observatory of Athens, Athens, 15236, Greece*

[2] *Research Institute for Water and Environment, University of Siegen, Siegen, 57076, Germany*

[3] *Department of Water Resources and Environmental Engineering School of Civil Engineering, National Technical University of Athens, Athens, 15780, Greece*

ABSTRACT

Highly turbulent water flows, often encountered near human constructions like bridge piers, spillways, and weirs, display intricate dynamics characterized by the formation of eddies and vortices. These formations, varying in sizes and lifespans, significantly influence the distribution of fluid velocities within the flow. Subsequently, the rapid velocity fluctuations in highly turbulent flows lead to elevated shear and normal stress levels. For this reason, to meticulously study these dynamics, more often than not, physical modeling is employed for studying the impact of turbulent flows on the stability and longevity of nearby structures. Despite the effectiveness of physical modeling, various monitoring challenges arise, including flow disruption, the necessity for concurrent gauging at multiple locations, and the duration of measurements. Addressing these challenges, image velocimetry emerges as an ideal method in fluid mechanics, particularly for studying turbulent flows. To account for measurement duration, a probabilistic approach utilizing a probability density function (PDF) is suggested to mitigate uncertainty in estimated average and maximum values. However, it becomes evident that deriving the PDF is not straightforward for all turbulence-induced stresses. In response, this study proposes a novel approach by combining image velocimetry with a stochastic model to provide a generic yet accurate description of flow dynamics in such applications. This integration enables an approach based on the probability of failure, facilitating a more comprehensive analysis of turbulent flows. Such an approach is essential for estimating both short- and long-term stresses on hydraulic constructions under assessment.

Keywords: Smart modeling; Turbulent flows; Data analysis; Stochastic analysis; Image velocimetry

*CORRESPONDING AUTHOR:
Evangelos Rozos, Institute for Environmental Research & Sustainable Development, National Observatory of Athens, Athens, 15236, Greece; Email: erozos@noa.gr

ARTICLE INFO
Received: 4 December 2023 | Revised: 29 January 2023 | Accepted: 20 February 2023| Published Online: 5 March 2024
DOI: https://doi.org/10.30564/jees.v6i1.6109

CITATION
Rozos, E., Leandro, J., Koutsoyiannis, D., 2024. Stochastic Analysis and Modeling of Velocity Observations in Turbulent Flows. Journal of Environmental & Earth Sciences. 6(1): 45–56. DOI: https://doi.org/10.30564/jees.v6i1.6109

1. Introduction

Highly turbulent flows exhibit complex behavior, characterized by rapid and irregular fluctuations in velocity, pressure, and other flow parameters [1]. Many hydraulic structures and systems, such as piers, dams, channels, pipelines, and pumps, are susceptible to high-intensity turbulent flows [2]. Knowledge of turbulent flow characteristics helps in assessing the hydraulic loads, including pressure fluctuations, impacts, and dynamic forces, acting on structures. This information is crucial for ensuring the structural integrity, stability, and safety of hydraulic constructions under various flow conditions. For this reason, various numerical methods, such as the large eddy and the direct numerical simulation, have been developed to study turbulent flows [3]. However, turbulent flows often involve gas-liquid interfaces, which significantly increase the complexity of flow descriptions and can challenge even the most sophisticated numerical models [4]. For this reason, more often than not, scale models of hydraulic systems are built to study turbulent flows. Nevertheless, the monitoring of these physical models, even within meticulously controlled environments, is a laborious and demanding task.

Turbulent flows pose inherent challenges in flow measurement due to their unpredictable fluctuations and irregular nature. Conventional mechanically-based methods and acoustic Doppler velocimeters often introduce disturbances to the flow, making accurate measurements difficult. While there are intrusive methods available that can provide reliable measurements of high frequency with minimal flow disturbance, they are limited in their ability to obtain simultaneous measurements at multiple locations [5,6]. On the other hand, image velocimetry has been widely suggested by researchers as a non-intrusive method that offers accurate and reliable measurements of flow in both natural [7,8] and man-made hydraulic structures [9].

Image velocimetry stands out as an exceptionally well-suited method for studying turbulent flows, offering distinct advantages over traditional techniques such as current meters and acoustic Doppler velocimetry. One of its primary merits lies in its non-intrusive nature, allowing for flow measurements without physically disrupting the system under investigation. This characteristic is particularly crucial when studying turbulent flows, where the introduction of probes or other intrusive devices can alter the flow dynamics. Also, image velocimetry enables the determination of velocity fields with high temporal and spatial resolution, providing a detailed and comprehensive view of the turbulent characteristics, and for this reason, has gained significant popularity in hydraulic laboratories [2,10].

Image velocimetry can be based on different methods of video analysis, including approaches based on correlation, feature-tracking, or optical-flow analysis. Correlation-based techniques, such as Particle Image Velocimetry (PIV), rely on tracking the movement of identifiable features or particles in consecutive images [11]. Feature/particle tracking methods (PTV) focus on tracking specific features or points of interest in the flow field across multiple frames to track the movement of features and estimate the flow velocities [12]. In space-time image velocimetry (STIV) a search line of arbitrary length is set in the mainstream direction of the image, and the flow velocity is calculated from the gradient of the striped pattern that appears in the space-time image generated by stacking the image intensity information in the time direction [13]. Lastly, optical flow (OF) methods provide estimates of pixel or image region motion between consecutive frames, based on inverse methods applied to brightness variations in the image sequence [7]. Depending on the employed inverse method, there are different alternatives for the optical flow (OF) algorithms, such as the Horn-Schunk method, Lucas-Kanade method, and Farneback method [14].

PIV and OF have emerged as the most suitable methods for turbulent flows. PIV's capability to capture detailed flow phenomena, including wall-normal vortices and low-speed streaks, has been demonstrated, offering pivotal information to understand underlying turbulence statistics such as streamwise velocity fluctuations, turbulence intensities, and Reynolds shear stress. This elucidates peak values and their locations near solid flow boundaries. PIV has served as an indispensable tool in studying bed shear stress from remotely measured surface turbulent dissipation fields in open channel flows [15]. On the other hand, the OF method, specifically employing the Farneback algorithm, provides denser spatial resolution and increased computational efficiency. This allows researchers to characterize the behavior of turbulent flow, and observe the formation of eddies, turbulent structures, and surface features like bumps and dimples [16].

Regarding the study of the impact of turbulent flows on nearby hydraulic structures, understanding Reynolds stresses and drag force is pivotal [17]. Typically, these stresses are estimated by the quantities $v_x'^2$, $v_x' \cdot v_y'$, and v_x^2, respectively, where v_x and v_y are the velocity vector components at a specific point of the flow field, and $v_x' = v_x - \langle v_x \rangle$ and $v_y' = v_y - \langle v_y \rangle$. The typical approach to obtaining foundational insights is to use the time-averaged values $\langle v_x'^2 \rangle$ and $\langle v_x' \cdot v_y' \rangle$ for the Reynolds stresses, and the maximum value, $\max(v_x^2)$, for the drag force. However, if the aforementioned quantities are obtained from observations of short time durations, the limitations of this approach become apparent when considering potential impacts over extended periods, where significantly larger magnitudes compared to the previously mentioned time-averaged and maximum values may emerge. Recognizing these limitations, a transition to a more comprehensive perspective becomes imperative. In this context, utilizing a probabilistic framework not only offers insights into dynamic behavior but also facilitates the analysis of stresses. This has been highlighted by scholars who suggest proceeding from Reynolds stress to PDF level of description [17]. Assuming v_x follows a normal distribution, the quantities $v_x'^2$ and v_x^2, representing the Reynolds normal stress and the drag force respectively, are expected to adhere to a central and non-central chi-square distribution respectively, with one degree of freedom [18]. In cases where the standard deviation is not 1, variable substitution is required [19].

As the probabilistic framework adeptly addresses normal stress, the complexity deepens when examining shear stress, specifically the product $v_x' \cdot v_y'$. In contrast to normal stress, where a closed-form solution aligns with the non-central chi-square distribution, for shear stress deriving the distribution of the product of the two random dependent variables, $v_x' \cdot v_y'$, is a formidable mathematical challenge [20,21]. An alternative practical approach is the utilization of a numerical stochastic model to navigate the intricacies of this product distribution. A multivariate stochastic model could be used to generate synthetic time series of velocity at various locations in the flow field. Subsequently, the corresponding values of Reynolds stresses and drag force could be estimated using the formulas mentioned earlier. Finally, by applying an empirical distribution to these time series, one could obtain the probability of exceedance.

Analyzing turbulent flows using image velocimetry yields vast datasets, demanding a nuanced approach to ensure statistically consistent results. The necessity to filter out spurious velocities further emphasizes the need for a methodologically rigorous framework. Moreover, the simultaneous monitoring of multiple locations introduces a layer of complexity that warrants a comprehensive probabilistic perspective. A stochastic model not only facilitates the probabilistic assessment of extreme velocity occurrences but also provides a systematic means to tackle the intricacies of the distribution of the product $v_x' \cdot v_y'$. At the same time, the stochastic model serves as a statistical filter to manage spurious velocities, ensuring that the obtained data reflects the true nature of turbulent flows.

In this study, we demonstrate the efficacy of integrating an image velocimetry algorithm with a stochastic model to address the previously mentioned challenges posed by turbulent flows. By harnessing the power of image velocimetry for non-intrusive, simultaneous measurements at multiple locations, and coupling it with a robust stochastic framework, we aim to provide a comprehensive understanding of turbulent flow dynamics. This holistic approach not only enables a probabilistic assessment of extreme velocity values but also navigates the complexities associated with drag force, and shear and normal stresses calculations. It should be noted that the application of stochastic models to turbulent flows has been suggested by various researchers [22,23]. However, unlike these previous studies, which employed a stochastic approach to enhance the accuracy of numerical modeling, our study takes a distinctive approach. We utilize a stochastic model not only to improve the analysis of image velocimetry data but also to provide a probabilistic assessment of the stress factors arising from the intense and highly varying flow conditions. This dual application sets our study apart, allowing for a more comprehensive understanding of turbulent flow dynamics and its implications for hydraulic structures.

2. Materials and methods

2.1 Case study—hydraulic jump

A hydraulic jump serves as a compelling example of localized turbulent flow. When supercritical flow abruptly transitions to subcritical flow, a surge of kinetic energy is dissipated, causing a sudden increase in turbulence within the jump region. This localized turbulence is characterized by rapid fluctuations in velocity and pressure. The intensified turbulent flow can induce dynamic hydraulic loads on adjacent structures, such as embankments or bridge foundations, potentially jeopardizing their stability and integrity. The energy dissipation inherent in hydraulic jumps makes them (the adjacent structures) particularly prone to erosive forces, which, coupled with the turbulent nature of the flow, can lead to the scouring of riverbeds and banks.

Understanding the dynamics of turbulent flow within hydraulic jumps is crucial for assessing the potential impacts on nearby constructions and implementing effective engineering solutions to mitigate risks and ensure the longevity and safety of hydraulic infrastructure. For this reason, in this study, we have chosen this characteristic case of turbulent flow to demonstrate our methodology, i.e., analyze the video of a hydraulic jump with image velocimetry and then process the obtained time series with a stochastic model.

The video used in this study was obtained from the supplementary material of the publication of Mortazavi et al. [3]. This video represents a hydraulic jump with inflow Froude number of 2, Weber number of 1820 and density ratio of 831. The video has 598 frames, a frame rate of 24 fps, and a resolution of 960 × 540 px. The first frame of this video is displayed in **Figure 1**.

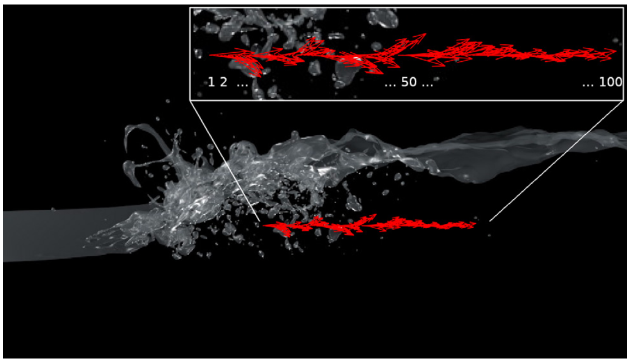

Figure 1. The vectors of the time-averaged velocities along the 100 points of the track line (marked by the origins of the vectors) are processed by the image velocimetry. The upper window is a zoom-in around the track line.

In this study, the Free-LSPIV particle image velocimetry algorithm [24–26] was used. Particle image velocimetry (other image velocimetry variants include particle tracking, space-time, optical flow etc. [27]) is based on the assumption that the most probable displacement of the particles within a flow captured in two subsequent frames of a video is the displacement that maximizes the correlation function. The process involves dividing the preceding frame into tiles, referred to as interrogation areas. Subsequently, these areas are compared for similarity (via the correlation function) with all subregions of the corresponding search areas, in the following frame. This enables a reliable estimation of motion yielding valuable insights into the velocity field of the fluid or particles under consideration [11].

The Free-LSPIV algorithm processes video frames along a predefined track line, with an arbitrary number of points representing the centers of interrogation areas. Sequential runs of Free-LSPIV, each using different predefined track lines, can be employed to obtain velocities over a specific area of the flow. However, for this study, a single track line was utilized. The algorithm outputs velocity vectors at these points for the time intervals between the video frames. In this case study, velocity vectors were obtained at 100 points (**Figure 1**).

The data obtained by Free-LSPIV were stored in the 2D matrix $\boldsymbol{V}$ with dimensions nt × $2n$. In this case, nt was 597 (representing the number of intervals between the 598 video frames), and n was 100 (indicating the number of points along the track line, as shown in **Figure 1**). This resulted in 200 columns of $\boldsymbol{V}$, which store the vector components along the principal flow directions (streamwise and vertical) for the 597 time steps. The matrix contained NaN (not a number) values corresponding to time instances and locations for which Free-LSPIV could not obtain velocity estimations due to the lack of distinct features (particles) in the specific locations of the corresponding frames.

Because some of the algorithms used in the analysis cannot handle NaN values (e.g., the fast Fourier transformation algorithm), 1D linear interpolations (applied separately for each column of the matrix $\boldsymbol{V}$) were used to fill the missing values.

2.2 Stochastic analysis of image velocimetry data

The stochastic model used in this study was a multivariate autoregressive of order 1. This is described by the following equation [28,29]:

$$\boldsymbol{v}_t = \boldsymbol{A}\, \boldsymbol{v}_{t-1} + \boldsymbol{B}\, \boldsymbol{\varepsilon}_t \tag{1}$$

$\boldsymbol{v}_t$ and $\boldsymbol{v}_{t-1}$ are $2n \times 1$ vectors of which elements are the transposed rows t and $t-1$ of the matrix $\boldsymbol{V}$, respectively, $\boldsymbol{A}$ is a $2n \times 2n$ matrix, $\boldsymbol{\varepsilon}_t$ is a $2n \times 1$ vector with independent and identically distributed random numbers following the N(0,1) distribution, and $\boldsymbol{B}$ is a $2n \times 2n$ matrix, where $2n$ is the number of the random variables (in this case, $2n$ equals 200 with the first 100 values corresponding to the streamwise vector components and the next 100 to the vertical vector components of the 100 points along the track line).

The matrices $\boldsymbol{A}$ and $\boldsymbol{B}$ can be calculated with the following formulas based on the available observations:

$$\boldsymbol{A} = \mathrm{cov}[\boldsymbol{V}, \boldsymbol{V}_1]\, (\mathrm{cov}[\boldsymbol{V}, \boldsymbol{V}])^{-1} \tag{2}$$

$$\boldsymbol{B}\boldsymbol{B}^{\mathrm{T}} = \mathrm{cov}[\boldsymbol{V}, \boldsymbol{V}] - \boldsymbol{A}\, \mathrm{cov}[\boldsymbol{V}, \boldsymbol{V}]\, \boldsymbol{A}^{\mathrm{T}} \tag{3}$$

where $\boldsymbol{V}_1$ is the vertical circular shift of $\boldsymbol{V}$ (the row t of $\boldsymbol{V}$ is the same as the row t+1 of $\boldsymbol{V}_1$).

The right-hand side of Equation (2) and Equation (3) can be computed directly from the data. However, a decomposition should be applied to the matrix obtained by the right-hand side of Equation (3) to obtain the matrix $\boldsymbol{B}$. In this study, the eigendecomposition method was employed [30]. According to this method, any square matrix, the right-hand side of Equation (3) in this case, that has eigenvalues λ_i and eigenvectors $\boldsymbol{z}_i$, $i = 1, \ldots, 2n$, equals the product $\boldsymbol{Z}\,\boldsymbol{L}\,\boldsymbol{Z}^{-1}$, where $\boldsymbol{Z}$ is the $2n \times 2n$ matrix with the eigenvectors $\boldsymbol{z}_i$ and $\boldsymbol{L}$ the $2n \times 2n$ diagonal matrix with its eigenvalues λ_i [31]. Since the right-hand side of Equation (3) is symmetric, the matrix $\boldsymbol{Z}$ is orthogonal (or orthonormal) [32], and hence $\boldsymbol{Z}^{-1} = \boldsymbol{Z}^{\mathrm{T}}$. If $\boldsymbol{L}^{0.5}$ is the matrix for which $\boldsymbol{L}^{0.5}\, \boldsymbol{L}^{0.5} = \boldsymbol{L}$, then Equation (3) becomes:

$$\boldsymbol{B}\boldsymbol{B}^{\mathrm{T}} = \boldsymbol{Z}\,\boldsymbol{L}\,\boldsymbol{Z}^{-1} = (\boldsymbol{Z}\,\boldsymbol{L}^{0.5})\,(\boldsymbol{L}^{0.5}\,\boldsymbol{Z})^{\mathrm{T}} \tag{4}$$

and therefore

$$\boldsymbol{B} = \boldsymbol{Z}\,\boldsymbol{L}^{0.5} \tag{5}$$

While various researchers have provided an intuitive description of the physical meaning of matrices $\boldsymbol{A}$ and $\boldsymbol{B}$, attributing the former to the strength of the influence of memory and the latter to the strength of randomness, concerns have been raised regarding the mathematical consistency of this definition, particularly with respect to the concept of "memory" [33].

Equation (1) applies to variables with a zero mean. Consequently, the observed time series should be standardized to have a zero mean before applying Equations (1) to (5). Subsequently, the generated time series from Equation (1) should be destandardized (by adding back the mean) to restore the intended statistical properties.

3. Results

The stochastic model described by Equation (1) was applied to produce 20000 × 200 synthetic velocity values (100 streamwise vector components and 100 vertical vector components at 20000-time steps). **Figure 2** displays the mean and standard deviation of the synthetic and observed velocity values at the 100 points along the track line. **Figure 3** displays the correlation coefficient between the streamwise components of the velocities at two subsequent points, and the correlation coefficient between the components of the velocity vector at all 100 points.

Figures 4 and 5 display the histogram and the second-order characteristics (the power spectrum and the climacogram) of the streamwise and vertical components of the velocity vector at the point $i = 50$ of the track line.

The red line in the power spectrum of **Figures 4 and 5** indicates the theoretically expected slope of –5/3 at the inertial sub-range, based on the Kolmogorov conceptual framework for turbulence [34]. The figures also provide the slope of the trend line that best fits the spectrum and the Hurst coefficient of the climacogram. The Hurst coefficient is related to the slope of the climacogram for the higher scales (or lower frequencies) according to the formula $H = 1 + \text{slope}/2$ [33].

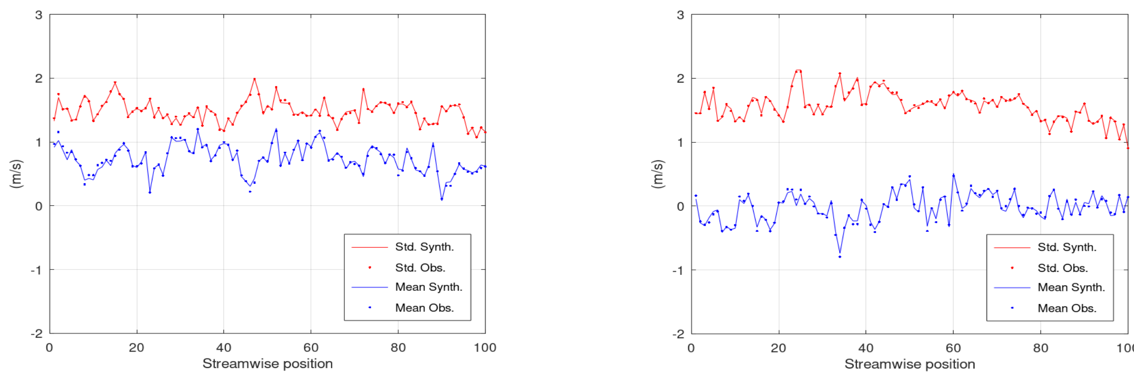

(A) (B)

Figure 2. Comparison of the mean and standard deviation values of the observed and synthetic velocities at the 100 points of the track line; (A) mean and standard deviation values of the components of the velocity vectors along the streamwise direction, i.e., mean(v_{xi}) and std(v_{xi}), (B) mean and standard deviation values of the vertical components of the velocity vectors, i.e., mean(v_{yi}) and std(v_{yi}), where $i = 1, \ldots, 100$ in both (A) and (B).

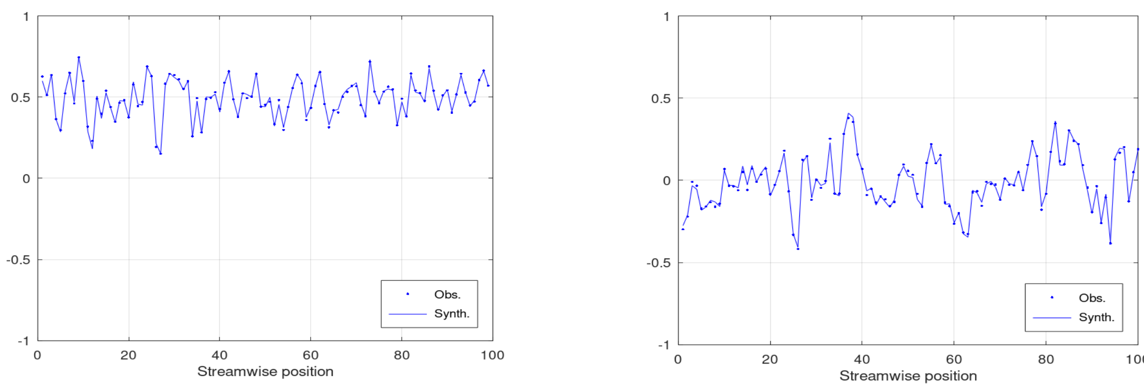

(A) (B)

Figure 3. Comparison of the correlation coefficients of the observed and synthetic velocities at the 100 points of the track line; (A) $\rho(v_{xi}, v_{xi+1})$, where $i = 1, \ldots, 99$; (B) $\rho(v_{xi}, v_{yi})$, where $i = 1, \ldots, 100$.

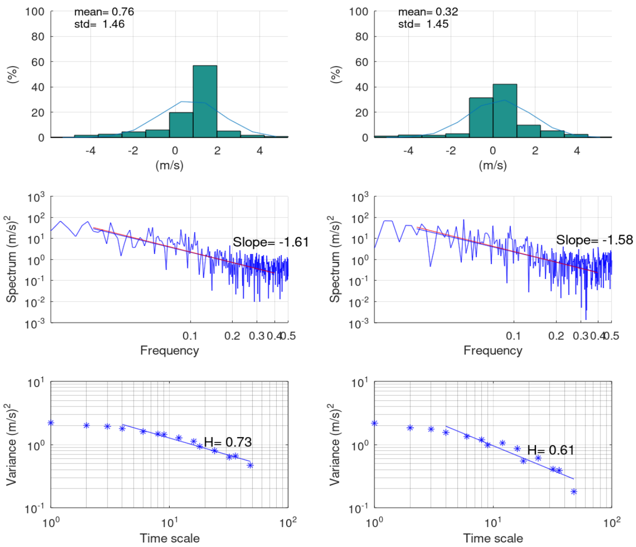

Figure 4. First- and second-order characteristics of the observed velocity (597 time steps) at point i = 50 of the track line. The left column corresponds to the streamwise component of the velocity vector and the right column corresponds to the vertical component.

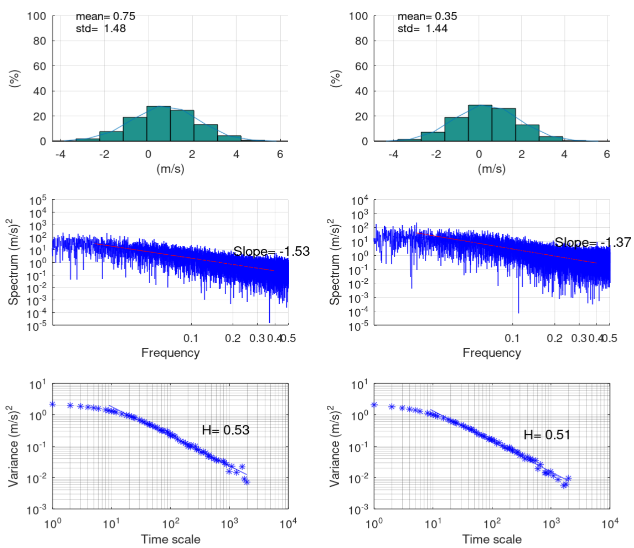

Figure 5. First- and second-order characteristics of the synthetic velocity (20000 time steps) at point i = 50 of the track line. The left column corresponds to the streamwise component of the velocity vector and the right column corresponds to the vertical component.

A collective comparison of the slope of the power spectrum of the observed and synthetic data is given in Table 1. The spectrum slope is estimated in the frequency region [0.02, 0.4] for all points of the track line. This region was selected because it gave the closest mean value to the expected theoretical, and at the same time the lowest standard deviation.

Table 1. The mean and the standard deviation of the 100 spectrum slopes of the velocity values at the 100 points along the track line.

	Mean	Standard deviation
Observed streamwise component	–1.68	0.21
Synthetic streamwise component	–1.66	0.20
Observed vertical component	–1.69	0.27
Synthetic vertical component	–1.66	0.22

A collective comparison of the H coefficient of the observed and synthetic time series is provided in **Table 2**.

Table 2. The mean and the standard deviation of the H coefficients of the two velocity vector components at the 100 points along the track line.

	Mean	Standard deviation
Observed streamwise component	0.70	0.078
Synthetic streamwise component	0.58	0.043
Observed vertical component	0.70	0.075
Synthetic vertical component	0.58	0.037

Figure 6 displays the return period plot of v_x^2, $v_x'^2$ and $|v_x' \cdot v_y'|$ at points i = 1 and 50 of the track line. The return period of a specific value is estimated with the formula $T/\Delta t = 1/(1 - P)$ [33], where Δt is the time step of the assessment, 1/24 second in this case, and P is the probability of non-exceedance of this specific value. The latter is estimated empirically with the Hazen plotting position, which is consistent with a set of statistical preconditions [35]. The probability of non-exceedance is estimated also for v_x^2 and $v_x'^2$ from the chi-square distribution with one degree of freedom.

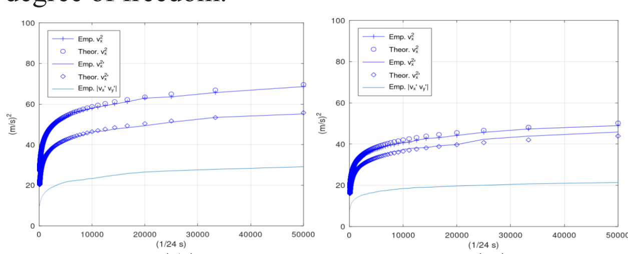

(A) (B)

Figure 6. Return-period plot of v_x^2, $v_x'^2$ and $|v_x' \cdot v_y'|$ at points (A) i = 1, and (B) i = 50 of the track line.

4. Discussion

Figures 2 to 6 and **Tables 1 and 2**, featuring the statistical metrics outlined in the preceding section, are dedicated to scrutinizing the effectiveness of the stochastic model in interpreting data acquired through the image velocimetry algorithm. The model showcased commendable performance in accurately capturing both first and select second-order statistics observed in the data. At all 100 points along the track line, it accurately reproduced the mean and standard deviation of the observed velocity time series, the correlation coefficient between the streamwise velocity components of two neighboring points, and the correlation coefficient between the two velocity components of any point. Yet, for this kind of application, it is crucial to ensure that the synthetic data manifests the distinctive statistical properties originating from the hydraulic conditions that define turbulent flows.

An essential characteristic of stochastic processes representing turbulent flows is the trend of the spectrum in the inertial sub-range of fully developed turbulence. Within this sub-range, smaller eddies transfer energy to larger eddies, creating a cascade of energy across various length scales. According to Kolmogorov, the spectrum in this sub-range tends to follow a power law with an exponent equal to –5/3 [34]. In our case study, the spectrum of both the synthetic and observed data demonstrated average slopes compatible with this power law in the frequency range [0.02, 0.4] (refer to **Figures 4 and 5**). Regarding the synthetic time series, this was encouraging since the mathematical analysis of autoregressive models, like the one used in this study, suggests that the log-log slope of the power spectrum of a time series produced with Equation (1) smoothly ranges from 0 for low frequencies to –2 for high frequencies, with the rate of decay determined by the values of the matrix $\boldsymbol{A}$ [33]. Noticeably, the average log-log slope of the synthetic time series in the inertial sub-range was virtually equal to the theoretically expected value of –5/3 (**Table 1**).

Another important characteristic of stochastic processes that represent turbulent flows is the long-term persistence, also known as Hurst-Kolmogorov (HK) behavior. The accurate representation of the HK dynamics is very important for assessing the hydraulic stresses induced by turbulent flows. According to Nordin et al. [36], the range of the cumulative sum of departures of any subset of the observed time series of the velocity of a turbulent flow with mean value u_m presents a scaling behavior according to the rule:

$$R \sim \sigma\, s^{H} \tag{6}$$

where σ is the standard deviation of the subset, s is the time scale or the subset length, H the Hurst coefficient, and $R = \max\{\Sigma_t\, u_t - t\, u_m\} - \min\{\Sigma_t\, u_t - t\, u_m\}$ with $t = 0, \ldots, s$. The value of R ranges from 0 to higher values, where 0 corresponds to a time series of a constant value. Higher values of R indicate both persistence and higher excursions from the mean value.

From Equation (6) it becomes evident that the Hurst coefficient plays an important role in the duration and magnitude of the deviations of the velocity from the mean value. According to **Table 2**, the average Hurst coefficient of the observed and synthetic velocities is 0.70 and 0.58 respectively. This deviation was expected because of the Markovian nature of the stochastic model employed in this study. The climacogram of the synthetic time series (**Figure 5**) exhibits the typical pattern of the climacogram of a Markovian process [33]. In this case study, the Hurst coefficient of the observed was relatively low. However, H values up to 0.9 are not uncommon in turbulent flows [37]. For such cases, a generalized Hurst-Kolmogorov stochastic model should be considered [1].

Figure 6 is the most important output of this study and could form the basis for a probabilistic assessment of the potential impacts of turbulent flow on nearby construction. The return period plots at points $i = 1$ and 50 provide a direct visual assessment of the stressful conditions at these assessed locations. The magnitude of the stresses decreases with distance from the hydraulic jump, which is manifested by the lowering of the curves.

Consider a scenario where the previous case study concerned the assessment of the stress on a construction at point 1 of the track line. If the study was limited exclusively to the analysis of the data obtained by the image velocimetry method, the reported maximum v_x^2 value during the 25-second video recording period would be 34.87 $(m/s)^2$. However, there is no specific reason why the assessment period should be constrained to the duration of the video or the duration of any other monitoring procedure (e.g., the duration of sampling with a current meter). The assessed construction will remain subject to stresses for extended periods. Ideally, the stress values used for the design or the estimation of impacts on the construction should be based on the following formulation: given the expected duration $k\,\Delta t$ of a stressful event, and an acceptable probability of exceedance at least once during the assessed period (probability of failure) equal to R, what are the expected maximum stress values. The handling of this probabilistic formulation is as follows. Given the values of k and R, and by employing the probability of failure equation [38]:

$$R = 1 - (1 - \Delta t / T)^k \tag{7}$$

One could solve for T, and then from **Figure 6** obtain the estimation for the design values.

Figure 6 indicates that a stress level of 34.87 $(m/s)^2$ corresponds to a return period of 308 time steps (each time step being 1/24 second). This results in a relatively short duration of 13 seconds, which is notably shorter than the expected duration of high flows capable of inducing intense turbulence and increased stresses on a structure.

It should be noted that in a comprehensive study, **Figure 6** should also include the confidence limits of the return period plots [33]. This would require generating not a single, but a set of synthetic time series.

Future research could focus on alternative stochastic models to address various issues that were unveiled in this study.

- As mentioned previously, models that accurately represent the Hurst-Kolmogorov behavior should be assessed. This will enable the capture of this important second-order characteristic for reproducing the effect of persistence.
- The stochastic model used in this case study is 1D in the sense that the index set of the process concerns one dimension, the time in Equation (1). By extending the set to three dimensions, one could explore comprehensive spatio-temporal approaches, like those employed in geostatistics [39]. However, multidimensional modeling is challenging and, for this reason, is employed only in a small portion of stochastic model applications.
- The histograms in **Figure 4** suggest that some of the observed time series do not follow normal distribution. It should be noted that Equation (3) is an underdetermined system of equations, therefore Equation (5) is only one of the infinite alternative solutions. For example, Koutsoyiannis has suggested a solution of Equation (3) that preserves the skewness [28]. This may prove advantageous in cases where the distribution of the involved random variables is not Gaussian.
- An alternative coordinate system could be employed to express the velocity vector into scalar variables. For example, in weather forecast modeling they have suggested employing polar coordinates since with Cartesian coordinates there is an incentive to minimize the wind magnitude in the face of predictive uncertainty. Using polar coordinates, accounting for both magnitude and angular direction, may offer advantages in such instances [40].

5. Conclusions

In this study, we presented a novel approach that integrates image velocimetry with a stochastic model to comprehensively analyze turbulent flows, with a focus on hydraulic jumps as a characteristic case. The synergy of these methodologies allowed for a nuanced understanding of flow dynamics, offering insights that contribute to both hydraulic engineering and structure design.

The proposed stochastic model, a multivariate autoregressive model of order 1, demonstrated commendable performance in capturing statistical properties of turbulent flows. Through the analysis of synthetic and observed data, we observed the model's ability to reproduce key characteristics of the statistical properties and structure.

The power law behavior in the inertial subrange of fully developed turbulence was verified, with the spectral analysis revealing an exponent close to the theoretical –5/3. This alignment with Kolmogorov's theory reaffirms the accuracy of the image velocimetry data and the stochastic model. Additionally, the study delved into the long-term persistence, or Hurst-Kolmogorov behavior, revealing insights into the scaling behavior of velocity deviations from mean values.

The significance of this work lies in its potential applications for assessing hydraulic stresses on nearby constructions in turbulent flow scenarios. By providing a probabilistic framework for extreme velocity values, the methodology presented here offers a valuable tool for hydraulic engineering practices. The return-period plot emerges as a pivotal output of the stochastic model, allowing for a probabilistic assessment of potential impacts on nearby constructions over extended durations.

In conclusion, the integrated approach presented in this study opens avenues for advancements in the field of turbulent flow analysis. By bridging image velocimetry and stochastic modeling, we not only validate the accuracy of our methodology but also contribute valuable insights that can inform the design, safety considerations, and risk assessments of hydraulic structures under diverse flow conditions. Moreover, the demonstrated efficacy of our integrated approach in hydraulic model experiments underscores its applicability in practical settings, enhancing the reliability and precision of flow analyses crucial for hydraulic engineering.

Author Contributions

Conceptualization, E.R. and D.K.; methodology, E.R.; software, E.R.; validation, J.L. and D.K.; formal analysis, E.R.; investigation, E.R.; resources, J.L.; data curation, E.R.; writing—original draft preparation, E.R.; writing—review and editing, J.L. and D.K.; visualization, E.R.; supervision, E.R.; project administration, E.R.

Conflict of Interest

The authors declare no conflict of interest.

Funding

This research received no external funding.

Acknowledgments

The authors wish to thank the Deutscher Akademischer Austauschdienst (DAAD) for covering the travel costs necessary for the completion of this study.

References

[1] Dimitriadis, P., Koutsoyiannis, D., Papanicolaou, P., 2016. Stochastic similarities between the microscale of turbulence and hydro-meteorological processes. Hydrological Sciences Journal. 61(9), 1623–1640. DOI: https://doi.org/10.1080/02626667.2015.1085988

[2] Gautam, P., Eldho, T.I., Mazumder, B.S., et al., 2019. Experimental study of flow and turbulence characteristics around simple and complex piers using PIV. Experimental Thermal and Fluid Science. 100, 193–206. DOI: https://doi.org/10.1016/j.expthermflusci.2018.09.010

[3] Mortazavi, M., Le Chenadec, V., Moin, P., et al., 2016. Direct numerical simulation of a turbulent hydraulic jump: Turbulence statistics and air entrainment. Journal of Fluid Mechanics. 797, 60–94. DOI: https://doi.org/10.1017/jfm.2016.230

[4] Leandro, J., Carvalho, R., Chachereau, Y., et al., 2012. Estimating void fraction in a hydraulic jump by measurements of pixel intensity. Experiments in Fluids. 52, 1307–1318. DOI: https://doi.org/10.1007/s00348-011-1257-1

[5] Murzyn, F. (editor), 2010. Assessment of different experimental techniques to investigate the hydraulic jump: do they lead to the same results. 3rd International Junior Researcher and

Engineer Workshop on Hydraulic Structures; 2010 May 4–6; Edinburgh, Scotland.

[6] Wang, H., Murzyn, F., 2017. Experimental assessment of characteristic turbulent scales in two-phase flow of hydraulic jump: from bottom to free surface. Environmental Fluid Mechanics. 17, 7–25. DOI: https://doi.org/10.1007/s10652-016-9451-6

[7] Jyoti, J.S., Medeiros, H., Sebo, S., et al., 2023. River velocity measurements using optical flow algorithm and unoccupied aerial vehicles: A case study. Flow Measurement and Instrumentation. 91, 102341. DOI: https://doi.org/10.1016/j.flowmeasinst.2023.102341

[8] Jin, T., Liao, Q., 2019. Application of large scale PIV in river surface turbulence measurements and water depth estimation. Flow Measurement and Instrumentation. 67, 142–152. DOI: https://doi.org/10.1016/j.flowmeasinst.2019.03.001

[9] Emadzadeh, A., Chiew, Y.M. (editors), 2017. Bubble dynamics and PIV measurements in a hydraulic jump. The 37th IAHR World Congress; 2017 Aug 13–18; Kuala Lumpur, Malaysia.

[10] Ayegba, P.O., Edomwonyi□Otu, L.C., 2020. Turbulence statistics and flow structure in fluid flow using particle image velocimetry technique: A review. Engineering Reports. 2(3), e12138. DOI: https://doi.org/10.1002/eng2.12138

[11] Fujita, I., Muste, M., Kruger, A., 1998. Large-scale particle image velocimetry for flow analysis in hydraulic engineering applications. Journal of hydraulic Research. 36(3), 397–414. DOI: https://doi.org/10.1080/00221689809498626

[12] Fujita, I., Kawamura, Y. (editors), 2001. Discharge measurements of flood flow by imaging technology and float method. Proceedings of the 29th Congress of IAHR; 2001 Sep 16–21; Beijing, China.

[13] Watanabe, K., Fujita, I., Iguchi, M., et al., 2021. Improving accuracy and robustness of space-time image velocimetry (STIV) with deep learning. Water, 13(15), 2079. DOI: https://doi.org/10.3390/w13152079

[14] Shi, R., Leng, X., Chanson, H., 2020. On optical flow techniques applied to breaking surges. Flow Measurement and Instrumentation. 72, 101710. DOI: https://doi.org/10.1016/j.flowmeasinst.2020.101710

[15] Johnson, E.D., Cowen, E.A., 2017. Estimating bed shear stress from remotely measured surface turbulent dissipation fields in open channel flows. Water Resources Research. 53(3), 1982–1996. DOI: https://doi.org/10.1002/2016WR018898

[16] Romagnoli, M., Carvalho, R., Leandro, J., 2013. Turbulence characterization in a gully with reverse flow. Journal of Hydraulic Engineering. 139(7), 736–744. DOI: https://doi.org/10.1061/(ASCE)HY.1943-7900.0000737

[17] Pope, S.B., 2001. Turbulent flows. Measurement Science and Technology. 12(11). DOI: https://doi.org/10.1088/0957-0233/12/11/705

[18] Papoulis, A., 1990. Probability and statistics. Prentice-Hall: New Jersey. pp. 219.

[19] Patnaik, P.B., 1949. The Non-Central χ2- and F-Distribution and their applications. Biometrika. 36 (½), 202–232. DOI: https://doi.org/doi:10.2307/2332542

[20] Nadarajah, S., Pogány, T.K., 2016. On the distribution of the product of correlated normal random variables. Comptes Rendus. Mathématique. 354(2), 201–204. DOI: https://doi.org/10.1016/j.crma.2015.10.019

[21] Cui, G., Yu, X., Iommelli, S., et al., 2016. Exact distribution for the product of two correlated Gaussian random variables. IEEE Signal Processing Letters. 23(11), 1662–1666. DOI: https://doi.org/10.1109/LSP.2016.2614539

[22] Zare, A., Georgiou, T.T., Jovanović, M.R., 2020. Stochastic dynamical modeling of turbu-

lent flows. Annual Review of Control, Robotics, and Autonomous Systems. 3, 195–219. DOI: https://doi.org/10.1146/annurev-control-053018-023843

[23] Czibere, T., 2006. Calculating turbulent flows based on a stochastic model. Journal of Computational and Applied Mechanics. 7(2), 155–188.

[24] Rozos, E., Dimitriadis, P., Mazi, K., et al., 2020. On the uncertainty of the image velocimetry method parameters. Hydrology. 7(3), 65. DOI: https://doi.org/10.3390/hydrology7030065

[25] Rozos, E., Mazi, K., Koussis, A.D., 2021. Probabilistic evaluation and filtering of image velocimetry measurements. Water. 13(16), 2206. DOI: https://doi.org/10.3390/w13162206

[26] Rozos, E., Mazi, K., Lykoudis, S., 2022. On the accuracy of particle image velocimetry with citizen videos—five typical case studies. Hydrology. 9(5), 72. DOI: https://doi.org/10.3390/hydrology9050072

[27] Wijaya, F., Liu, W.C., Huang, W.C., 2023. Comparative assessment of different image velocimetry techniques for measuring river velocities using unmanned aerial vehicle imagery. Water. 15(22), 3941. DOI: https://doi.org/10.3390/w15223941

[28] Koutsoyiannis, D., 1999. Optimal decomposition of covariance matrices for multivariate stochastic models in hydrology. Water Resources Research. 35(4), 1219–1229. DOI: https://doi.org/10.1029/1998WR900093

[29] Matalas, N.C., 1967. Mathematical assessment of synthetic hydrology. Water Resources Research. 3(4), 937–945. DOI: https://doi.org/10.1029/WR003i004p00937

[30] Goodfellow, I., Bengio, Y., Courville, A., 2016. Deep learning. MIT Press: Cambridge. pp. 40.

[31] Rawlings, J.O., Pantula, S.G., Dickey, D.A., 1998. Applied regression analysis: A research tool. Springer: New York. pp. 58.

[32] Searle, S.R., 1982. Matrix algebra useful for statistics. John Wiley & Sons: New York.

[33] Koutsoyiannis, D., 2023. Stochastics of hydroclimatic extremes—A cool look at risk, edition 3. Kallipos Open Academic Editions: Athens. DOI: https://doi.org/10.57713/kallipos-1

[34] Biferale, L., Boffetta, G., Castaing, B., 2003. Fully developed turbulence. The Kolmogorov legacy in physics. Springer-Verlag: Heidelberg. pp. 149–172.

[35] Hyndman, R.J., Fan, Y., 1996. Sample quantiles in statistical packages. The American Statistician. 50(4), 361–365.

[36] Nordin, C.F., McQuivey, R.S., Mejia, J.M., 1972. Hurst phenomenon in turbulence. Water Resources Research. 8(6), 1480–1486. DOI: https://doi.org/10.1029/WR008i006p01480

[37] Dimitriadis, P., Papanicolaou, P. (editors), 2012. Statistical analysis of turbulent positively buoyant jets. European Geosciences Union General Assembly 2012; 2012 Apr 22–27; Vienna, Austria.

[38] Te Chow, V., Maidment, D.R., Mays, L.W., 1988. Applied hydrology. McGraw-Hill: New York.

[39] Kitanidis, P.K., 1993. Geostatistics. The handbook of hydrology. McGraw-Hill: New York.

[40] Lam, R., Sanchez-Gonzalez, A., Willson, M., et al., 2023. Learning skillful medium-range global weather forecasting. Science. 382(6677), 1416–1421. DOI: https://doi.org/10.1126/science.adi2336

BILINGUAL PUBLISHING GROUP

Journal of Environmental & Earth Sciences

https://journals.bilpubgroup.com/index.php/jees

REVIEW

Effect of No Tillage and Conventional Tillage on Wheat Grain Yield Variability: A Review

Kenza Kadiri Hassani [1,2,3*], ***Rachid Moussadek*** [2,3], ***Bouamar Baghdad*** [4], ***Abdelmjid Zouahri*** [3], ***Houria Dakak*** [3], ***Hassnae Maher*** [2,3,5], ***Abdelhak Bouabdli*** [1]

[1] *Laboratory of Geosciences, Department of Geology, Faculty of Sciences, Ibn Tofail University, Kenitra B.P. 242, Morocco*

[2] *International Center for Agricultural Research in the Dry Areas (ICARDA), Rabat P.O. Box 1014, Morocco*

[3] *Research Unit on Environment and Conservation of Natural Resources, Regional Center of Rabat, National Institute of Agricultural Research, Rabat P.O. Box 6356, Morocco*

[4] *Georesources Environmentalist Consultant/Expert, Associate Professor at Casablanca School of Architecture and Landscape—Honoris United Universities, Casablanca, B.P. 20100, Morocco*

[5] *Laboratory of Materials, Nanotechnology and Environment, Department of Chemistry, Faculty of Sciences, Mohammed V University, Rabat B.P. 703, Morocco*

ABSTRACT

Conservation Agriculture (CA) covers more than 205 million hectares in the world. This made it possible to face and mitigate the challenges of climate change, reducing soil erosion and providing multiple ecosystem services. The first elementary factor influenced is the yield evaluation. It has a direct effect on farmers' choices for sustainable production. The present article records a review focused on wheat yield average positive change compared between conventional tillage (CT) and no tillage (NT) systems. The international database collected showed that NT is adaptable everywhere. The results of wheat yield differentiation showed the influence of crop rotation depending on stations located in different climatic zones. In more than 40 years of research, specialists have succeeded in demonstrating the importance of crop productivity like wheat. The whole integrates also experimentations where the initiation starts more than ten years.

Keywords: Climate change; No tillage; Crop rotation; Wheat; Yield

*CORRESPONDING AUTHOR:

Kenza Kadiri Hassani, Laboratory of Geosciences, Department of Geology, Faculty of Sciences, Ibn Tofail University, Kenitra B.P. 242, Morocco; International Center for Agricultural Research in the Dry Areas (ICARDA), Rabat P.O. Box 1014, Morocco; Research Unit on Environment and Conservation of Natural Resources, Regional Center of Rabat, National Institute of Agricultural Research, Rabat P.O. Box 6356, Morocco; Email: kenza.kadiri-hassani@uit.ac.ma

ARTICLE INFO

Received: 16 January 2024 | Revised: 29 March 2024 | Accepted: 31 March 2024 | Published Online: 22 April 2024

DOI: https://doi.org/10.30564/jees.v6i1.6172

CITATION

Kadiri Hassani, K., Moussadek, R., Baghdad, B., et al., 2024. Effect of No Tillage and Conventional Tillage on Wheat Grain Yield Variability: A Review. Journal of Environmental & Earth Sciences. 6(1): 57–70. DOI: https://doi.org/10.30564/jees.v6i1.6172

1. Introduction

The agricultural challenges faced many obstacles to maintaining sustainable productivity and preserving the environment [1]. Climate change has a hard impact on the environment and economic ways as it was reported by Schlegel et al., and Moussadek et al. [2,3]. These alterations particularly affect productivity at the international market level. Today, technical and technological progress is being recognized for a better confrontation to these phenomena [4]. Since the end of the Second World War, a certain modernization of agriculture has been established. It concerned also the pollution of groundwater and the disturbance of the nitrogen cycle and carbon cycle. They all are repercussed on developing new strategies [5].

The continual evolution made it possible to adopt new alternative models that can combine several options under CA. It allowed permanent soil covered for years, ensuring sustainability and limiting the use of inputs [3]. The NT system used to take in account the agriculture conditions. The results obtained during the period 1960–2000 made it possible to translate how we can have productivity on the same surface area under CA. The basics of NT include the importance of adopting this practice for many kinds of environments allowing the minimum optimization of inputs used [1,5].

The extension and the determination of CA could after years be resilient to drought effect with better water storage as it was explained by Bouzza [6]. It helps to protect the growing season. Yield evaluation is linked to growth effects.

These are taken into consideration for cereal productions where NT was tested a lot under different aspects. Cereals yield interest represents a large part of agricultural productivity for many countries [7]. According to a couple of programs developed in Mediterranean areas wheat yield profitability varies between 8 and 20% compared to CT [3]. The variability of wheat yield is also attached to the different climates and crop rotation. This work aims to compare the wheat yield of two systems (CT/NT) under each climate and crop rotation adapted.

2. Materials and method

The set of data used was carefully collected and checked from the original papers. That integrates different stations all over the world localized in Morocco, Tunisia, Algeria, Spain, Mexico, USA, Canada, China, Brazil and Australia. It was actualized following the process reported by Su et al. [8], Pittelkow et al. [9] and also Ponisio et al. [10] in their meta-analysis. This is all, in addition to more values of the Maghreb data situation (**Table 1**). It implied the common factors of location, crop sequences, wheat yield under NT and CT, soil texture and climate type. After years of experimentations, searchers analyzed the value of the type of rotation that should be specified. The grain wheat yield variability (%) (GWYV) calculated: ((NTyield-CTyield)/CTyield) × 100 shows us the guidelines in our case depending on crop rotation with qualified soils (Clay and loam) (**Table 1**).

3. Results and discussions

The world is targeted with serious warming signs for projections of the future. The vulnerability indicates strongly the decrease in crop development with an approaching influence of drought. The adoption of NT is a resolution that responds to the distress situation. Climate change is directly relied on agricultural challenges. Uncertainties persist and impact the attention on soil and water resources. The recent data reported by Schmidt et al. [64] point to the alarming temperature deviation between 1930 and 2023.

Over the years, NT proved its place in CA and how it can cope with different phenomena. This work continuously joins the meta-analysis carried out by Su et al. [10]. It marks the interest of the advances of the NT in the Maghreb area. Many conclusions are retained in the long term [15]:

-Reducing energy consumption and inputs used.

-Improving more greenhouse gas balance.

-Restoring organic matter which efficiently is favorable on soil organic stocks.

-Protecting soil against erosion by monitoring crop rotation and residues.

-Ensuring crop yield productivity.

The profitability of wheat yield under CA evolution describes the perspectives for sustainable agriculture.

Table 1. The grain wheat yield variability (%) evaluation under NT and CT.

Location	Year of activity	Years of NT	Crop rotation system	Yield on NT (t/ha)	GWYV (%)	Authors
Algeria						
Setif	2018		Wheat-Tritical-Pea	1,50	24	*Chouter, et al.,* [11]
	2017		Wheat-Lentil	2,68	10	
	2016		Continuous wheat	1,31	70	
	2012			2,20	13	*Taibi, et al.,* [12]
	2011			2,00	–17	
	2010			3,20	28	
	2009			3,75	56	
	2008			1,70	17	
	2010	2		0,30	19	*Chennafi, et al.,* [13]
	2009			0,22	–4	
Oued Smar	2017	-	Wheat-bersim	6,41	5	*Yachi,* [14]
				5,59	1	
Morocco						
Abda	1982	10	Wheat-fallow	3,10	29	*Mrabet,* [15]
		19	Continuous wheat	1,60	0	
Ain Sbit	2021	1	Wheat - lentil	6,99	-	*Raji,* [16]
				6,62	1912	
		2		4,58	316	
		1		7,17	229	
				4,06	152	
		2		7,20	140	
				5,36	48	
		1		11,89	18	
		2		2,20	17	
				7,44	–5	
Chaouia	1996	2	Continuous wheat	6,88	10	*Mrabet,* [17]
				2,03	–1	
	1995	1		12,51	–2	
				4,15	–5	
	1982	10	Wheat-fallow	3,70	42	*Bouazza,* [6]
	-	3	Wheat-chickpeas	1,87	146	*Mrabet,* [18]
	-	9		2,53	72	*Mrabet,* [19]
	-	9	Different rotation	2,21	16	*Mrabet,* [20]
	1982	10	Continuous wheat	1,90	36	*Mrabet,* [17]
		19		2,47	5	
Gharb	-	3		2,8	24	*Razine and Raguine,* [21]
Merchouch	2020	18	Durum wheat-legume	4,15	26	*Maher, et al.,* [22]
				4,62	7	
				4,18	7	
				4,22	5	
				3,17	–1	

Table 1 continued

Location	Year of activity	Years of NT	Crop rotation system	Yield on NT (t/ha)	GWYV (%)	Authors
Merchouch	2018	15	Wheat-chickpea-barley-lentil	2,15	13	*Devkota, et al.,* [23]
	2016	13		3,00	33	
	2015	12		0,90	80	
	2014	11		2,80	47	
	2010	7	Soft wheat-lentil	3,80	6	*Moussadek, et al.,* [3]
	2009	6		1,70	–11	
	2008	5		4,70	12	
	2007	4		2,60	44	
	2006	3		0,50	25	
	2005	2		4,60	15	
	2004	1		1,50	50	
Saïs	-	4	Different rotation	2,55	2	*Mrabet and Moussadek,* [24]
	-			2,72	–1	
	2020	-		4,11	21	*Sellami, et al.,* [25]
	2019	-		2,60	27	
Zaer	-	4	Wheat-lentil	1,97	40	*Mrabet and Moussadek,* [24]
	-			2,99	10	
	-			2,71	9	
Tunisia						
Kef	2014	-	Fababean-durum wheat-barley	2,70	5	*Chaieb, et al.,* [26]
Koudiat	2013		Durum wheat-fababean	3,82	7	*Mouelhi, et al.,* [27]
			Durum wheat-barley	1,96	7	
			Durum wheat-oat	2,17	6	
	2012		Durum wheat-barley	2,46	8	
			Durum wheat-fababean	4,29	7	
			Durum wheat-oat	2,19	–7	
	2011		Durum wheat-fababean	3,75	19	
			Durum wheat-barley	2,98	19	
			Durum wheat-oat	2,85	6	
	2010		Durum wheat-fababean	3,43	10	
			Durum wheat-oat	3,03	7	
			Durum wheat-barley	3,21	6	
	2009		Durum wheat-oat	3,42	9	
			Durum wheat-fababean	3,46	4	
			Durum wheat-barley	3,40	–12	
Krib	-	4	Durum wheat-pea-oat	3,68	6	*Ben Moussa-Machraoui, et al.,* [28]
Mahassen	-		Durum wheat-barley	1,43	72	
-	-	5	Continuous wheat	2,18	12	*M'hedhbi, et al.,* [29]
Mateur		2		3,90	18	*Vadon, et al.,* [30]
Australia						

Table 1 continued

Location	**Year of activity**	**Years of NT**	**Crop rotation system**	**Yield on NT (t/ha)**	**GWYV (%)**	**Authors**
Biloela	1999	17	Continuous wheat	2,50	67	*Radford and Thornton* [1]
	1998	16		1,77	25	
	1997	15		2,04	31	
	1996	14	Maize-wheat	3,17	57	
	1991	9	Continuous wheat	2,02	5	
	1990	8		1,60	29	
	1987	5	Sorghum-wheat	0,65	2	
Queensland, Gindie	1991	2	Wheat-chickpeas	1,60	4	*Armstrong, et al., 2003* [31]
Victoria, Rutherglen	1983	1	Continuous wheat	2,22	7	*Coventry, et al., 1992* [32]
Western Australia, Merredin	1982	6		1,03	76	*Hamblin, et al., 1984* [33]
	1981	5		0,98	72	
Brazil						
Parana, Londrina, Embrapa Soybean	2008	20	Winter wheat-summer soybean; winter lupine -summer maize; winter oat-summer soybean	2,13	36	*Franchini, et al.,* [34]
	2006	18		2,51	27	
	2005	17		2,88	1	
	2004	16		3,27	6	
		16		3,21	3	
	2003	15		1,02	4	
	1997	9		1,97	51	
				1,85	40	
	1990	2		0,65	7	
Canada						
Alberta, Beaverlodge	2005	2	Barley-wheat-canola	1,93	35	*Soon, et al.,* [35]
Alberta, Champion	1993	1	Continuous wheat	3,74	71	*Blackshaw, et al.,* [36]
Alberta, Rycroft	1994	6	Fallow/green manure-canola-wheat-barley	3,25	15	*Arshad and Gill,* [37]
Alberta, Three Hills	2003	10	Continuous wheat	2,76	3	*Wang, et al.,* [38]
	2002	9		0, 97	147	
	2001	8		2,23	18	
	2000	7		2,32	44	
Saskatchewan, Cantuar	1990	10	Fallow-wheat	0,60	15	*McConkey, et al.,* [39]
	1989	9	Wheat-fallow	1,27	11	
Saskatchewan, Melfort	1997	5	Canola-wheat-barley-barley; Canola-barley-pea-wheat; Canola-pea-flax-barley	5,10	2	*Bailey, et al.,* [40]
	1996	4		5,20	7	
	1994	2		3,96	14	
	2001	8	Canola-wheat-barley-barley; canola-barley-pea-wheat; canola-pea-flax-barley	2,07	61	*Kutcher, et al.,* [41]
Saskatchewan, Rosthern	2007	4	Canola-wheat-wheat	1,98	12	*Baan, et al.,* [42]
	2006	3		3,29	1	

Table 1 continued

Location	Year of activity	Years of NT	Crop rotation system	Yield on NT (t/ha)	GWYV (%)	Authors
Saskatchewan, Scott	1990	13	Wheat-oilseed-wheat; fallow oilseed-wheat	2,66	17	*Brandt,* [43]
	1990			2,71	12	
	1987	10		2,03	23	
	1981	4		2,18	18	
				2,45	2	
Saskatchewan, Stewart Valley	1993	13	Continuous wheat	2,76	–1	*McConkey, et al.,* [39]
			Fallow-wheat	3,05	–18	
	1990	10	Continuous wheat	2,38	10	
			Fallow-wheat	3,55	7	
	1989	9		2,28	37	
Saskatchewan, Swift Current	1993	3	Continuous wheat	2,59	0	
		13		2,46	1	
	1990	10		2,28	18	*McConkey, et al.,* [44]
				2,61	5	*McConkey, et al.,* [39]
		9		2,58	14	
		7		1,60	14	
	1987		Fallow-wheat	2,45	1	
	1990	10	Continuous wheat	2,61	5	*Selles, et al.,* [45]
			Wheat-fallow	2,88	–2	
	1988	8	Continuous wheat	0,65	23	
		8	Wheat-fallow	1,66	15	
	1987	7		2,45	1	
Saskatchewan, Tisdale	2007	4	Canola-wheat-wheat	1,88	10	*Baan, et al.,* [42]
China						
Dongping, Shandong Province	2016	5	Maize-wheat	10,56	11	*Latifmanesh, et al.* [46]
				9,53	10	
	2015	4		10,27	11	
				11,00	8	
				9,61	5	
Gansu	2016	1		8,73	18	*Guo, et al.* [47]
Heyang, Shanxi		10		2,74	13	*Sun,* [48]
				2,88	6	
	2012	6		3,38	16	
				3,28	7	
	2010	4		3,28	16	
	2009	3		2,54	9	
				2,18	5	
	2008	2		2,65	3	
				3,26	2	
Tai’an, Shandong Province	2015	14	Winter wheat-summer maize	8,3	0	*Liu,* [49]
	2014	13		8,2	1	
				8,2	9	*Xu,* [50]

Table 1 continued

Location	Year of activity	Years of NT	Crop rotation system	Yield on NT (t/ha)	GWYV (%)	Authors
Mexico						
Ciudad Obregon	2008	4	Continuous wheat	4,95	25	*Verhulst, et al.,* [51]
				4,87	19	
				7,57	3	
				7,52	1	
	2007	3		5,18	10	
				4,63	1	
	2006	2		8,20	6	
				4,77	1	
Spain						
Agramunt	2002	13	Barley-wheat	2,6	30	*Cantero-Martinez, et al.,* [52]
Cordoba	2005	20	Wheat-sunflower; wheat-fababean; wheat-chickpea; wheat-fallow	2,63	20	*López-Bellido, et al.,* [53]
		20		2,85	17	
	2003	18		4,94	21	
	1991	6		1,91	–1	*López-Bellido, et al.,* [54]
	1990	5		2,51	–10	
	1989	4		4,50	–11	
	1987	2		4,70	0	
	2007	22	Wheat-chickpea	3,48	41	*Melero, et al.,* [55]
				8,49	32	
			Wheat-fababean	4,70	20	
			Wheat-fallow	11,76	18	
			Wheat-wheat	3,75	14	
			Wheat-sunflower	2,07	11	
			Wheat-wheat	9,34	10	
			Wheat-sunflower	5,11	5	
Selvanera	2003	17	Barley-canola-wheat,	2,48	–9	*Cantero-Martinez, et al.,* [52]
	2001	15		5,13	5	
	1999	13		3,16	2	
	1993	7		5,42	22	
USA						
Kansas Tribune	2013	23	Wheat-sorghum-fallow	1,18	74	*Schlegel, et al.,* [2]
	2008	18		1,48	160	
	1992	2		3,91	36	
Kansas, Garden City	1988	4		1,53	89	*Norwood,* [56]
Kansas, Saline County	2005	2	Sorghum-winter wheat-winter wheat; maize-soybean-winter wheat-winter wheat	3,06	12	*Carignano, et al.,* [57]
Kansas, Tribune	1994	4	Wheat-fallow; wheat-sorghum-fallow; wheat-wheat	3,49	11	*Schlegel, et al.,* [58]

Table 1 continued

Location	Year of activity	Years of NT	Crop rotation system	Yield on NT (t/ha)	GWYV (%)	Authors
North Dakota, Mandan	1995	12	Spring wheat-winter wheat-sunflower	2,28	34	*Halvorson, et al.,* [59]
	1989	6		1,26	7	
	1988	5		1,14	47	
Oklahoma	2016	6	Winter wheat-cowpea	5,82	22	*Kandel, et al.,* [60]
South Carolina, Florence	1990	12	Maize-wheat-cotton	2,87	48	*Karlen, et al.,* [61]
Texas, Burleson County	2000	17	Continuous wheat	1,12	78	*Ribera, et al.,* [62]
	1996	13	Sorghum-wheat-soybean; wheat-soybean	2,26	13	
	1995	12		2,75	35	
	1994	11		2,4	28	
			Continuous wheat	1,84	9	
	1992	5	Sorghum-wheat-soybean; wheat-soybean	2,60	9	
	1988	8	Continuous wheat	2,41	27	
Texas, Bushland	1995	6	Wheat-sorghum-fallow	0,80	186	*Baumhardt and Jones,* [63]
	1993	11		2,07	37	
	1992	10	Continious wheat	1,84	63	*Jones and Popham,* [64]
	1991	8	Wheat-soybean-fallow	2,06	29	
	1989	6	Wheat-fallow	1,26	24	
	1987	6	Continious wheat	1,51	29	

3.1 The general interest of wheat yield under NT

Research carried out over the last four decades on CA, has shown the benefits of the direct interactivity between farmers, specialists and State support. This cohesion made it possible to invest efficiently as detailed by Mrabet et al. [5]. The adaptability of NT on multiple levels is oriented to knowing how to achieve crop productivity despite drought situations [3]. Wheat yield results obtained under NT and CT evaluated in the same conditions as Mediterranean ones confirm the process. In 1990 Bouzza [6] centralized the intensity of water storage and the GWYV positively under NT compared to CT. These are highlighted more by Mrabet et al. [18], with +146%. All the GWYV calculated are classified in **Table 1**. This visibility is marked by potentialities that should be adopted in all the continents and turn the attention to how to extend the system [14]. These relevant aspects are also explored by Moussadek et al. [3], after only four years of NT, the yield variation takes the reflection to +0,44 at Merchouch station between the period of 2004–2008 (Morocco). This is in continual adequation of what Devkota et al. [22] , obtained after 18 years at the same station with +80% yield variability. The last five years of successive drought seasons in North Africa (Morocco, Algeria and Tunisia) support the previous conclusions. Raji [16], results on the table presented note a value of +1912% at Ain Sbit (Morocco), some farmers didn't harvest any wheat yield under CT at the period concerned. It's in total adequacy with Chouter et al. [11], experimentations at Setif (Algeria). They join the fact that under drought effect NT could be more performant. They join previous searchers, it is attached to the nature of crop rotation and climate influence. All of these approaches were also expected in Australia, Brazil, Canada, China, Mexico, Spain and the USA as cited in **Table 1**.

3.2 The long-term influence of crop rotation and climate under NT

Crop rotation and residue retention affect the stock organic carbon and can increase wheat yield [3]. When both are controlled, it could make the vision of high wheat productivity for a long-term effect. This intensity revealed the power of GWYV and the crop rotation choice under NT. Schlegel et al.[2], experimentation defined a variation of +160% on the wheat-sorghum and fallow rotation in the loamy soil of the Kansas area (USA). It was in continual adequacy with values obtained by Norwood [55], with +89% at the same place. In the same directive, Baumhardt and Jones [62], on Texas's experimentations and monitored precisely the potential of wheat yield advantages compared the two systems. This variability is projected on many crops rotations advanced in **Table 1.** The exploration of crop rotation is accommodated with the veritable crop choice. Years of studies, in warm and temperate zones solicitation by searchers like Sun [47] led to consequences on wheat-maize rotation and mentioned the efficacity of wheat yield evolution under NT. Their perseverance is totally accorded by Latifmanesh and Guo [45-46], in different stations of China. Another rotation marked by specialists is the continuous-wheat rotation. It is comparable depending on the climates where the dry seasons are significant. McConkey et al. [38], confront after more than ten years of NT, two rotations: continuous wheat and wheat-fallow. The values were joined by Selles et al. [44] at Saskatchewan's stations (Canada), where the continental climate is predominant without alarming drought seasons. It reports the evidence of wheat yield attachment detailed by Blacksnaw et al. and Wang et al. [35,37]. They affirmed also that the disposition of climate takes a look at crop spreading. Long-term NT studies, taken up at the level described in the table, leaned researchers into the profitability of the yield and its relativity which is in total coordination with the results in the Mediterranean zone. It detects the comparative yield under three crop rotations: wheat-wheat, wheat-fallow, and cereals-legumes. During the last five years drought circumstances defined the implication of legumes like crop rotation in a resilient system. The semi-arid zones have the last five years, been affected by hard dry effects, experimentations after more than 10 years target when wheat productivity is associated with cereals-legumes systematic rotation. Many of those are explored at semi-arid stations like Merchouch (Morocco). The steps of challenging climate and crop rotation system adapted, in all cases ensuring the positive arrangement of NT compared to CT. It consolidates with every soil aspect and wheat productivity the sustainability of the process in the long term.

4. Conclusions

All the authors cited in this review based on different experimental stations of many countries referenced, agree with the profitability in different stages of wheat yield under NT compared to CT. The valorization of a few inputs used can make an impressive value of GWYV. These yields are conducted by climates and crop rotation influence. It leaves the continuity of ecological, economic and environmental profitability. Indeed, the interest in varietal choice applications is centralized also to improve yield efficiency for the long term.

Author Contributions

Conceptualization, Methodology and Perspectives approaches, Visualization, Validation, K.H.K., M.R., B.B., B.A, Z.A., D.H. and M.H.; Writing original draft, K.H.K.; Review and Editing, K.H.K., M.R., B.B., B.A and M.H.; Supervision, M.R., B.B., B.A and Z.A.; Project administration and Funding acquisition, M.R.

Conflict of Interest

All authors are agreed for the publication of this manuscript version and declare that there are no conflicts of interest.

Acknowledgments

The present article is integrated as part of a project between MCGP, EIA and CAMA. We would like to sincerely thank the National Institute for Agronomic Research (INRA of Rabat), the International Center for Agricultural Research in the Arid Zones (ICARDA) and the Faculty of Sciences of Kenitra for their essential support.

References

[1] Radford, B.J., Thornton, C.M., 2011. Effects of 27 years of reduced tillage practices on soil properties and crop performance in the semi-arid subtropics of Australia. International Journal of Energy, Environment and Economics. 19, 565–588.

[2] Schlegel, A.J., Assefa, Y., Haag, L.A., et al., 2018. Long-Term tillage on yield and water use of grain sorghum and winter wheat. Agronomy Journal. 110(1), 269–280. DOI: https://doi.org/10.2134/agronj2017.02.0104

[3] Moussadek, R., Laghrour, M., Mrabet, R., et al., 2023. Crop yields under climate variability and no-tillage system in dry areas of Morocco. Ecological Engineering & Environmental Technology. 24(1), 221–232. DOI: https://doi.org/10.12912/27197050/155024

[4] Mrabet, R., Moussadek, R., 2013. Reducing climate risks for sustainable development guides on soil management techniques for adaptation to climate change in Morocco. GIZ: Bonn. (in French).

[5] Mrabet, R.,N., Bahri, H., Zaghouane, O., et al., 2022. Adoption and spread of conservation agriculture in North Africa. In Burleigh Dodds series in agricultural science. 185–246. DOI: https://doi.org/10.19103/as.2021.0088.06

[6] Bouzza, A., 1990. Water Conservation in wheat rotations under several management and tillage systems in semiarid areas [PhD thesis]. Lincoln: University Of Nebraska. p. 125.

[7] Mrabet, R., 2011. No-Tillage agriculture in West Asia and North Africa. Rainfed Farming Systems. 1, 1015–1042. DOI: https://doi.org/10.1007/978-1-4020-9132-2_40

[8] Su, Y., Gabrielle, B., Makowski, D., 2021. A global dataset for crop production under conventional tillage and no tillage systems. Scientific Data. 8(1). DOI: https://doi.org/10.1038/s41597-021-00817-x

[9] Pittelkow, C.M., Liang, X., Linquist, B.A., et al., 2014. Productivity limits and potentials of the principles of conservation agriculture. Nature. 517(7534), 365–368. DOI: https://doi.org/10.1038/nature13809

[10] Ponisio, L.C., M'Gonigle, L.K., Mace, K., et al, 2015. Diversification practices reduce organic to conventional yield gap. Proceedings of the Royal Society B: Biological Sciences. 282(1799), 20141396. DOI: https://doi.org/10.1098/rspb.2014.1396

[11] Chouter, A., Benniou, R., Sebbane, M., Louahdi, N., 2022. Effect of tillage systems on durum wheat production with different rotations in semi arid area of Algeria. Agricultural Science Digest. 44(1), 53–57. DOI: https://doi.org/10.18805/ag.DF-438

[12] Taibi, H.H.Y., Smail-Saadoun, N., Labidi, S., et al., 2020. The influence of no-till farming on durum wheat Mycorrhization in a Semi-Arid Region: A long-term field experiment. Journal of Agricultural Science. 12(4), 77. DOI: https://doi.org/10.5539/jas.v12n4p77

[13] Chennafi, H., Hannachi, A., Touahria, O., et al. 2011. Tillage and residue management effect on durum wheat [Triticum turgidum (L.) thell. ssp. turgidum conv. durum (Desf.) mackey] growth and yield under semi arid climate. Advances in Environmental Biology. 5(10), 3231–3240.

[14] Yachi A., 2022. Problems of the introduction of direct seeding in Algeria: Agronomic and energy analysis [PhD Thesis]. Algiers: National Higher School of Agronomy. p. 168. (in French).

[15] Mrabet, R., 2008. No-Tillage systems for sustainable dryland agriculture in Morocco. INRA: Paris. pp. 153.

[16] Raji J., 2022. The impact of no tillage on soil

quality and crop yields: Case of soft wheat (Ain Sbit, Khemisset province, central Morocco) [Master's Thesis]. Rabat: IAV HASSAN II. p. 63.

[17] Mrabet, R. 2000. Differential response of wheat to tillage management systems in a semiarid area of Morocco. Field Crops Research. 66(2), 165–174.
DOI: https://doi.org/10.1016/s0378-4290(00)00074-5

[18] Mrabet, R. (editor), 2001. The direct seeding system: for sustainable and environmental Moroccan agriculture. Seminar on Climate Hazards and Agricultural policies; 2001 May 4–25; Morocco: Moroccan Association of Agro-Economy, Rabat. p. 337–348.

[19] Mrabet, R., 2011. Effects of residue management and cropping systems on wheat yield stability in a semiarid Mediterranean clay soil. American Journal of Plant Sciences. 2(2), 202–216.
DOI: https://doi.org/10.4236/ajps.2011.22022

[20] Razine, M., Raguin, M., 2006. Direct seeding of cereals: Experience of the agricultural field of Sidi Kacem. Bull. Transfer. Technol. 163, 1–4. (in French).

[21] Maher, H., Moussadek, R., Ghanimi, A., et al., 2023. Effect of tillage and nitrogen fertilization on soil properties and yield of five durum wheat germoplasms in a dry area of Morocco. Applied Sciences. 13(2), 910.
DOI: https://doi.org/10.3390/app13020910

[22] Devkota, M., Devkota, K.P., Kumar, S., 2022. Conservation agriculture improves agronomic,economic, and soil fertility indicators for a clay soil in a rainfed Mediterranean climate in Morocco. Agricultural Systems. 201, 103470.
DOI: https://doi.org/10.1016/j.agsy.2022.103470

[23] Mrabet, R., Moussadek, R., Fadlaoui, A., et al., 2012. Conservation agriculture in dry areas of Morocco. Field Crops Research. 132, 84–94.
DOI: https://doi.org/10.1016/j.fcr.2011.11.017

[24] Sellami, W., Bendidi, A., Daoui, K., et al., 2023. Tillage systems effect on wheat yield in the Saïs region of Morocco. Universal Journal of Agricultural Research. 11(1), 22–31.
DOI: https://doi.org/10.13189/ujar.2023.110103

[25] Chaieb, N., Rezguia, M., Ayedb, S., et al., 2020. Effects of tillage and crop rotation on yield and quality parameters of durum wheat in Tunisia. Journal of Animal and Plant Sciences. 44(2), 7654–7676.
DOI: https://doi.org/10.35759/janmplsci.v44-2.7

[26] Mouelhi, B., Slim, S., Arfaoui, S., et al., 2016. Effect of sowing method and crop rotation on growth parameters and yield components of durum wheat (Triticum durum Desf.) variety "Karim". Journal of New Sciences. 28, (11). (in French)

[27] Ben Moussa-Machraoui, S., Errouissi, F., Ben-Hammouda, M., et al., 2010. Comparative effects of conventional and no-tillage management on some soil properties under Mediterranean semi-arid conditions in northwestern Tunisia. Soil & Tillage Research. 106(2), 247–253.
DOI: https://doi.org/10.1016/j.still.2009.10.009

[28] M'hedhbi, K., Chouen, S., Ben-Hammouda, M., 2003. A recent Tunisian experience with direct drilling. World Congress on Conservation Agriculture. Iguassu Falls: Parana, Brazil. pp. 132–135.

[29] Vadon, B., Lamouchi, L., Elmay, S., et al., 2006. Farmers' organizations: A lever for developing conservation agriculture in the Maghreb. Mediterranean Options: Series A. 69, 87–99. (in French).

[30] Armstrong, R., Millar, G., Halpin, N.V., et al., 2003. Using zero tillage, fertilisers and legume rotations to maintain productivity and soil fertility in opportunity cropping systems on a shallow Vertosol. Australian Journal of Experimental Agriculture. 43(2), 141.
DOI: https://doi.org/10.1071/ea01175

[31] Coventry, D., Hirth, J.R., Reeves, T., 1992. Interactions of tillage and lime in wheat-subterranean clover rotations on an acidic sandy clay loam in south-eastern Australia. Soil & Tillage

Research. 25(1), 53–65.
DOI: https://doi.org/10.1016/0167-1987(92)90062-g

[32] Hamblin, A., 1984. The effect of tillage on soil surface properties and the water balance of a xeralfic alfisol. Soil and Tillage Research. 4(6), 543–559.
DOI: https://doi.org/10.1016/0167-1987(84)90004-7

[33] Franchini, J.C., Debiasi, H., Balbinot, A.A., et al., 2012. Evolution of crop yields in different tillage and cropping systems over two decades in southern Brazil. Field Crops Research. 137, 178–185.
DOI: https://doi.org/10.1016/j.fcr.2012.09.003

[34] Soon, Y.K., Malhi, S.S., Lemke, R., et al., 2011. Effect of polymer-coated urea and tillage on the dynamics of available N and nitrous oxide emission from Gray Luvisols. Nutrient Cycling in Agroecosystems. 90(2), 267–279.
DOI: https://doi.org/10.1007/s10705-011-9428-2

[35] Blackshaw, R.E., Semach, G., Li, X., et al., 2000. Tillage, fertiliser and glyphosate timing effects on foxtail barley (Hordeum jubatum) management in wheat. Canadian Journal of Plant Science. 80(3), 655–660.
DOI: https://doi.org/10.4141/p99-132

[36] Arshad, M., Gill, K.S., 1997. Barley, canola and wheat production under different tillage-fallow-green manure combinations on a clay soil in a cold, semiarid climate. Soil and Tillage Research. 43(3–4), 263–275.
DOI: https://doi.org/10.1016/s0167-1987(97)00017-2

[37] Wang, H., Lemke, R., Goddard, T., et al., 2007. Tillage and root heat stress in wheat in central Alberta. Canadian Journal of Soil Science. 87(1), 3–10.
DOI: https://doi.org/10.4141/s06-016

[38] McConkey, B., Campbell, C.A., Zentner, R.P., et al., 1996. Long-term tillage effects on spring wheat production on three soil textures in the Brown soil zone. Canadian Journal of Plant Science. 76(4), 747–756.
DOI: https://doi.org/10.4141/cjps96-127

[39] Bailey, K.L., Johnston, A., Kutcher, H.R., et al., 2000. Managing crop losses from foliar diseases with fungicides, rotation, and tillage in the Saskatchewan Parkland. Canadian Journal of Plant Science. 80(1), 169–175.
DOI: https://doi.org/10.4141/p99-069

[40] Kutcher, H.R., Johnston, A., Bailey, K.L., et al., 2011. Managing crop losses from plant diseases with foliar fungicides, rotation and tillage on a Black Chernozem in Saskatchewan, Canada. Field Crops Research. 124(2), 205–212.
DOI: https://doi.org/10.1016/j.fcr.2011.05.018

[41] Baan, C., Grevers, M., Schoenau, J.J., 2009. Effects of a single cycle of tillage on long-term no-till prairie soils. Canadian Journal of Soil Science. 89(4), 521–530.
DOI: https://doi.org/10.4141/cjss08041

[42] Brandt, S., 1992. Zero vs. conventional tillage and their effects on crop yield and soil moisture. Canadian Journal of Plant Science. 72(3), 679–688.
DOI: https://doi.org/10.4141/cjps92-084

[43] McConkey, B., Ulrich, D., Dyck, F.B., 1997. Snow management and deep tillage for increasing crop yields on a rolling landscape. Canadian Journal of Soil Science. 77(3), 479–486.
DOI: https://doi.org/10.4141/s96-080

[44] Selles, F., McConkey, B., Campbell, C., 1999. Distribution and forms of P under cultivator and zero-tillage for continuous and fallow-wheat cropping systems in the semi-arid Canadian prairies. Soil and Tillage Research. 51(1–2), 47–59.
DOI: https://doi.org/10.1016/s0167-1987(99)00027-6

[45] Latifmanesh, H., Deng, A., Nawaz, M.M., et al., 2018. Integrative impacts of rotational tillage on wheat yield and dry matter accumulation under corn-wheat cropping system. Soil and Tillage Research. 184, 100–108.
DOI: https://doi.org/10.1016/J.STILL.2018.07.008

[46] Guo, Y., Yin, W., Hu, F., et al., 2019. Reduced irrigation and nitrogen coupled with no-tillage and plastic mulching increase wheat yield in maize-wheat rotation in an arid region. Field Crops Research. 243, 107615.
DOI: https://doi.org/10.1016/j.fcr.2019.107615

[47] Sun, L., Wang, R., Li, J., et al., 2019. Reasonable fertilization improves the conservation tillage benefit for soil water use and yield of rain-fed winter wheat: A case study from the Loess Plateau, China. Field Crops Research. 242, 107589.
DOI: https://doi.org/10.1016/j.fcr.2019.107589

[48] Liu, Z., Gao, T., Tian, S., et al., 2020. Soil organic carbon increment sources and crop yields under long-term conservation tillage practices in wheat-maize systems. Land Degradation & Development. 31(9), 1138–1150.
DOI: https://doi.org/10.1002/ldr.3531

[49] Xu, J., Han, H., Ning, T., et al., 2019. Long-term effects of tillage and straw management on soil organic carbon, crop yield, and yield stability in a wheat-maize system. Field Crops Research. 233, 33–40.
DOI: https://doi.org/10.1016/j.fcr.2018.12.016

[50] Verhulst, N., Govaerts, B., Nelissen, V., et al., 2011. The effect of tillage, crop rotation and residue management on maize and wheat growth and development evaluated with an optical sensor. Field Crops Research. 120(1), 58–67.
DOI: https://doi.org/10.1016/j.fcr.2010.08.012

[51] Cantero-Martínez, C., Angás, P., Lampurlanés, J., 2007. Long-term yield and water use efficiency under various tillage systems in Mediterranean rainfed conditions. Annals of Applied Biology. 150(3), 293–305.
DOI: https://doi.org/10.1111/j.1744-7348.2007.00142.x

[52] López-Bellido, L., Muñoz-Romero, V., Benítez-Vega, J., et al., 2012. Wheat response to nitrogen splitting applied to a Vertisols in different tillage systems and cropping rotations under typical Mediterranean climatic conditions. European Journal of Agronomy. 43, 24–32.
DOI: https://doi.org/10.1016/j.eja.2012.05.002

[53] López-Bellido, L., Fuentes, M., Castillo, J.E., et al., 1996. Long-term tillage, crop rotation, and nitrogen fertilizer effects on wheat yield under rainfed Mediterranean conditions. Agronomy Journal. 88(5), 783–791.
DOI: https://doi.org/10.2134/agronj1996.00021962008800050016x

[54] Melero, S., López-Bellido, R.J., López-Bellido, L., et al., 2011. Long-term effect of tillage, rotation and nitrogen fertiliser on soil quality in a Mediterranean Vertisol. Soil and Tillage Research. 114(2), 97–107.
DOI: https://doi.org/10.1016/j.still.2011.04.007

[55] Norwood, C.A., 1994. Profile water distribution and grain yield as affected by cropping system and tillage. Agronomy Journal. 86(3), 558–563.
DOI: https://doi.org/10.2134/agronj1994.00021962008600030019x

[56] Carignano, M., Staggenborg, S.A., Shroyer, J.P., 2008. Management practices to minimize tan spot in a continuous wheat rotation. Agronomy Journal. 100(1), 145–153.
DOI: https://doi.org/10.2134/agronj2007.0092

[57] Schlegel, A.J., Dhuyvetter, K.C., Thompson, C.P., 1999. Agronomic and economic impacts of tillage and rotation on wheat and sorghum. Journal of Production Agriculture. 12(4), 629–636.
DOI: https://doi.org/10.2134/jpa1999.0629

[58] Halvorson, A.D., Black, A.L., Krupinsky, J.M., et al., 1999. Sunflower response to tillage and nitrogen fertilization under intensive cropping in a wheat rotation. Agronomy Journal. 91(4), 637–642.
DOI: https://doi.org/10.2134/agronj1999.914637x

[59] Kandel, T.P., Gowda, P.H., Northup, B.K., 2019. Impacts of tillage systems, nitrogen fertilizer rates and a legume green manure on light interception and yield of winter wheat.

Cogent Food & Agriculture. 5(1), 1580176.
DOI: https://doi.org/10.1080/23311932.2019.1580176

[60] Karlen, D.L., Hunt, P.G., Matheny, T.A., 1996. Fertilizer 15 nitrogen recovery by corn, wheat, and cotton grown with and without pre-plant tillage on norfolk loamy sand. Crop Science. 36(4), 975–981.
DOI: https://doi.org/10.2135/cropsci1996.0011183x003600040026x

[61] Ribera, L.A., Hons, F.M., Richardson, J.W., 2004. An economic comparison between conventional and no-tillage farming systems in burleson county, Texas. Agronomy Journal. 96(2), 415–424.
DOI: https://doi.org/10.2134/agronj2004.4150

[62] Baumhardt, R.L., Jones, O.R., 2002. Residue management and tillage effects on soil-water storage and grain yield of dryland wheat and sorghum for a clay loam in Texas. Soil & Tillage Research. 68(2), 71–82.
DOI: https://doi.org/10.1016/s0167-1987(02)00097-1

[63] Jones, O.R., Popham, T.W., 1997. Cropping and tillage systems for dryland grain production in the southern high Plains. Agronomy Journal. 89(2), 222–232.
DOI: https://doi.org/10.2134/agronj1997.00021962008900020012x

[64] Global Temperature Anomalies from 1880 to 2023 [Internet]. NASA Scientific Visualization Studio [cited 2024 Jan 12]. Available from : https://svs.gsfc.nasa.gov/5207/

BILINGUAL PUBLISHING GROUP

Journal of Environmental & Earth Sciences

https://journals.bilpubgroup.com/index.php/jees

CASE REPORT

Environmental Impact Assessment of Onshore Wind Farms in the Region of Central Greece Using a Modified RIAM Method

Olga Korozi, Dimitra G. Vagiona*

Department of Spatial Planning and Development, Aristotle University of Thessaloniki, Thessaloniki 54124, Greece

ABSTRACT

Wind energy is one of the most basic forms of renewable energy, which shows an increasing rate of development worldwide and also at the European level. However, this rapid deployment of wind farms makes the need for an impact assessment of this type of projects on the natural and man-made environment imperative. The present paper aims to identify and assess the environmental impacts of wind farm projects in the Region of Central Greece. A modified Rapid Impact Assessment Matrix (RIAM) method is used for this purpose. The methodology includes the identification of the existing onshore wind farm projects in the study area, the appropriate modifications of the RIAM method to respond to the characteristics of the projects and the study area, the qualitative assessment of their potential impacts during construction and operational phases and the computation of the Environmental Performance Grade (EPG) of projects based on the pro-posed modified RIAM method. The results reveal that although there are some slight negative impacts on the natural environment of the study area, the examined wind farms contribute positively both to the atmosphere and to the socio-economic environment of the study. This study extends the potential for using RIAM as a tool in environmental impact assessment studies of renewable energy projects.

Keywords: Environmental impact assessment; Environmental components; Region of central Greece; Rapid impact assessment matrix (RIAM); Environmental performance grade (EPG)

*CORRESPONDING AUTHOR:
Dimitra G. Vagiona, Department of Spatial Planning and Development, Aristotle University of Thessaloniki, Thessaloniki 54124, Greece; Email: dimvag@plandevel.auth.gr

ARTICLE INFO
Received: 22 December 2023 | Revised: 25 March 2024 | Accepted: 11 April 2024 | Published Online: 26 April 2024
DOI: https://doi.org/10.30564/jees.v6i1.6173

CITATION
Korozi, O., Vagiona, D.G., 2024. Environmental Impact Assessment of Onshore Wind Farms in the Region of Central Greece Using a Modified RIAM Method. Journal of Environmental & Earth Sciences. 6(1): 71–82. DOI: https://doi.org/10.30564/jees.v6i1.6173

1. Introduction

The systematic process of identifying, predicting, and evaluating the environmental effects of a proposed project or activity is widely known as Environmental Impact Assessment (EIA) [1]. The goal of an EIA is to identify and assess the impacts of a project or activity on the natural and anthropogenic environment, ideally from conception to decommissioning, and before any decision about its implementation. The output of the above process is the Environmental Impact Study or Statement (EIS). Phylip-Jones and Fischer [2] investigated the quality of EIS and its content regarding twenty wind farm projects in the United Kingdom and Germany and concluded that although there are some weaknesses, the information included in relevant studies strongly contributes to decision-making. One of the most complicated parts of the EIA process is the impact significance. There are several components and factors, that may vary from project to project, that should be considered when determining the significance of an impact, making comparisons among projects a challenging task [3].

The impact assessment is carried out using various qualitative and quantitative methods (i.e. overlapping maps, checklists, matrices, mathematical models). Descriptive characterizations, colour gradations, numerical ratings, Likert rating scales or a combination of the above can be used in the impact assessment. The simplest methods of determining impacts involve using a list of impacts (checklists, impact matrices) to ensure that all impacts have been considered in the analysis. For example, Kaldellis et al. [4] present an indicative list of impacts that the development of an onshore wind farm may cause. There are also more complex impact assessment methods, which use numerical values to derive a composite value for the impacts of projects/activities. Zolfagharian et al. [5] assess the environmental impacts of construction projects in Malaysia by determining the hazard of their impacts. Several more complex applications can be also found in the literature, which integrate multicriteria analysis into evaluation matrices. An example of such an application is the Rapid Impact Assessment Matrix (RIAM) [6,7]. The RIAM matrix was initiated by Pastakia [6] and Pastakia and Jensen [7], who present a summary impact assessment matrix, in their attempt to transparently incorporate subjective judgments into the environmental impact assessment process. Examples of applications of the RIAM method in the environmental impact assessment process appear frequently in the international literature.

Pastakia and Bay [8] performed an initial environmental evaluation (IEE) to evaluate potential development options to preserve or enhance the Rupa Tal lake and valley in Nepal. Four different alternatives were considered, and the IEE was able to specify a number of crucial elements for their comparison, while the Rapid Impact Assessment Matrix illustrated the of impacts that each alternative would cause. Kuitunen et al. [9] compared the social and environmental impacts of various projects, plans, and programs carried out in the same geographic area using RIAM. Shakib-Manesh et al. [10] evaluated a number of solutions for the restoration of the water system in Eastern Finland using a combination of a straightforward MCA approach, RIAM, and an Expert Panel. Suthar and Sajwan [11] used the RIAM to assess the site suitability of a possible new municipal solid waste disposal site for the city of Dehradun (India), considering ecological, social, cultural and economic components in the decision-making process. Vagiona [12] uses a modified Rapid Impact Assessment Matrix as an online tool to calculate the degree of environmental performance of fourteen (14) different projects in Greece.

Although the RIAM method was originally deployed for the comparison of alternatives within one project, this paper illustrates the use of RIAM as a tool for the sustainability assessment of onshore wind farms in the Region of Central Greece. A comparison of the Environmental Performance Grade (EPG) of the existing onshore wind farms is performed for this purpose.

The advantages of the proposed approach in impact assessment can be summarized as follows: (i) it can be easily applied in practical evaluation of environmental impacts of developmental projects; (ii) it presents flexibility and adaptability in environmental components as well as assessment criteria; (iii) it is simple in computations and understandable in the interpretation of results; (iv) it provides numerical values although it is considered a qualitative approach and (v) provides a holistic approach to sustainability. The results suggest that the modified RIAM can be a reliable tool to identify the suitability and sustainability of wind farm project deployment.

The remainder of this paper is organized as follows. Section 2 presents the main environmental impacts of onshore wind farm installations. Section 3 describes the methodological approach developed for the EPG of onshore wind farm projects, while in Section 4, the results from the application of the modified RIAM method on the existing wind farm projects in the Region of Greece are presented. The main conclusions of this research are revealed and discussed in Section 5.

2. Onshore wind farm projects and impact assessment

Wind energy systems are regarded as being eco-friendly [13] and are constantly improving regarding compatibility with human life and wildlife among all renewable systems [14].

The main environmental impacts that are discussed frequently are related to acoustic-noise pollution [15], visual pollution [16], disturbances or wildlife safety for birds [17], disturbances or wildlife safety for bats [18], local climate change [19], soil erosion and deforestation [15], lightning from towers [15], and electromagnetic interferences and radiation [15].

More specifically, during the construction phase of a wind energy facility, certain activities, such as excavation and associated road works, may affect the soil characteristics and natural environment of the study area. With the deforestation of the land, the surface is exposed both to strong winds and climatic conditions with consequent soil erosion. Sewage and various oils from the construction site can cause soil erosion. Additionally, the use of heavy machinery during the construction phase may disturb the local ecological balance.

Although wind farms have a relatively low impact on the environment compared to conventional power generation facilities, the negative impacts of onshore wind farms in the operational phase focus on: the aesthetics-visional features (landscape alteration), the acoustic environment (noise pollution) and the impacts in fauna (bird strikes).

The visual nuisance and aesthetics of a wind farm installation is a subjective factor, which depends on the condition of a wind farm, as well as on the observer's view and judgement. Noise, which is the consequence of the operation of wind turbines, depends both on the level of acoustic emissions due to the operation of the wind turbine and the distance of the wind farm from the nearest residential area.

High noise emissions are usually caused by large wind turbines. However, in these cases, the height of the turbines exceeds 100 meters and therefore does not affect humans and wildlife [15]. In many cases wind farm proposals may face strong social reactions from people living near the proposed projects who support that noise from wind turbines will disrupt their quality of life [20–22].

Regarding the potential negative effects of wind turbines on avifauna, many studies have indicated that wind turbines do not pose a threat to birds, given that their mortality from this cause is only a small percentage of their total mortality. Statistically, the possibility of bird deaths associated with wind energy projects is significantly lower compared to bird deaths caused by other factors such as collisions with tall buildings, infrastructure networks (electricity, telecommunications) and public utility projects, cats, vehicles, pesticides [23].

Few cases of bird mortality have been reported for wind turbines under 50 meters in height, while isolated problems have been pointed out in wind farms located on migratory bird routes. The strict restrictions that have been established in recent years for the installation of anthropogenic activities in environmentally sensitive areas (e.g. NATURA zones, RAMSAR areas), but also the integration of the criterion of the distance of a wind farm installation from migratory bird routes in the sitting process should contribute to the protection from collisions.

Finally, according to research by Sengupta, D.L. [24], the electromagnetic radiation produced by wind farms can distort or even change the signal from nearby television or radio stations and affect nearby navigation and microwave communication.

3. Methodological framework for environmental performance grade of onshore wind farm projects

The proposed methodological framework includes the identification of the existing onshore wind farm projects within the study area, the determination of the environmental components as well as the assessment criteria based on the project's features and the characteristics of the study area, the qualitative assessment of their potential impacts during the construction and operational phases, and the computation of the projects' Environmental Performance Grade (EPG).

Appropriate modifications of the RIAM method to reflect the environmental impacts of the selected type of projects and the characteristics of the environment of the study area are performed. The qualitative evaluation of their potential effects during the construction and operational phases contributes to the computation of the projects' EPG that is based on the proposed modified RIAM method.

3.1 The study area

The Region of Central Greece is one of the thirteen Regions of the country and consists of five Regional Units (Boeotia, Evia, Evrytania, Phthiotis, Phocis). The Region of Central Greece is located in the central continental part of the Greek territory and is the second largest region of the country with a total area of 15,554 km², representing almost 11.8% of its total area. The total population of Central Greece has declined over a decade. Specifically, in Boeotia, Phtiotis, Evrytania and Phocis there is a decrease of 10.1%, 12.9%, 13.2% and 10.3% respectively, while Evia is the only one where the population remains stable [25].

According to the statistical data from Hellenic Wind Energy Association [26] the Region of Central Greece has the largest wind power potential in the country. The existing onshore wind farm projects are located in the Regional Units of Evia, Boeotia, Phocis and Phtiotis of the Region of Central Greece and are depicted in **Figure 1**.

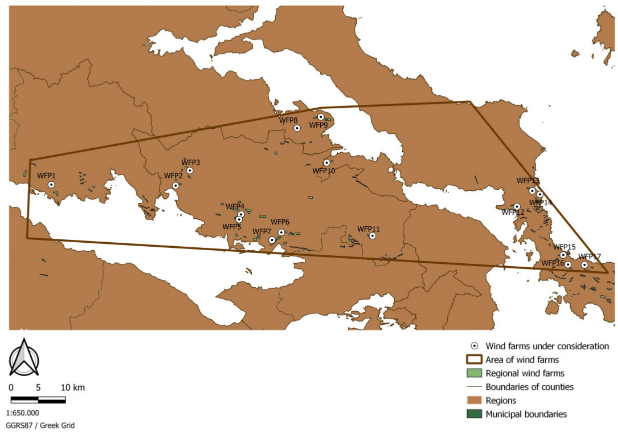

Figure 1. Existing Wind Farms in the Region of Central Greece.

Historical cultural environment

In the study area, there is a wealth of important archaeological sites and discoveries from the prehistoric, classical, byzantine and modern periods through which tourism is enhanced throughout the year. In addition, it has an important cultural heritage which consists of remarkable Neolithic findings as well as sites of the post-Byzantine period (1453–1830). The cultural heritage of the region includes a wealth of folklore (museums, galleries, cultural events, folklore centers). A basic example of the cultural wealth of the Region, apart from the above archaeological sites, are the traditional settlements (one in Boeotia, three in Evia, four in Evrytania, two in Phthiotis and seven in Phocis), the castles and the fortresses.

Climatic characteristics

In the Central Greece, during the year there are variations in temperature, with some months being colder or warmer than others. More specifically, according to the recordings of all four meteorological stations closest to the wind farms (Aliartos, Lamia, Skyros, Tanagra), the lowest temperatures are recorded in January with the average temperature ranging from 7–10 °C and the warmest month is July with temperatures of 25–27 °C.

Morphological topological characteristics

According to the Regional Climate Change Adaptation Plan (RCAP) [27], the Region of Central Greece, due to its large area, presents complex morphological and landscape characteristics which divide it into two parts, the continental part of Central Greece (Evrytania, Phocis, Phthiotis, Boeotia) and the islands (Skyros, Evia). Although the length of its coastline is quite significant (1682 km), it is one of the most mountainous regions of the Greek territory as its mountainous character (47.4%) dominates its total area. In particular, the main mountainous part of the region is located in the Regional Units of Evrytania and Phocis, where the southern side of Pindos extends to the Gulf of Corinth. The largest part of the area (49.02%) is characterized by flat to slightly sloping relief (0°–10° slope), followed by 35.29% of the area which consists of strongly sloping to steeply sloping relief (10°–30° slope), and finally, 15.69% consists of extremely steep relief (> 30° slope).

Natura 2000 and other protected areas

The Natura 2000 aims at preserving the natural European environment and the long-term protection of endangered species (divided into two categories: Special Areas of Conservation—SAC and Special Protection Areas—SPA). In the study area, there are 27 areas covered by the Natura 2000, of which 10 are located in Evia, 7 in Phocis, 6 in Phthiotis, 2 in Boeotia and 2 in Evrytania. Other protected areas that can be found in the study area are: (i) Biodiversity Protection Areas and (ii) National Parks, Wildlife Sanctuaries, Protected Landscapes and Protected Natural Formations.

3.2 Environmental components

According to the existing Greek legislation [28] the present condition of the environment of the study area includes the description of the following aspects of the environment: climate, bioclimate, morphology, aesthetics/visional features, geology, tectonics, soils, natural environment, land uses, built environment, historical and cultural environment, socio-economic environment, infrastructure, air quality, acoustic environment-noise, vibrations, radiation, surface waters and groundwater.

Initially, the construction and operation of the wind farms are not expected to have any direct impact on the climatic and bioclimatic characteristics of both the immediate as well as the wider study area. The studied wind farms are mainly located on the ground, which makes it difficult to change the geological and tectonic characteristics of the area. Furthermore, the wind facilities are located at distances in accordance with the existing legislation from settlements and residential areas [29], so that they do not cause disturbances in the residential environment. In addition, the installation areas of the wind farms under study as well as their accompanying projects are located outside of declared archaeological sites and consequently no effects on the historical-cultural environment of their construction area are expected. No electromagnetic interference problems are identified from the installation and operation of the wind farms, as the national legislation in the context of the licensing is framed by a series of measures (e.g. observance of minimum distances from telecommunications or broadcasting stations) according to which the selection of their optimal location is performed. During the construction and operational phase of the wind facilities, the surface and underground waters of the area are not expected to be affected and any effect is considered negligible.

Therefore, in this paper, the environmental assessment focuses on specific Environmental Components (EC) that are defined through the process of scoping and cover all potential environmental impacts of the examined projects (**Table 1**).

The importance of the eight environmental factors is qualitatively rated, based on a five-point scale as follows: 1 = not important, 2 = slightly important, 3 = moderately important, 4 = very important, and 5 = extremely important.

Table 1. Environmental components.

Environmental Component (EC)	Description
Morphology (EC1)	Study of landforms, including their nature, origin, development processes, and composition of materials
Aesthetics/Visional Features (EC2)	Shape, texture, colours and appearance of land
Natural Environment (EC3)	Flora and fauna, protected areas
Land Uses (EC4)	The distinction of land use types in zoning
Socio-economic Environment (EC5)	Features of the population, changes in the population, employment, occupation, education, and income trends
Infrastructures (EC6)	The technical structures such as road network, water supply network, sewage facilities, electrical grids, telecommunications
Air Quality (EC7)	The concentration of air pollutants such as CO, SO_2, NO, NO_2, O_3 and total suspended particulates that mainly contributes to the quality of atmospheric environment
Acoustic Environment (EC8)	The noise level in the study area from various sources

3.3 Assessment criteria and computation of environmental performance grade

The scoring scales and the assessment criteria used to evaluate each component are based on the original RIAM method as initiated by Pastakia and Jensen [6] and modified by Vagiona [12].

Two Primary Assessment Criteria (PAC) and three Secondary Assessment Criteria (SAC) are used to calculate the EPG: impact importance (PAC1), magnitude (PAC2), permanence (SAC1), reversibility (SAC2) and cumulatively (SAC3). The first two can individually change the EPG obtained, while the rest three should not individually be capable of changing the EPG obtained. These assessment criteria are evaluated using the scales presented in **Table 2**.

The impact significance of each environmental component is calculated as follows (Equation 1):

$$\alpha ij=PC1ijxPC2ijx(SC1ij+SC2ij+SC3ij) \quad (1)$$

Table 2. Environmental components.

	Assessment Criteria	Scale	Description
PAC1	Nature	1	positive impact (improvement) in status quo
		0	no change in status quo
		–1	negative impact in status quo
PAC2	Magnitude	1	low impact
		2	moderate impact
		3	significant impact
SAC1	Permanence	1	short term
		2	medium term
		3	long term (almost permanent)
SAC2	Reversibility	0	not applicable
		1	reversible
		2	partially reversible impact
		3	irreversible
SAC3	Confrontability	0	not applicable
		1	confrontable
		2	partially confrontable
		3	unconfrontable

where, i = 1,2, denotes the two basic phases of a project's life cycle, namely, construction phase (i = 1) and operational phase (i = 2) and j = 1,…,8, corresponds to the jth environmental component.

The EPG of each examined wind farm project is derived using the weighted sum model. The total score, Aij, of each j-th, j = 1,…,8, environmental component and for each i-th, i = 1,2, phase of the project life cycle, (construction phase (i = 1), the operational phase (i = 2)), is calculated as follows (Equation 2):

$$A_{ij} = \frac{a_{ij} w_j}{\sum_{j=1}^{8} w_j} \tag{2}$$

where, wj, j = 1,…,8, is the qualitative weight of the j-th environmental component and aij, i = 1,2, j = 1,…,8, is the impact significance as obtained from Equation (1). It should be noted that the minimum value of the impact significance between the construction and operational phases is used in Equation (2).

The EPG of each wind farm project is, finally, derived by the aggregation (sum) of all the environmental components' scores.

4. Results

4.1 Qualitative environmental impact assessment of WFP2

WFP2 is located in the Municipality of Karystos with a total installed capacity of 19.8 MW. Moderate effects of local extent and partial reversibility on the soil morphology occur during the construction phase of the project with mild to very weak effects during its operation. The installation and operation of the WFP2 have little impact on the landscape and the aesthetic environment as it is quite far away from the nearest settlement (almost 1.2 km) and the disturbances caused by the machinery are considered to be temporary and fully reversible. The wind farm abstains 5km from a Special Protection Area (SPA-GR2420012) which makes the impacts on the natural environment of the area weak and partially manageable. Due to the advanced technology of wind turbines, no particular impacts on the natural environment are caused during its operation. The construction of the project causes weak and partially reversible impacts on land uses. The installation and operation of the project are not expected to have a negative impact either on the social and economic environment of the area or on the existing anthropogenic activities. On the contrary, it positively affects the economic and social environment of the region. The transfer of the necessary mechanical equipment and machinery to the installation site of the wind farm project will increase the traffic in the area, contributing to heavy traffic during peak hours and causing problems in the acoustic environment.

The modified Rapid Impact Assessment Matrix for each one of the onshore wind farm projects have been developed and the individual scores for each environmental component are indicatively presented for WFP2 in **Tables 3 and 4** for the construction and operational phase respectively.

Table 3. Individual score for each environmental component in the construction phase for WFP2.

Environmental Component	PC1	PC2	SC1	SC2	SC3	a1j
EC1	–1	2	2	2	2	–12
EC2	–1	2	1	1	1	–6
EC3	–1	1	3	3	2	–8
EC4	–1	1	1	2	2	–5
EC5	1	2	2	3	2	14
EC6	–1	2	2	2	2	–12
EC7	–1	2	3	2	2	–14
EC8	–1	3	2	2	2	–18

Table 4. Individual score for each environmental component in the operational phase for WFP2.

Environmental Component	PC1	PC2	SC1	SC2	SC3	a2j
EC1	–1	1	2	2	2	–6
EC2	–1	2	2	2	2	–12
EC3	–1	1	2	2	2	–6
EC4	–1	1	2	2	1	–5
EC5	1	3	3	3	2	24
EC6	–1	2	1	1	1	–6
EC7	1	3	3	3	3	27
EC8	–1	2	2	2	2	–12

4.2 Computation of EPG

The impact significance of environmental components in construction and operational phase for all wind farm projects has been calculated using Equation (1) and presented in **Tables 5 and 6** respectively. Positive and negative aij values indicate, from a physical perspective, that the proposed wind farm project has, throughout its i-th phase, a positive or negative impact on the j-th environmental component, respectively. Higher absolute aij values in the negative range indicate more significant negative effects, while higher positive aij values indicate more significant positive impacts.

Table 5. Impact significance of environmental components in the construction phase.

	EC1	EC2	EC3	EC4	EC5	EC6	EC7	EC8
WFP1	–12	–15	–16	–3	24	–12	–14	–18
WFP2	–12	–6	–8	–5	14	–12	–14	–18
WFP3	–18	–10	–18	–4	24	–10	–12	–4
WFP4	–18	–18	–6	–3	18	–8	–16	–10
WFP5	–14	–10	–6	–3	14	–18	–16	–8
WFP6	–12	–6	–7	–3	14	–10	–16	–5
WFP7	–14	–6	–16	–3	14	–9	–16	–6
WFP8	–5	–8	–8	–3	14	–12	–8	–8
WFP9	–18	–12	–24	–3	14	–12	–24	–12
WFP10	–12	–18	–16	–10	16	–15	–24	–12
WFP11	–14	–12	–16	–3	16	–21	–14	–12
WFP12	–21	–6	–5	–3	14	–12	–16	–8
WFP13	–21	–6	–16	–6	14	–18	–16	–12
WFP14	–16	–15	–27	–3	12	–18	–16	–18
WFP15	–14	–14	–6	–3	16	–18	–14	–14
WFP16	–12	–10	–5	–6	14	–9	–21	–10
WFP17	–12	–6	–6	–3	16	–18	–18	–8

Table 6. Impact significance of environmental components in the operational phase.

	EC1	EC2	EC3	EC4	EC5	EC6	EC7	EC8
WFP1	–12	–18	–14	–5	24	–10	27	–12
WFP2	–6	–12	–6	–5	24	–6	27	–12
WFP3	–6	–4	–27	–4	24	–6	27	–12
WFP4	–6	–12	–6	–6	24	–6	27	–6
WFP5	–5	–12	–7	–5	24	–12	27	–12
WFP6	–6	–6	–8	–6	24	–12	27	–6
WFP7	–6	–12	–16	–5	24	–12	27	–12
WFP8	–6	–6	–7	–6	24	–12	27	–6
WFP9	–18	–12	–16	–6	24	–12	27	–18
WFP10	–6	–14	–24	–12	27	–10	24	–12
WFP11	–12	–18	–14	–6	27	–8	27	–12
WFP12	–12	–10	–5	–10	27	–10	27	–12
WFP13	–18	–12	–16	–12	27	–12	24	6
WFP14	–16	–12	–16	–8	27	–16	27	–12
WFP15	–7	–12	–6	–5	27	–16	24	–12
WFP16	–18	–7	–6	–12	27	–10	27	–14
WFP17	–14	–10	–6	–10	27	–12	27	–12

The final EPG of each wind farm project, based on Equation (2), is presented in **Figure 2**.

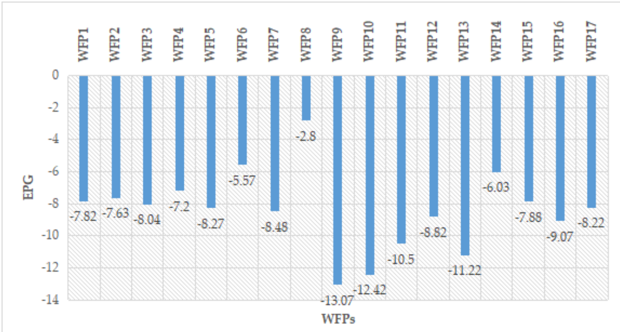

Figure 2. EPG scoring for WFPs.

The wind farms of the present research have a negative impact in terms of the natural and anthropogenic environment of the study area. WFP6, WFP8 and WFP14 cause weak negative effects on the natural and anthropogenic environment of the area, followed by eleven (11) stations which cause moderate negative effects and finally three (3) stations (WFP13, WFP10 and WFP9) cause the most significant negative effects. WFP9 received one of the highest negative grades as during its installation and operation the environmental components related to the morphology of the ground, the aesthetic and acoustic environment are strongly affected, as the nearest settlement with visual contact to the wind farm is only 0.55 km. The impact of WFP9 on the natural environment of the area is characterized as high intensity due to its proximity to the Wetland (Glaukos River Estuary). WFP10 has the second-highest EPG due to its impact on the natural and aesthetic environment of the surrounding area. The installation and operation of WFP13 significantly affect the environmental components related to the terrain morphology and the technical infrastructure due to new road construction and the extension of the existing road network.

However, the construction and operation of all WFPs positively affect specific environmental components. More specifically, their installation and operation contribute to the socio-economic environment of the study area as new jobs are created and employment is increased, while during their operation, cheaper electricity is ensured, and regional development is enhanced. In addition, during the operational phase of the examined wind farms, their greatest positive effect concerns the atmospheric environment of the study area as their main goal is the production of renewable "green" energy and the minimization of emissions of harmful pollutants into the atmosphere.

5. Discussion and conclusions

Wind farm installations like all forms of Renewable Energy Sources (RES) contribute to solving the problems created by the climate crisis as they produce electricity with zero harmful gaseous pollutants during their construction and operational phases. Wind energy should be deployed in compliance with the constraints and limitations set by the existing legal framework in order not to negatively affect the natural and anthropogenic environment and to promote sustainable development. Therefore, the aim of this paper is the evaluation and assessment of the environmental impacts of the existing wind farms in the Region of Central Greece, which was carried out through a modified RIAM method.

The RIAM method is a quantified impact calibration system. In this work, a modified RIAM is used which is applied for the construction and operational phase of the selected projects. Initially, the potential impacts of onshore wind farm facilities on the natural and anthropogenic environment during the construction and operational phase are analyzed. The environmental impact assessment is further enhanced by the computation of the EPG. The EPG could provide an innovative indicator for assessing the overall environmental impacts of a project, including environmental, economic and social dimensions.

The initial stage of the methodology includes the mapping of the existing wind farms and the analysis of the current state of the environment of the Region of Central Greece. Information related to the natural and the anthropogenic environment which either affects or is affected directly or indirectly by the installation and operation of the wind farms is provided. The environmental components that are affected by wind farm projects are identified and the individual score for each environmental component for each examined WFP is provided both in construction and operational phase. Impact significance of environmental components in both phases of the life cycle is then calculated and the EPG is finally computed.

From the application of the proposed methodology, it emerged that the negative impacts during the construction phase of the WFPs are mainly related to the morphology of the ground, the technical infrastructures and the atmospheric environment of the study area. The necessary work for the installation of such projects causes important impacts on the morphology of the soil, such as the destruction of the soil relief as well as the destruction of the soils that have been created by natural processes. The transfer of the necessary construction materials has as a consequence to increase the traffic of heavy vehicles in the area causing intense traffic load during peak hours. Finally, the atmospheric environment is directly affected by the installation of the WFPs as several pollutants are emitted from the gases produced by vehicles and mechanical equipment as well as from the diffusion of dust within the construction site.

However, during the operation of the WFPs, the most important positive impacts are related to the socioeconomic and atmospheric environment of the study area. The WFPs, during their operational phase, create new job opportunities and support local communities while at the same time contributing to the energy autonomy of the region and consequently of the entire country. Finally, the WFPs produce electricity without emitting greenhouse gases and other harmful pollutants to the atmosphere, which makes their influence on the atmospheric environment extremely important.

Author Contributions

Conceptualization, O.K. and D.V.; methodology, O.K. and D.V.; software, O.K. and D.V.; validation, O.K. and D.V.; formal analysis, O.K. and D.V.; investigation, O.K. and D.V.; resources, O.K. and D.V.; data curation, O.K. and D.V.; writing/original draft preparation, O.K. and D.V.; writing/review and editing, D.V.; visualization, O.K. and D.V.; supervision, D.V. All authors have read and agreed to the published version of the manuscript.

Conflict of Interest

The authors declare no conflict of interest.

Funding

This research received no external funding.

References

[1] Glasson, J., Therivel, R., Chadwick, A., 2012. Introduction to environmental impact assessment, 4th ed. Routledge: London, United Kingdom. DOI: https://doi.org/10.4324/9781315881218

[2] Phylip-Jones, J., Fischer, T.B., 2013. EIA for wind farms in the United Kingdom and Germany. Journal of Environmental Assessment Policy and Management. 15(2), 1–30. DOI: https://doi.org/10.1142/S1464333213400085

[3] Briggs, S., Hudson, M.D., 2013. Determination of significance in ecological impact assessment: past change, current practice and future improvements. Environmental Impact Assessment Review. 38, 16–25. DOI: https://doi.org/10.1016/j.eiar.2012.04.003

[4] Kaldellis, J.K., Apostolou, D., Kapsali, M., et al., 2016. Environmental and social footprint of offshore wind energy. Comparison with onshore counterpart. Renewable Energy. 92, 543–556. DOI: https://doi.org/10.1016/j.renene.2016.02.018

[5] Zolfagharian, S., Nourbakhsh, M., Irizarry, J., et al., 2012. Environmental impacts assessment on construction sites. Construction Research Congress. 1750–1759. DOI: https://doi.org/10.1061/9780784412329.176

[6] Environmental Impact Assessment Using the Rapid Impact Assessment Matrix (RIAM) [Internet][cited on 2023 January 2]. The Rapid Impact Assessment Matrix (RIAM)—A New Tool for Environmental Impact Assessment. Available from: https://www.scirp.org/reference/ReferencesPapers?ReferenceID=1190583

[7] Pastakia, C.M.R., Jensen, A., 1998. The Rapid Impact Assessment Matrix (RIAM) for EIA. Environmental Impact Assessment Review. 18(5), 461–482.
DOI: https://doi.org/10.1016/S0195-9255(98)00018-3

[8] Environmental Impact Assessment Using the Rapid Impact Assessment Matrix (RIAM) [Internet][cited on 2023 January 2]. Initial environmental evaluation of alternative methods to conserve the Rupa Tal, Nepal. Available from: http://www.pastakia.com/riam/pix/publicate/RupaTal-pp.htm

[9] Kuitunen, M., Jalava, K., Hirvonen, K., 2008. Testing the usability of the Rapid Impact Assessment Matrix (RIAM) method for comparison of EIA and SEA results. Environmental Impact Assessment Review. 28(4–5), 312–320.
DOI: https://doi.org/10.1016/j.eiar.2007.06.004

[10] Shakib-Manesh, T.E., Hirvonen, K.O., Jalava, K.J., et al., 2014. Ranking of small scale proposals for water system repair using the Rapid Impact Assessment Matrix (RIAM). Environmental Impact Assessment Review. 49, 49–56.
DOI: https://doi.org/10.1016/j.eiar.2014.06.001

[11] Suthar, S., Sajwan, A., 2014. Rapid Impact Assessment Matrix (RIAM) analysis as decision tool to select new site for municipal solid waste disposal: A case study of Dehradun city, India. Sustainable Cities and Society. 13, 12–19.
DOI: https://doi.org/10.1016/j.scs.2014.03.007

[12] Vagiona, D., 2015. Environmental performance value of projects: an environmental impact assessment tool. International Journal of Sustainable Development and Planning. 10(3), 315–330.
DOI: https://doi.org/10.2495/SDP-V10-N3-315-330

[13] Lintott, P.R., Richardson, S.M., Hosken, D.J., et al., 2016. Ecological impact assessments fail to reduce risk of bat casualties at wind farms. Current Biology. 26, R1135–R1136.
DOI: https://doi.org/10.1016/j.cub.2016.10.003

[14] Wang, S., Wang, S., Smith, P., 2015. Ecological impacts of wind farms on birds: questions, hypotheses, and research needs. Renewable and Sustainable Energy Reviews. 44, 599–607.
DOI: https://doi.org/10.1016/j.rser.2015.01.031

[15] Nazir, M.S., Ali, N., Bilal, M., et al., 2020. Potential environmental impacts of wind energy development: a global perspective. Current Opinion in Environmental Science and Health. 13, 85–90.
DOI: https://doi.org/10.1016/j.coesh.2020.01.002

[16] Szumilas-Kowalczyk, H., Pevzner, N., Giedych, R., 2020. Long-term visual impacts of aging infrastructure: challenges of de-commissioning wind power infrastructure and a survey of alternative strategies. Renewable Energy. 150, 550–560.
DOI: https://doi.org/10.1016/j.renene.2019.12.143

[17] Marques, A.T., Santos, C.D., Hanssen, F., et al., 2020. Wind turbines cause functional habitat loss for migratory soaring birds. Journal of Animal Ecology. 89, 93–103.
DOI: https://doi.org/10.1111/1365-2656.12961

[18] Conkling, T.J., Loss, S.R., Diffendorfer, J.E., et al., 2021. Limitations, lack of standardization, and recommended best practices in studies of renewable energy effects on birds and bats. Conservation Biology. 35(1), 64–76.
DOI: https://doi.org/10.1111/cobi.13457

[19] Abbasi, S.A., Tabassum, A., Abbasi, T., 2016. Impact of wind-energy generation on climate: a rising spectre. Renewable and Sustainable Energy Reviews. 59, 1591–1598.
DOI: https://doi.org/10.1016/j.rser.2015.12.262

[20] Kaldellis, J.K., Kavadias, K.A., Paliatsos, A.G., 2003. Environmental impacts of wind energy applications: Myth or reality? Fresenius environmental bulletin. 12(4), 326–337.

[21] Klick, H., Smith, E.R.A.N.,, 2010. Public understanding of and support for wind power in the United States. Renewable Energy. 35(7), 1585–1591.
DOI: https://doi.org/10.1016/j.renene.2009.11.028

[22] Kaldellis, J.K., Garakis, K., Kapsali, M., 2011. Noise impact assessment on the basis of onsite

acoustic noise immission measurements for a representative wind farm. Renewable Energy. 41, 306–314.

[23] Sayed, E.T., Wilberforce, T., Elsaid, K., et al., 2021. A critical review on environmental impacts of renewable energy systems and mitigation strategies: Wind, hydro, biomass and geothermal. Science of the Total Environment. 766, 144505.
DOI: https://doi.org/10.1016/j.scitotenv.2020.144505

[24] University of Michigan [Internet]. Electromagnetic Interference Effects of Wind Turbines [cited on 2023 March 1]. Available from: https://deepblue.lib.umich.edu/bitstream/handle/2027.42/20990/rl0773.0001.001.pdf?sequence=2

[25] Hellenic Statistical Authority (ELSTAT) [Internet][cited on 15 March 2023]. Available from: https://www.statistics.gr/statistics/pop

[26] Hellenic Wind Energy Association (HWEA) [Internet][cited on 2023 Mar 15]. Available from: https://eletaen.gr/wp-content/uploads/2023/04/2023-01-26-2022-HWEA_Statistics-Greece-1.pdf

[27] Regional Plan of Central Greece for Adaptation to Climate change [Internet]. (accessed on 15 March 2023) Available from: https://drive.google.com/file/d/1SxkTG8wzukYsDeZCZ4m5knIgWr4qH5KX/view (in Greek)

[28] MD 170225/2014 Specification of the environmental license file content for A' type activities (OGG 135/B/27-01-2014). (accessed on 15 March 2023). Available online: https://www.elinyae.gr/sites/default/files/2019-07/135b_14.1411457099343.pdf (in Greek)

[29] Ministry of Environment, Energy and Climate Change (MEECC). Specific Framework for Spatial Planning and Sustainable Development for Renewable Energy Sources (SFSPSD/RES). JMD 49828/2008 OGHE B′ 2464/3-12-08. 2008. Available online: https://ypen.gov.gr/wp-content/uploads/2020/11/FEK2464B_2008_RES.pdf (accessed on 15 February 2022). (in Greek)

BILINGUAL PUBLISHING GROUP

Tel:+65 65881289

E-mail: contact@bilpublishing.com

Website:https://journals.bilpubgroup.com

2661-3190

01

9 772661 319241